AMERICAN UNIVERSITY OF BEIRUT

MULTIPORT RF ENERGY HARVESTERS

by
ALINE JEAN EID

A thesis
submitted in partial fulfillment of the requirements
for the degree of Master of Engineering
to the Department of Electrical and Computer Engineering
of the Faculty of Engineering and Architecture
at the American University of Beirut

Beirut, Lebanon
June 2017

AMERICAN UNIVERSITY OF BEIRUT

MULTIPORT RF ENERGY HARVESTERS

by
ALINE JEAN EID

Approved by:

Dr. Joseph Costantine, Assistant Professor — Advisor
Electrical and Computer Engineering

Dr. Mariette Awad, Associate Professor — Member of Committee
Electrical and Computer Engineering

Dr. Youssef Tawk, Assistant Professor — Member of Committee
Electrical, Computer and Communication Engineering, Notre Dame University, Louaize

Dr. Ali Ramadan, Assistant Professor — Member of Committee
Electrical Engineering, Fahad Bin Sultan University

Date of thesis defense: June 9, 2017

AMERICAN UNIVERSITY OF BEIRUT

THESIS, DISSERTATION, PROJECT RELEASE FORM

Student Name: _____
Last First Middle

◯ Master's Thesis ◯ Master's Project ◯ Doctoral Dissertation

☐ I authorize the American University of Beirut to: (a) reproduce hard or electronic copies of my thesis, dissertation, or project; (b) include such copies in the archives and digital repositories of the University; and (c) make freely available such copies to third parties for research or educational purposes.

☐ I authorize the American University of Beirut, to: (a) reproduce hard or electronic copies of it; (b) include such copies in the archives and digital repositories of the University; and (c) make freely available such copies to third parties for research or educational purposes
after:

One ---- year from the date of submission of my thesis, dissertation, or project.

Two ---- years from the date of submission of my thesis, dissertation, or project.

Three ---- years from the date of submission of my thesis, dissertation, or project.

_____

Signature Date

ACKNOWLEDGMENTS

First, I would like to thank God for all the progress that I have achieved in my life and especially during my master studies. Also, I would like to thank him for surrounding me with amazing people that are helping me achieve my ambitions.

I would like to express my recognition and sincere gratitude to my advisor Prof. Joseph Costantine for his continuous support, motivation, and supervision during the last two years. His professionalism is the key element in the success of this work.

Also, I would like to address full appreciation to the rest of my thesis committee: Prof. Mariette Awad, Prof. Youssef Tawk and Prof. Ali Ramadan for their guidance and encouragement.

Special thanks to the University Research Board (URB) and the Munib and Angela Masri Institute of Energy and Natural Resources at the American University of Beirut (AUB) for providing financial support throughout this research.

I would like to thank the members of the Antennas and Radio Frequency Lab at the American University of Beirut for their continuous support and efforts exerted in the preparation of the testing area. Also, I would like to show my gratitude to Fatima El Zahraa AsadAllah, Serge Mghabghab, Sandy Saab and Mahmoud Abdallah for the nights we were working together, and for the research-related discussions that we held.

Last but not least, my deepest gratitude goes to my family members who were patient enough to supply me continuously with unlimited love and confidence.

AN ABSTRACT OF THE THESIS OF

Aline Jean Eid for Master of Engineering
Major: Electrical and Computer Engineering

Title: Multiport RF Energy Harvesters

RF energy harvesting allows the transformation of wireless RF energy into collectable dc power and constitutes the basis of green wireless charging and energy transfer technology. Various components, such as deployed sensors and small portable devices benefit from this technology to power their continuous operation. Harvesting low powered RF signals and rectifying them into a notable dc output is a challenging task. Such task requires understanding of the rectifying component's limits to maximize the desired outcome.

The aim of the work presented in this thesis is to design an efficient RF energy harvesting system for low input power levels operating over the Wi-Fi 802.11 b/g band. We propose a novel design of RF harvesters and rectifiers solely based on using zero-bias Schottky diodes. Our design objective is to identify the most suitable technique that results in an increased output dc power while maintaining the same transmitted power from the RF source. A tradeoff analysis is executed between various matching networks for better rectification efficiency and dc output.

Our designed rectifiers prove the ability to harvest and rectify the RF signals with a very good efficiency across a multitude of frequencies. We have then integrated these circuits into a multiport RF energy harvesting system that relies on two combining architectures: RF combining and dc combining. The multi-port rectifier system demonstrates excellent harvesting capabilities with an increased output dc voltage in both combining scenarios. We also discuss the harvesting of very small RF energy from ambient Wi-Fi signals that are collected from commercial Wi-Fi routers. The rectifier is tested in ambient conditions and efficiency results display a comparable performance to harvesting from dedicated RF signals.

In this thesis, Support Vector Machines (SVM) is also employed to yield a system that can predict with a good accuracy the location and level of maximum power available at a certain day and time. In summary, the limits of Schottky diode's rectification abilities are pushed, while investigating optimal matching networks. The systems designed are deployed in a multiport scenario when combined input and output are used. Such system, not only harvests from dedicated RF signals but also collects

ambient Wi-Fi signals with a machine learning prediction ability of the maximum available power.

CONTENTS

ACKNOWLEDGMENTS V

ABSTRACT VI

LIST OF ILLUSTRATIONS XI

LIST OF TABLES XV

Chapter

I. INTRODUCTION 1

II. BACKGROUND OF RF ENERGY HARVESTING SYSTEMS AND KNOWLEDGE 5

A. Introduction 5

B. RF Energy Harvesting using Schottky Diodes and Transistors 6

C. Integrated Techniques in an RF Energy Harvester 8

D. RF Energy Harvesting from Ambient RF Sources 13

E. Application of Machine Learning in Antennas and RF Circuits Design 17

F. Summary 20

III. A LOAD INDEPENDENT TAPERED RF HARVESTER . 21

A. Introduction 21

B. Rectifier's Circuit Topology 21

C. Design and Performance Results 25

D. Summary 35

IV. A COMPACT RF ENERGY HARVESTER WITH AN IMPROVED MATCHING NETWORK 36

A. Introduction 36

B. RF Energy Harvesting System Overview 36

C. Rectifier Designs with a Stub Based Meandered Matching Network 38

1. Shorted Shunt Stub Matching Network 38
2. Open Shunt Stub Matching Network 41
3. Performance comparison between the open- and short-circuited stub matching techniques 43

D. Rectifier Designs with a Stub Based Meandered Matching Network 44

1. Proposed dual lines matching technique 44
2. Improved matching network technique 49

E. Rectifiers' Performance Comparison with Respect to Frequency, Load and Input Power 52

F. Summary 57

V. MULTIPORT RF ENERGY HARVESTERS 58

A. Introduction 58

B. Design of the Multiport System 58

C. Single Transmitter - Multiple Receivers - RF Energy Harvesting System 61

1. RF Combining 61
2. DC Combining 63
3. RF combining vs dc combining 66

D. Multiple Transmitters - Multiple Receivers - RF Energy Harvesting System 67

E. Summary 69

VI. AMBIENT RF ENERGY HARVESTING FROM WI-FI 70

A. Introduction 70

B. Principles of Harvesting from Ambient Wi-Fi signals 70

C. Ambient RF Energy Harvesting Experimental Setup 73

1. Ambient Wi-Fi Signals Vs Dedicated Point to Point RF Signals Energy Harvesting 74
2. Efficiency Response with Respect to Frequency 76
3. Efficiency Response with Respect to Distance 77

D. Ambient RF Harvesting Effect on Wi-Fi Users 78

E. Summary 80

VII. IMPROVING WI-FI HARVESTING EFFICIENCY USING SUPPORT VECTOR MACHINES 82

A. Introduction 82

B. Wi-Fi Activity Prediction Methodology 83

1. Data Collection and Preprocessing 83
2. Wi-Fi activity prediction approach 85

C. Results Interpretation 86

D. Summary 92

VIII. CONCLUSION AND FUTURE WORK 93

ILLUSTRATIONS

Figures Page

1. Block diagram of a basic RF energy harvesting system 2

2. Microstrip rectifier design. [9] 7

3. Rectenna System: (a) Proposed stacked patch antenna, (b)Fabricated rectifier on 0.8-mm-thiek NPC-F260 and the spice parameters of diode HSMS2850. [10] 8

4. Origami package with harvester electronics inside. [11] 9

5. (a) 3D model of the proposed rectenna, (b) Topology of the proposed rectifying circuit with a two-branch impedance matching network. [12] 10

6. Rectenna array implementation. [15] 11

7. Photographs of the 1by4 quasi-Yagi array: (a) Top side, (b) Back side. [16] . 12

8. Photograph of the fabricated rectifier. [16] 12

9. Layout of the proposed rectenna [19] 13

10. Measured received power versus frequency and measured output voltage of the proposed rectenna. [13] 14

11. Rectenna experiment in ambient environment (a) [21], (b) [22] 15

12. Measurement of harvested DC voltage from the ambience [23] 16

13. Key challenge with Wi-Fi power delivery [26] 17

14. The proposed impedance transformer network. 24

15. Return Loss Results for different scenarios of the lines characteristic impedances: (a) Z0L and Z0F equal to 20 Ω, (b) Z0L and Z0F equal to 100 Ω, (c) Z0L equal to 20 Ω and Z0F equal to 100 Ω, (d) Z0L equal to 100 Ω and Z0F equal to 20 Ω. 25

16. Rectifier Design (a) Layout, (b) Fabricated prototype. 26

17. The transition between TLs using triangular tapering technique. 27

18. Impedance variation of a matching section with a triangular taper for d (ln Z/Z0)/dz [1] 28

19. PCE and output voltage results for the proposed rectifier for RL = 2470 Ω... 29

20. Slot antenna prototype: (a) Top view, (b) Bottom view. 30

21. Reflection coefficient of the slot antenna. 31

22. (a) Gain plots for the slot antenna with and without ground plane (at f = 2.45 GHz and φ = 0˚, θ), (b) Slot antenna with a λg/4 distant copper sheet from beneath. 31

23. Experiment 2 with the transmitting-receiving system. 32

24. Measured flat efficiency results for the proposed rectifier for Pin = -5 dBm, -10 dBm and -15 dBm with a wide range of load values. 33

25. Variation of the input impedance with respect to the load: (a) Real part, (b) Imaginary part. 35

26. Block diagram of the proposed RF energy harvesting system. 37

27. Rectifier design with short-circuited stub (a) Schematic, (b) Layout, (c) Fabricated prototype. 40

28. Efficiency and output voltage results for the rectifier design with single short-circuited stub matching network. 41

29. Rectifier design with open-circuited stub (a) Schematic, (b) Layout, (c) Fabricated prototype. 42

30. Efficiency and output voltage results for the rectifier design with single open-circuited stub matching network. 43

31. Rectifier design along with the proposed impedance transformer network. ... 45

32. Smith chart representation of the proposed impedance transformer matching network. 46

33. Rectifier design for the proposed impedance transformer matching network (a) Layout, (b) Fabricated prototype. 48

34. Efficiency and output voltage results for the rectifier with tapered series lines matching technique. 49

35. Rectifier design with improved matching network (a) Layout, (b) Fabricated prototype. 51

36. Efficiency and output voltage results for the rectifier with improved matching technique. 51

37. Measured PCE results for different load values of all rectifiers at Pin = 0dBm and f = 2.45GHz. 53

38. Input impedance plots with respect to load variations for the proposed rectifier "IMN" and the 50 Ω single stub MN rectifier "OS". 54

39. Measured PCE results with respect to frequency for Pin = 0 dBm and RL (optimal)..... 55

40. Input impedance plots with respect to frequency for the proposed rectifier "IMN" and the 50 Ω single stub MN rectifier "OS". 56

41. Measured PCE results with respect to input power at 2.45 GHz and RL= 1kΩ. 57

42. Single element meander antenna design on HFSS. 59

43. Photo of fabricated meander antenna array. 59

44. Plot of simulated and measured reflection coefficient of meander antenna array. 60

45. Plot of simulated and measured radiation pattern of meander antenna array.. 60

46. RF Combining schematic. 62

47. Four-to-one RF combining experimental setup. 63

48. DC combining schematic. 65

49. DC combining experimental setup of four rectifying circuits. 66

50. (a) The one to one transmitting-receiving system, (b) RF combining experimental setup. 68

51. RF Energy Harvesting: (a) Dedicated signals, (b) Ambient Wi-Fi signals. 71

52. Router normal activity. 72

53. Router activity after applying the packet injection algorithm. 73

54. Experimental setups: (a) Ambient harvesting setup, (b) Dedicated harvesting setup. 75

55. Efficiency comparison between Dedicated and Ambient energy harvesting scenarios..... 76

56. Efficiency results for the used rectifier. 76

57. Measured PCE results with respect to frequency for Pr=-5dBm, Pr=- 10dBm, and Pr=-12dBm. 77

58. Efficiency plot with respect to distance. 78

59. Video streaming duration for router with and without packet injection. 79

60. Data Rates for router with and without packet injection. 79

61. Data collected for three consecutive Tuesdays in location A. 84

62. Power Patterns for three consecutive Tuesdays in location A. 86

63. Comparison of actual power with predicted power using ANN And SVM in location A for a week period..... 87

64. ANN Architecture. 87

65. Power on predicted path using SVM for a one day period. 90

66. Rectifier's efficiency on predicted path using SVM for a one day period. 91

67. Efficiency and output voltage results for the used rectifier circuit. 91

TABLES

Table Page

1. Comparison between short and open shunt stub MN 44

2. Sample of actual vs predicted power 89

CHAPTER I

INTRODUCTION

There has been a lot of effort spent in the past decade on researching new ways to provide sufficient energy to power devices. Radio Frequency (RF) energy harvesting has proven to be an attractive technique that relies on collecting ambient RF energy in order to re-purpose it. Such technique has the potential to provide efficient and continuous recharging possibilities.

The spectrum encompasses frequency bands that extend from the very high frequency range (VHF) (30–300 MHz) to ultra-high frequency (UHF) (300–3000 MHz) while the term microwave is typically used for frequencies between 3 and 300 GHz [1]. RF signals originate from the propagating electromagnetic waves of TV stations, mobile phones, radio stations, Wi-Fi routers and other sources that are abundantly available.

The work in this thesis focuses on expanding the potential of RF harvesting and rectification efficiencies through a series of techniques that understand and extend the limits of the rectifying component. The goal of this work is to collect ambient RF energy, convert it into dc power and supply small electrical and portable devices with charging capabilities. Not only this new technique eliminates the need for manually replacing batteries, but it is also an environment friendly solution since it enables the "recycling" of ambient energy. In fact, RF energy harvesting allows wireless devices to become self-sustaining [2].

The main element in an RF energy harvesting system is the rectenna which is a combination of the rectifier and the antenna. This concept which was first introduced in

1964 by William C. Brown [3] refers to an antenna that is integrated with an RF rectifying circuit. The antenna that is the front end of the receiver is connected to an efficient rectifier for RF-to-dc power conversion. Figure 1 shows a block diagram of a basic energy harvesting system, where an antenna harvests ambient electromagnetic energy. The harvested energy is rectified and filtered. The recovered dc either powers a low powered device directly, or is stored in a capacitor or battery for higher power low duty-cycle operation. This process can be directed towards the charging of battery dependent devices such as mobile devices or distant sensor networks. Such technique is the basis of what is now known as wireless charging or wireless power transfer from RF energy and constitutes a great advantage for any mobile or distant device.

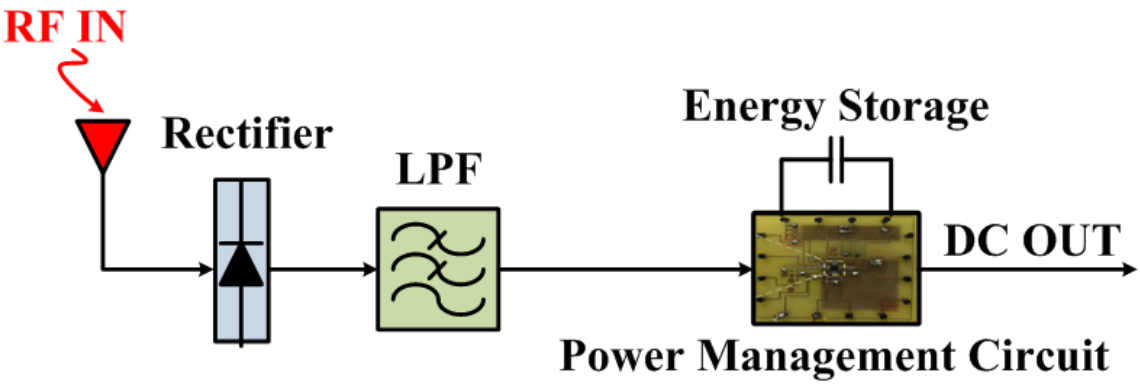

Figure 1: Block diagram of a basic RF energy harvesting system

RF and microwave wireless power transfer systems can occur at three different levels and regions: near-field power transfer that consists of tens of watts with a limited distance of a meter-range, microwave power transfer (MPT) equivalent to tens of milliwatts that can go up to a few meters distance, and ambient microwave power harvesting (MPH) which denotes signals up to hundreds of microwatts, but without a

distance limitation if the receiver is in the proximity of a concentrated area of RF transmitters or base-stations. Among these three types, this work focuses on a demonstration of harvesting very small RF energy from the ambient environment. The core enabling part of an RF harvesting system is the rectifying circuit. This is due to its role in converting the limited available RF power into an exploitable dc energy. For that purpose, efforts were redirected toward pushing the maximum efficiency of the rectifying circuit in order to enable it to handle a lower input RF power [4].

At low RF power levels proper selection of the Schottky diode and appropriate design of the impedance matching network are necessary to overcome the limitations of the low power input. A boost converter can also be used at the output to increase the collected dc voltage level. However, in this work, different techniques are applied to increase the output dc power of the harvesting system without altering the input RF power levels.

In a far field, very low power densities of RF energy can be extracted from the environment since the propagation energy drops down rapidly as distance from the source is increased. Since the investigated harvesting systems are intended to operate within an ambient environment, the antenna front end of the rectenna system must exhibit a wide beam with a relatively good gain.

The purpose of this work is to present methods that could be approached for increasing the efficiency of the harvesting system at lower power levels. The techniques include optimized matching network topologies, combining architectures, ambient harvesting and learning algorithms implementation. For this reason, the research proposed in this thesis is first based on theoretical analysis, simulations carried out using three software packages: Ansys Electronics Desktop (AEDT), Advanced Design

System (ADS) and MATLAB, in addition to measurement data that results from numerous experimental setups. Measurement result verify and validate the analytical and simulated predicted data.

This thesis is composed of eight chapters that are divided as follows: Chapter II carries out a survey of RF energy harvesting knowledge and systems. It serves as a general description of the techniques that are presented in literature. Chapter III introduces a novel rectifying circuit resulting in a load independent efficiency response. Chapter IV employs a tradeoff analysis between various matching techniques for a better rectification efficiency. This work results in a compact, tapered RF energy harvester with an improved matching technique. Chapter V discusses combining architectures and ends up in the implementation of three multiport RF energy harvesting systems. In chapter VI, ambient RF energy harvesting is discussed and results in a harvesting system from wireless routers. In chapter VII, machine learning techniques are employed for a smarter harvesting performance. Finally, chapter VIII ends with a conclusion that summarizes the results that this research has achieved and highlights future directions.

CHAPTER II

BACKGROUND OF RF ENERGY HARVESTING SYSTEMS AND KNOWLEDGE

A. Introduction

In this chapter, a survey of RF-dc microwave rectifiers' research is executed. The aim of the survey is to take a closer look at rectenna elements proposed by various specialized researchers in order to gain insight into rectenna designs, rectifier geometries, matching networks, performance parameters, simulation and measurement techniques.

The surveyed literature is divided into four categories where the first category presents the most popular rectifying elements in literature. Some work covers the Schottky diode configurations, performance and limitations whereas other research presents those of a transistor.

Section II. B of this chapter discusses the various RF energy harvesting systems that resort to Schottky diodes and transistors. Section II. C addresses the design of RF energy harvesters using various techniques such as the integration of 3D structures, novel fabrication techniques and flexible materials. Other approaches are presented in this section, aiming for an increased efficiency with the implementation of multiport or multifrequency operation rectifying systems. Section II. D moves from the traditional dedicated RF transmission sources to ambient harvesting from RF sources available everywhere. Finally, section II. E introduces some of the work that merges the application of machine learning algorithms in RF and antennas designs.

B. RF Energy Harvesting using Schottky Diodes and Transistors

Different types of devices operating as rectifiers are listed, however the focus is mainly directed towards Schottky diodes and transistors. In [5], [6], limitations accompanied with the use of Schottky diodes are clearly presented along with a study on the maximum attained efficiency at low input power levels. Ideally the Schottky diode conducts no current (OFF state) until the input voltage exceeds the diode voltage threshold or the breakdown voltage. Above or below these input voltage values, the diode conducts infinite current. It is important to note that losses can arise due to the junction capacitance, series resistance, threshold voltage, and reverse breakdown. This is intensively detailed in [5] where the best predicted efficiencies given by the SMS7630 and VDI W-Band ZBD diodes present, respectively, 4.7% and 6.7% power conversion efficiencies at a −35dBm input power level.

The CMOS technology for the design of RF rectifiers is investigated in [7]. A high sensitivity rectifier is achieved with 40% efficiency at -17dBm. Another alternative of the Schottky diode-based designs is the diode-connected MOSFET Dickenson charge pump due to its desired process compatibility with the CMOS circuits. However, these designs suffer from the efficiency loss induced by a large threshold voltage leading to relatively low PCE values. Therefore, the work done in [8] reveals the superiority of the heterojunction tunnel field-effect transistor HTFET RF rectifiers and their capability to result in a high PCE at a low RF input power range.

Other efficient rectenna designs are proposed in literature and rely only on the use of Schottky diodes. They resort to different diode configurations such as single diode in series [9], in shunt [10] or multiple diodes in voltage multipliers topologies [11], [12], [13]. For example, an 868 MHz-single-series rectifier circuit shown in Figure 2 is

discussed in [9]. Its corresponding efficiency is 47% for a 0dBm input power and a load of 9530 Ω.

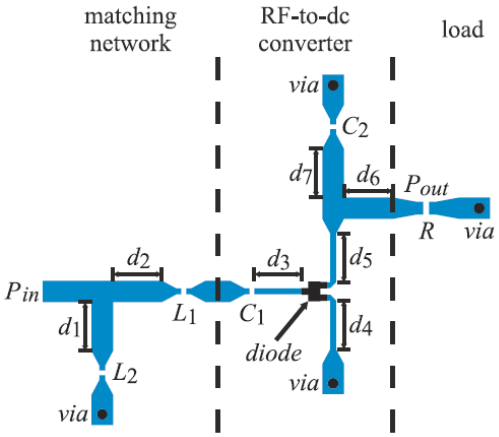

Figure 2: Microstrip rectifier design. [9]

In [10], a wideband and efficient rectenna suitable for 2.4 GHz-band RF energy harvesting from Wi-Fi applications is presented. The rectenna system shown in Figure 3 consists of a driven patch and four parasitic patches along with the rectifying circuit. The harvester exhibits a high efficiency in the band of 2.41-2.47 GHz with the power level as low as -20 dBm. Especially, at 2.472 GHz, the measured efficiency of rectifier is 4.3%, 24.3%, 48.5%, 63% for different input powers of -30, -20, -10, 0 dBm, respectively.

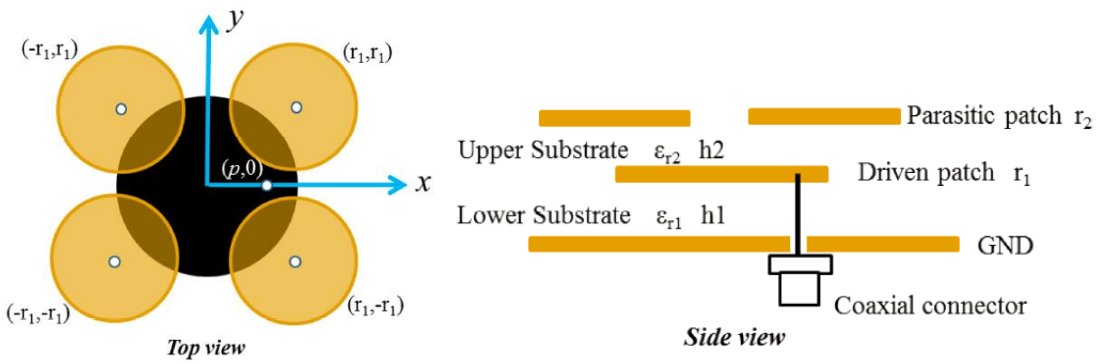

(a)

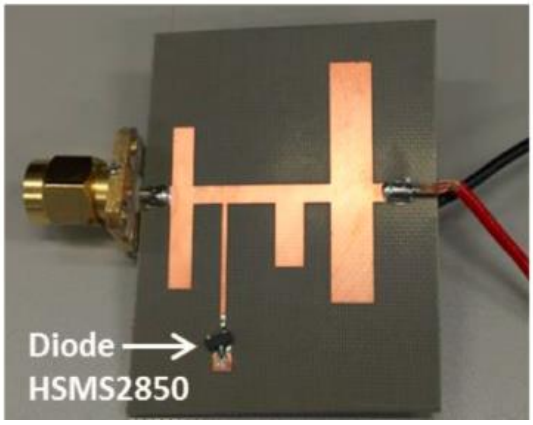

(b)

Figure 3: Rectenna System: (a) Proposed stacked patch antenna, (b)Fabricated rectifier on 0.8-mm-thiek NPC-F260. [10]

C. Integrated Techniques in an RF Energy Harvester

Some of the work presented in literature employ novel 3D structures using inkjet printing such as a cube enabling simultaneous harvesting or a flexible wearable RF energy harvester. In the design presented in [11], two patch antennas operating at 2.4 GHz are fabricated on the surface of a 3D cube. This printed cube using Inkjet printing is reduced in size with sides of 4.2cm x 4.2cm as shown in Figure 4. Each of these two antennas is connected to a rectifier circuit consisting of a voltage doubler configuration of HSMS285 zero bias diode. For this design, dc combining is used therefore the output is combined at a single dc terminal that drives the load. As a result of the measurement

done, a voltage level of 100mV is obtained at -15dBm input power and a load of 2 kΩ when one port is excited. When both ports are excited for the same input power 150mV is measured at the output.

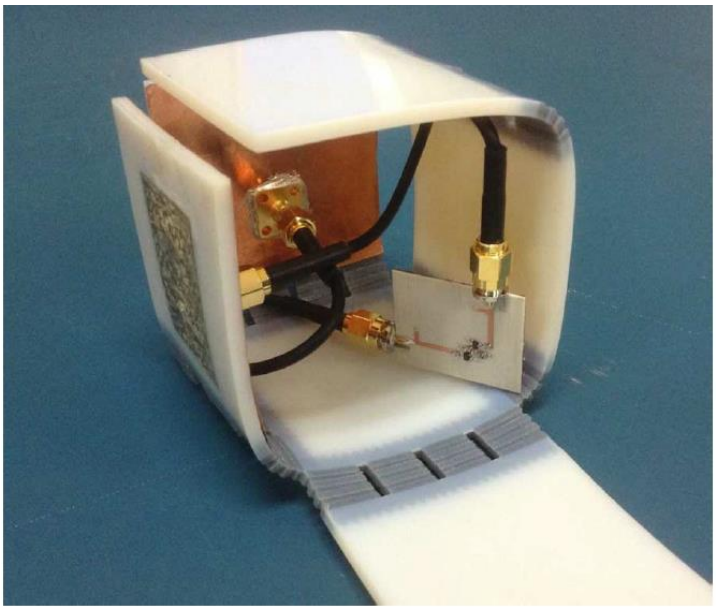

Figure 4: Origami package with harvester electronics inside. [11]

Other examples cover the integration of various techniques in order to increase the input power to the system such as addressing multiband operation [12], [13], as well as building arrays instead of single element systems [14], [15].

In [12], a novel broadband rectenna for ambient wireless energy harvesting is presented over the frequency band from 1.8 to 2.5 GHz. It consists of a novel broadband dual-polarized cross-dipole antenna which has an embedded flower-shaped slot filter for harmonic rejection to further improve the rectenna efficiency. The antenna as well as the matching network are built on a low-cost FR4 substrate. To insure a maximum power transfer between the antenna and the rectifier, a novel two-branch impedance matching circuit is proposed. It consists of a 50Ω microstrip line with an H-shaped slot

filter on the ground plane. For the rectifier, a modified voltage doubler configuration is designed using the Schottky diode SMS7630. The rectenna design is shown in Figure 5. The measured power sensitivity of this design is down to −35dBm where efficiency is 5% and reaches 55% when the input power to the rectifier is −10dBm. The measured maximum efficiency is about 70% at 2.15 GHz when the input power to the rectifier is 0dBm.

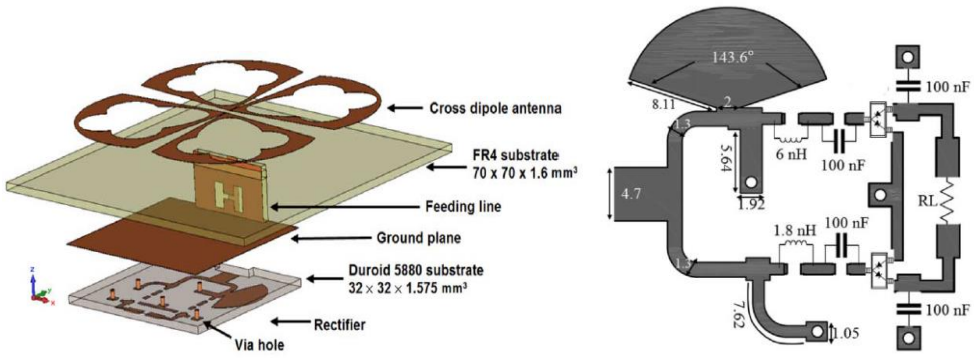

(a) **(b)**

Figure 5: (a) 3D model of the proposed rectenna, (b) Topology of the proposed rectifying circuit with a two-branch impedance matching network. [12]

The single rectenna element presented in [12] is now transformed into a multiport system as shown in Figure 6 by the implementation of a rectenna array operating on several frequency bands between 1.8 GHz and 2.5 GHz [15]. The measured efficiency of the rectenna array is increased from 20% to 70% when the ambient power density varies between -30 dBm and -10 dBm.

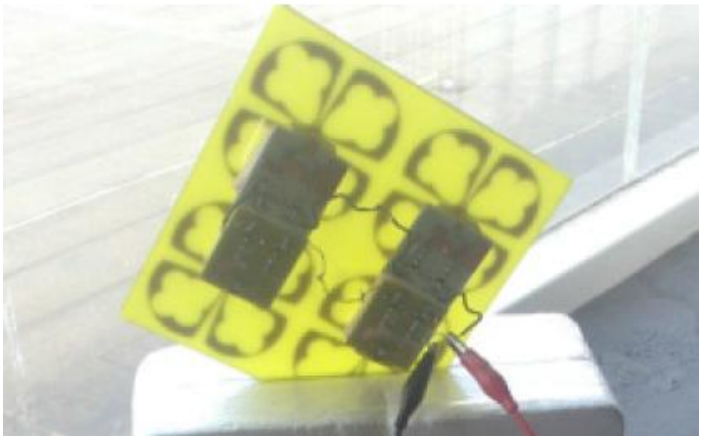

Figure 6: Rectenna array implementation. [15]

An array implementation is also targeted in [16] with a novel dual band rectenna that harvests ambient RF power of GSM-1800 and UMTS-2100 bands efficiently. The antenna design is initiated with a 1 by 2 sub-array of quasi-Yagi antenna and is then extended to a 1 by 4 array as seen in Figure 7. This array has a high gain of 10.9 and 13.3dBi at 1.85 and 2.15 GHz. Such gain leads to the reception of higher power for rectification due to the fact that the effective aperture area of an antenna is proportional to its gain. As for the designed rectifier shown in Figure 8, the Schottky diode HSMS 2852 from Avago is used in a series configuration. Since the operation is at both 1.8 and 2.1 GHz bands, a dual-band rectifier with the corresponding matching network is implemented. For single-tone input, the efficiency can reach 34% at 1.84 GHz and input power of -20dBm. Measurement results show that a power conversion efficiency of 40% and an output dc voltage of 224 mV is achieved over a 5 kΩ resistor when the dual-tone input power density is 455 μW/m2.

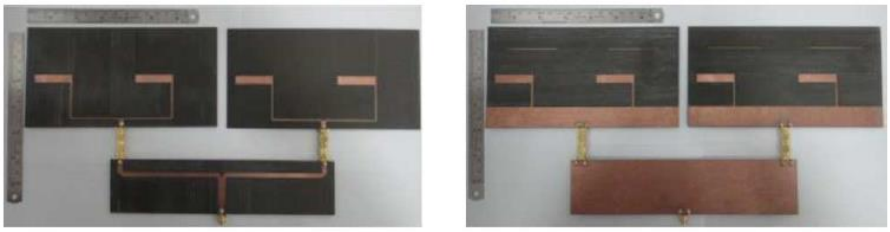

(a) **(b)**

Figure 7: Photographs of the 1by4 quasi-Yagi array: (a) Top side, (b) Back side. [16]

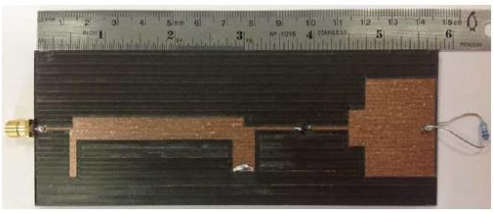

Figure 8: Photograph of the fabricated rectifier. [16]

The harvested energy is supplemented in some cases by additional resources as discussed in [17]. A proposed harvester consists of a dual port rectangular slot antenna, a 3-D printed package, a solar cell, an RF-dc converter, a power management unit (PMU), a microcontroller unit, and an RF transceiver. In addition to the antenna and rectifying device selection, the choice of the matching network topology is at the base of any successful RF design. Recent work has focused on this intermediate stage between the antenna and the rectifier such as through optimizing the length and width of a matching stub in order to achieve the highest efficiency [18], [19], [20].

For example, in [19], the idea of conjugate matching a rectifier to the antenna is introduced. The RF harvesting component consists of an antenna, a rectifier, an RF matching circuit and a dc collection circuit with dc load. Initially, the W-Band ZBD Schottky diode from VDI is chosen. An antenna with a high impedance is chosen to minimize the size of the matching circuit which is the folded dipole in this case. An

inductive feed is used to match the antenna to the highly reactive diode as seen in Figure 9. The maximum rectified power is 15.05 µW. As previously mentioned, the high impedance required for the W-band ZBD diode becomes a problem for high efficiency energy harvesters. A modified version of the rectifier uses the Skyworks SMS7630-079 GaAs Schottky diode. The impedance required for maximum efficiency is lower in this case, about 50+j250Ω obtained by load-pull simulations. The rectified power is increased by 20% compared to the VDI diode prototype, with a maximum rectified power of 18.05 µW at approximately 25º from the symmetry plane.

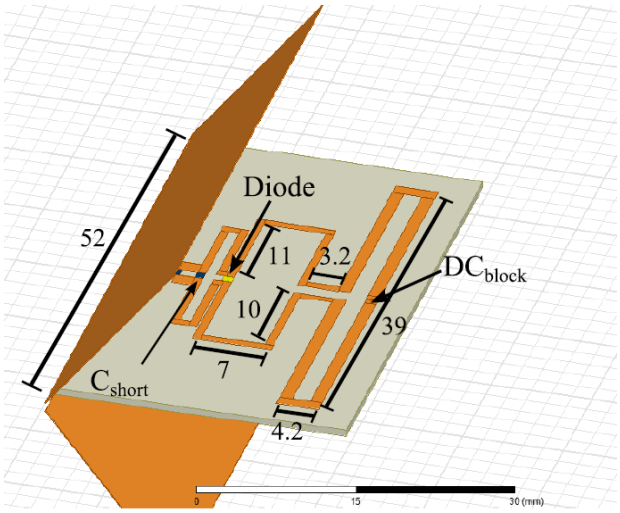

Figure 9: Layout of the proposed rectenna. [19]

D. RF Energy Harvesting from Ambient RF Sources

Wireless energy harvesting (WEH) from ambient electromagnetic fields is an emerging technology that can be exploited as a power source for many small electronic devices. A number of key challenges are identified but the optimum design of rectennas for ambient WEH is challenging. For example, in [13], ambient RF energy harvesting is tested on a novel six-band dual circular polarization (CP) rectenna. A public square is

chosen to evaluate the rectenna as an outdoor ambient environment. The square is not in the line of sight of any high-power RF sources such as DTV towers and mobile base stations. The received ambient signal levels as a function of frequency are shown in Figure 10. For cellular mobile bands, the signal level in outdoor measurement is between −35 to −25dBm. Due to the limits of the Wi-Fi router distribution, the received Wi-Fi signals are only available at low levels around −37 dBm at the indoor environment. This rectenna's overall measured conversion efficiency is up to 26% for the for a wide range of load between 10 and 75 kΩ.

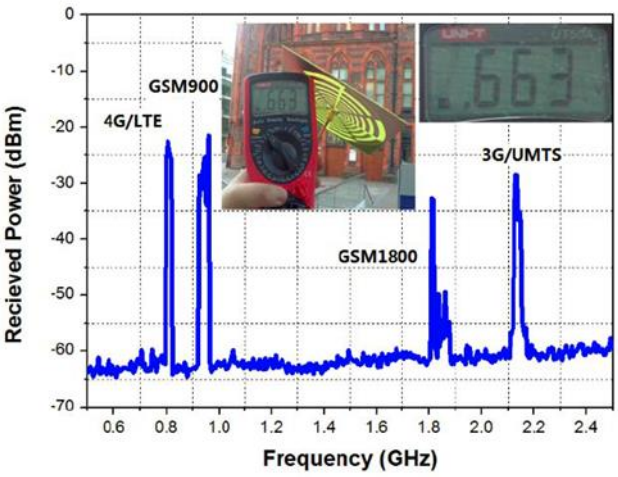

Figure 10: Measured received power versus frequency and measured output voltage of the proposed rectenna. [13]

Ambient energy harvesting at GSM bands (900 MHz and 1800 MHz) is discussed by many researchers. For example, a dual band rectenna is introduced in [21] for that purpose. The efficiency of the rectenna is 40.8% and 20% at 1834 MHz and 890 MHz, respectively with an incident power of – 20 dBm. This rectenna provides the possibility of harvesting the ambient electromagnetic energy for powering low power electronic devices as seen in Figure 11(a). The same dual band operation is discussed in [22]. The

RF energy harvesting system shown in Figure 11(b) is built and tested in the ambient environment. The trial test shows that an excess of 0.5V can be harvested from the environment without a source nearby.

(a) **(b)**

Figure 11: Rectenna experiment in ambient environment (a) [21], (b) [22]

In addition to the work presented above, a triple-band rectifier design is proposed in [23] for the ambient RF energy harvesting. The circuit operates at three frequency bands - GSM 1800, UMTS 2100 and LTE 2600, and is able to achieve high RF-to-DC conversion efficiency, reaching 35% at input power of -20 dBm. From the voltage reading of 0.381 V and load RL of 5.6kΩ (Figure 12), the equivalent harvested power is approximately 25μW. The same topic is addressed in [24] that proposes another technique for simultaneous wireless communication and power transfer. In order to obtain a sufficient energy, a broadband rectenna is adopted to harvest the ambient RF energy over six frequency bands at the same time. The objective is to maximize the energy efficiency at the output of the rectifying system.

Figure 12: Measurement of harvested DC voltage from ambient. [23]

It can be noticed that the work presented in the literature about ambient RF energy harvesting focuses more on available RF sources far from the one collected from commercial Wi-Fi routers. The reasons behind such interest is discussed in [25] and [26]. In [25], a new class of RF energy harvesters called “waveform aware harvesters” is suggested. These rectifiers are optimized for their performance with non-CW signals which will form significant advantages in ambient energy harvesting, where the available RF energy is in the form of communication waveforms of a variety of types. The work presented in [25] presents an initial proof-of-concept demonstration of a waveform aware harvester optimized for harvesting energy at 2.4 GHz from Wi-Fi (802.11b/g) signals with a realistic traffic model. It also provides an optimized recovery of harvested energy from single 802.11b/g transmission bursts on the order of 1 ms in duration.

In [26], the key challenges faced in harvesting from an actual Wi-Fi router highlighted. There is a fundamental mismatch between the requirements for power delivery and the Wi-Fi protocol. Figure 13 shows the voltage at the harvester in the presence of Wi-Fi transmissions. This figure clearly explains how the silent periods

present during Wi-Fi transmissions limit the ability of the harvester in meeting a minimum voltage.

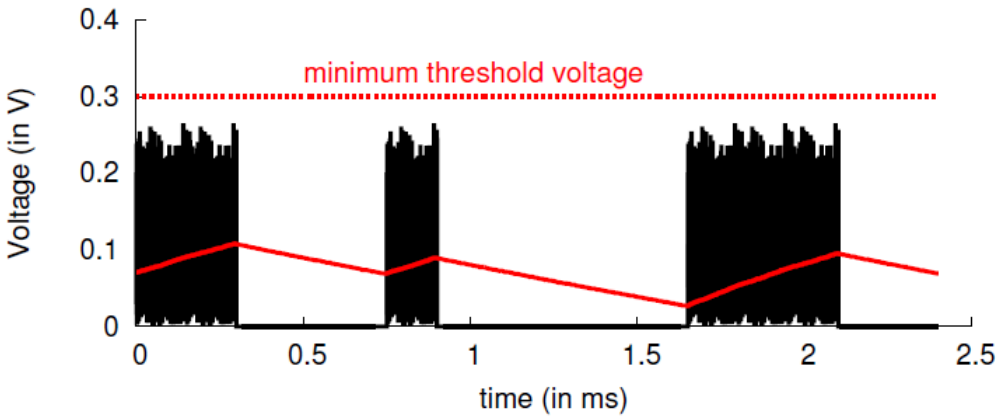

Figure 13: Key challenge with Wi-Fi power delivery. [26]

In [26], PoWi-Fi is introduced as a solution for harvesting from actual Wi-Fi signals. Existing Wi-Fi chipsets are implemented to cater for this purpose. At a high level, a router running PoWi-Fi imitates a continuous transmission while minimizing the impact on Wi-Fi performance. To accomplish this task, it injects small amounts of superfluous broadcast traffic on multiple Wi-Fi channels (e.g., channel 1, 6, and 11) such that the cumulative occupancy across the channels is high. A multi-channel harvester that efficiently harvests power across multiple Wi-Fi channels is also designed. This transmission mechanism at the router introduces additional power traffic on each Wi-Fi channel without interfering with other Wi-Fi networks.

E. Application of Machine Learning in Antennas and RF Circuits Design

"Machine learning (ML) is a branch of artificial intelligence that systematically applies algorithms to synthesize the underlying relationships among data and

information" [27]. Machine learning helps in developing programs that improve their performance for a given task through experience and training. The work in [27] discusses the theories, concepts, and applications of efficient learning machines. Machine learning algorithms can be introduced to the RF energy harvesting domain, since applying such techniques insures optimization of the efficiency and maintenance of reliability.

For example, in [28], two machine learning techniques, linear regression (LR) and decision trees (DT) are implemented to model the harvested energy using real-time power measurements in the radio spectrum. To ensure a reliable performance, energy prediction modelling is a key component for optimizing energy harvesting because it equips the harvesting node with adaptation to energy availability. Numerical results show that (LR) outperforms (DT) by attaining a minimum of 85% prediction accuracy. These models are useful for defining the scheduling policies of harvesting nodes. In [29], the learning algorithms are used to overcome the problems imposed by harvesting sufficient RF energy at low powers. Most of power management systems are not efficient at ultra-low power sources due to power consumption in control circuitry. The solution for this issue can be either power consumption reduction which is limited by physical constraints or harvesting from another energy source. This paper presents the use of particle swarm optimization technique where the converter efficiency is used as the fitness function while the circuit's inductor and the activation time (on-time) are chosen as optimized parameters. This leads to an optimized power management circuit that improves the efficiency of the dc-dc converter by 9.25% in comparison with conventional power management circuits over a wide range of input power. This allows the harvesting of more power from RF sources and hence a higher dc output voltage.

The matching network residing inside the rectifying circuit can also be optimized to improve the rectification process and reach higher efficiencies. For example, in [30], a genetic algorithm and a data mining method are used for this purpose. The proposed matching circuit can potentially have higher dc output power at 92.0% and 69.6 % of potential load combinations with a maximum matching performance improvement of 21.4 % and 37.6 % compared to conventional matching methods.

The matching network optimization is also targeted in the work presented in [31]. The maximization of the received power from compact multiple antenna systems in random RF fields is investigated using two novel impedance matching approaches. The first approach is based on optimal impedance matching where convex optimization is used to propose a sparse optimal impedance matching technique. The second approach is obtained by further relaxing the sparse optimal impedance matching method to obtain a suboptimal impedance matching (SOM) method referred to as multiport ladder matching (MLM). Simulation results show that the sparse optimal impedance matching approach provides the maximum received power while MLM captures more power than in conventional single-port matching (SPM). Additionally, they can maintain an acceptable bandwidth, which indicates the effectiveness of the sparse optimal and multiport ladder impedance matching approaches.

The integration of machine learning in the design of antennas and RF circuits has led to smart and efficient designs. Not only is it adding an advantage to the design of RF energy harvesters but also to the electromagnetics area in general. This contribution is presented in several approaches in literature such the use of neural networks and SVM in cognitive radio applications [32], smart antennas and antenna arrays structure [33] - [35].

F. Summary

This chapter introduces different rectifiers' designs presented in the literature where several rectifying elements and techniques are implemented. The surveyed designs are grouped into four sections. Section B discusses the limitations accompanied with the use of Schottky diodes in a rectifier along with a study on the maximum attained efficiency at low input power levels. The implementation of CMOS based rectifiers is also discussed where good sensitivity can be obtained especially at low power levels. However, the focus of the work presented is based on expanding the capabilities of Schottky diode based RF rectifiers. Section C discusses the implementation of several techniques in an RF energy harvester such as flexible materials, 3D inkjet printing, multiband operation and multiport systems. In section D, several papers are presented to describe the harvesting from ambient RF sources such as GSM, 3G, LTE bands. Also, challenges accompanied with harvesting from ambient wireless routers are listed and a PoWiFi router is proposed to overcome some of these challenges. Section E is concerned about the role of machine learning in the optimization of RF energy harvesting systems and many other applications such as cognitive radio and smart antenna designs.

CHAPTER III

A LOAD INDEPENDENT TAPERED RF HARVESTER

A. Introduction

Generally speaking, an RF energy harvesting system relies on an efficient and well-designed rectenna, which is a combination of an antenna and an RF rectifying circuit. A crucial parameter is the RF-to-dc power conversion efficiency (PCE). It defines the status of the rectifier and determines how efficiently a rectenna system transforms RF energy into dc power. The power conversion efficiency (PCE) is given by Eq. 1 as follows.

$$PCE = \frac{P_L}{P_{RF}} * 100\% = \frac{V^2_L}{R_L * P_{RF}} * 100\% \quad (1)$$

where P_L represents the dc power collected at the output, P_{RF} is the RF power captured by the antenna, V_L denotes the dc voltage at the output, and R_L denotes the load impedance.

In this chapter, a tapered dual line matching network is proposed to be integrated in a rectifier circuit. This matching network insures that the PCE remains stable over a large range of load impedances, while optimizing its performance at input powers that are below or equal to 0dBm.

B. Rectifier's Circuit Topology

The topology of the rectifier circuit discussed in this section is based solely on a Schottky diode. The proposed rectifier that is described in the circuit diagram of Figure

14 is composed of a dual transmission line matching network topology, a tuning stub, a shunt Schottky diode configuration and an RF choke. The first transmission line is characterized by an impedance (Z_{0L}), phase shift constant (β_L), length (L_L) and width (WL). This line constitutes the "load transmission line (TL)". The function of this line is to transform the diode impedance (Z_{out}) into (Z_I). The second transmission line in series is the "feed TL" that is characterized by an impedance (Z_{0F}), phase shift constant (β_F), length (L_F) and width (W_F). A capacitor (C) of 1 µF is integrated between the two transmission lines in order to block the dc voltage generated by the diode from reaching the generator. By tuning the lengths and characteristic impedances of both transmission lines, (Z_{in}) of the entire network is optimized to be 50 **Ω**. The substrate used in this work is Rogers 3203 with a thickness of 0.508 mm and a dielectric constant of 3.02. By assuming negligible conductor and dielectric losses, the impedances (Z_I) and (Z_{in}) can be calculated as displayed in Eq. (2) and Eq. (3):

$$Z_I = Z_{0L}\frac{Z_L + jZ_{0L}\tan\beta_L L_L}{Z_{0L} + jZ_L\tan\beta_L L_L} \tag{2}$$

$$Z_{in} = Z_{0F}\frac{Z_I + jZ_{0F}\tan\beta_F L_F}{Z_{0F} + jZ_I\tan\beta_F L_F} \tag{3}$$

The lengths of both transmission lines are iteratively swept and optimized over a full spatial period (0 to $0.5*\lambda_g$). Several characteristic impedance values are investigated as shown in the return loss results of Figure 15 (a-d). The amount of power loss in each design can be evaluated based on the return loss results presented in Figure 15. Choosing the design with the best return loss leads to the minimization of losses, which constitutes a major contribution in this design.

The maximum value chosen for either (Z_{0L}) or (Z_{0F}) is 100 Ω to take into consideration practical fabrication tolerances whereas the minimum impedance value is 20 Ω to keep the overall design as compact as possible with minimum amount of losses. In the first scenario, shown in Figure 15(a), (Z_{0L}) and (Z_{0F}) are chosen to be equal to each other and equal to 20 Ω (lower than 50 Ω). In the second scenario of Figure 15(b), the two quantities are still considered equal to each other at 100 Ω (higher than 50 Ω). In the third scenario, given in Figure 15(c), (Z_{0L}) is chosen to be 20 Ω while (Z_{0F}) is 100 Ω. Finally, for the fourth scenario in Figure 15(d), (Z_{0L}) is chosen to be at 100 Ω higher than (Z_{0F}), which is chosen to be equal to 20 Ω.

It is noticed that the return loss of the network is optimal when the "load" TL has a higher impedance than that of the "feed" TL. This corresponds to the fourth scenario that is shown in Figure 15(d). For this case, the highest return loss is achieved for a "load" TL length of 21 mm or 14.8 mm and a feed TL length of 7.4 mm or 32.4 mm. These two lengths are displayed by the two peaks of the return loss curve in Figure 15(d). In order to preserve the compactness of the design, the first set of values (Feed TL=7.4 mm, Load TL= 21 mm) is chosen for the design of the matching network.

In this design, the SMS-7630 diode from Skyworks [36] is chosen. It has a low built-in potential of about 170 mV with an approximate forward current of 1 mA, internal resistance R_s = 20 Ω and a junction capacitance C_{j0} = 0.14pF. The proposed network, shown in Figure 14, aims at matching the load composed of the SMS7630 zero-bias diode to the 50 Ω source.

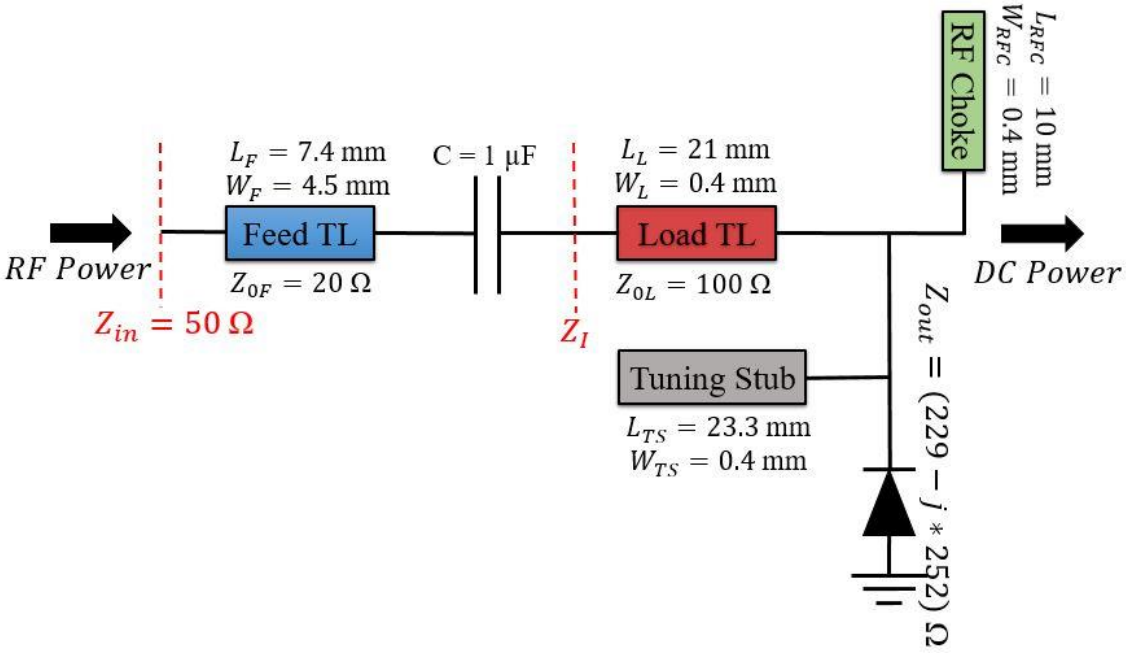

Figure 14: The proposed impedance transformer network.

The Schottky diode's impedance (Z_{out}) varies with both frequency and input power. For this rectifier design, (Z_{out}) is taken equal to (229-j*252) Ω for an input power level of -10dBm at 2.45 GHz and it is matched to the source's 50 Ω impedance. The rectifier is designed and simulated with the Agilent Advanced Design System (ADS) software [37], using large signal S-parameters (LSSP) and harmonic balance (HB) simulations. Non-linear models are utilized for the diodes and the passive components are simulated with models that include parasitic effects.

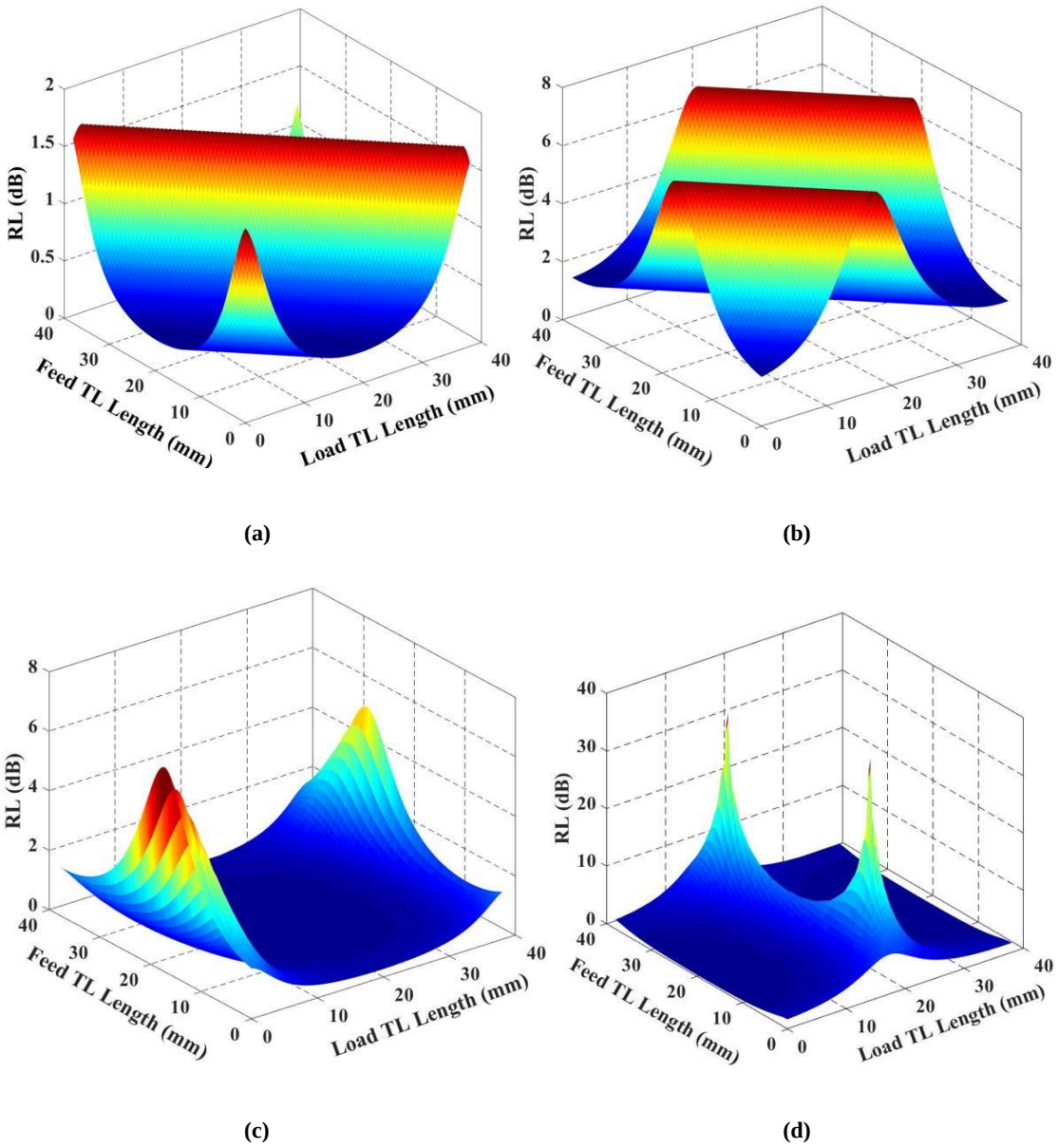

Figure 15: Return Loss Results for different scenarios of the lines characteristic impedances: (a) Z_{0L} and Z_{0F} equal to 20 Ω, (b) Z_{0L} and Z_{0F} equal to 100 Ω, (c) Z_{0L} equal to 20 Ω and Z_{0F} equal to 100 Ω, (d) Z_{0L} equal to 100 Ω and Z_{0F} equal to 20 Ω.

C. Design and Performance Results

The layout of the proposed rectifier is shown in Figure 16(a). Impedance transformation is achieved through the feed and load TLs as discussed in section B. Tapering techniques are implemented in order to achieve a smooth transition from the

20 Ω characteristic impedance of the “feed line” to its 100 Ω counterpart of the “load line”.

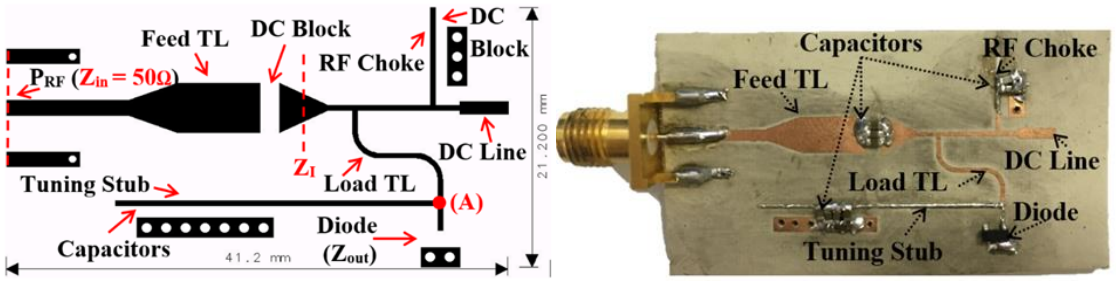

(a) **(b)**

Figure 16: Rectifier Design (a) Layout, (b) Fabricated prototype.

In reality, the tapered behavior of the impedance can be explained from equations (4) and (5) [1], where the impedance of a tapered line is studied in function of the position.

$$Z(z) = \begin{cases} Z_0 e^{2(z/L)^2 \ln Z_L/Z_0}, & for\ 0 \le z \le L/2 \\ Z_0 e^{(4z/L - 2z^2/L^2 - 1)\ln Z_L/Z_0}, & for\ L/2 \le z \le L \end{cases} \quad (4)$$

$$\frac{d(lnZ/Z_0)}{dz} = \begin{cases} 4z/L^2 \ln Z_L/Z_0, & for\ 0 \le z \le L/2 \\ (4/L - 4z/L^2)\ln Z_l/Z_0, & for\ L/2 \le z \le L \end{cases} \quad (5)$$

where Z_0 denotes the impedance at position zero, Z_L the impedance to be achieved and $Z_{(z)}$ its variation with respect to the distance.

The matching network designed for this rectifier circuit consists of two primary transmission lines with different characteristic impedances. First of all, the RF power is fed to the rectifier through a Z_1 = 50 Ω transmission line as seen in Figure 17. A triangular tapered connection “T1” is used for transition from the feeding line to TL_1 of Z_2 = 20 Ω. The study in this work shows that a line of characteristic impedance 100 Ω TL_2 should follow TL_1. Therefore, another transition “T2” is required to avoid the abrupt transition from low to high characteristic line impedance. For the same input RF

power, a stable PCE response is translated through collecting similar output DC power over a wide frequency range. This output remains stable when the percentage of RF power this diode is receiving almost frequency independent. This independence is provided through the tapering junctions “T1” and “T2” that widen the matching network operational range.

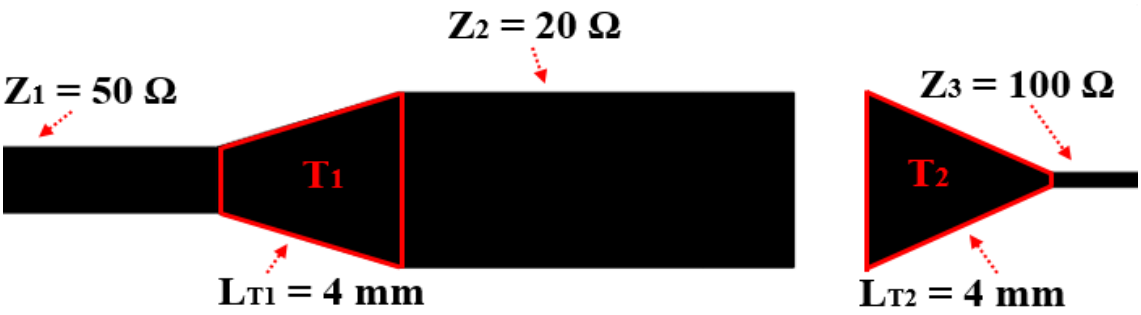

Figure 17: The transition between TLs using triangular tapering technique.

From [1], one can verify using Eq. 5 below and Figure 18 that the variation of the impedance at various locations of the tapered lines does not always depend on the load impedance as shown in Figure 18 that is taken from [1]. In fact, when the impedance is calculated at the input of the line up to a distance L/2 the variation of the impedance in function of the load is minimal.

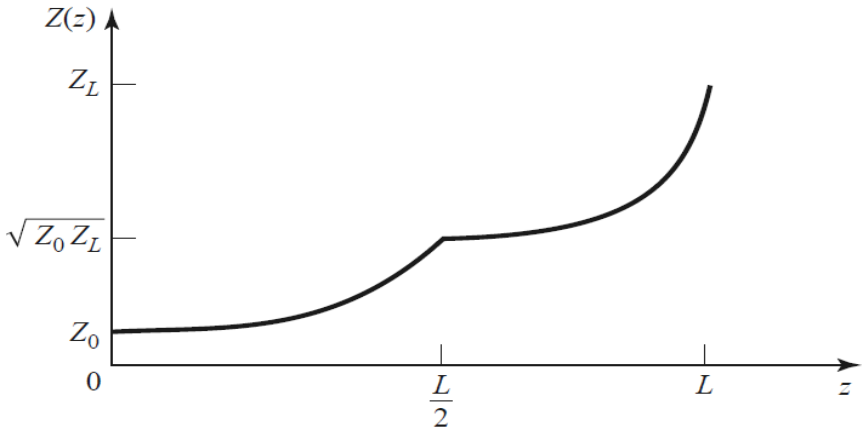

Figure 18: Impedance variation of a matching section with a triangular taper for d (ln Z/Z0)/dz [1]

The design is built using Rogers 3203 with thickness 0.508 mm as shown in Figure 16(b) with dimensions equal to 41.2 mm x 21 mm. The “RF Choke” functionality is achieved using a shorted quarter-wavelength (λ/4) stub. The shorting of the λ/4 stub is achieved through 1 μF capacitors. The λ/4 stub behaves as an open-circuit impedance at the fundamental and third harmonic frequencies. It also presents the second harmonic with a short circuit impedance. To that effect, it suppresses the leakage of RF power towards the dc line. The “dc line” of length 6 mm and width 1 mm is incorporated as a microstrip section that is used to extract the output dc voltage. To account for fabrication errors and diode parasitic effects, a “tuning stub” that has a length of 23.3 mm and a width of 0.4 mm is included in the circuit. The reflection coefficient of the proposed rectifier shows a magnitude of -23 dB at 2.45 GHz while the transmission coefficient measured between the input and point (A) shown in Figure 16(a) has a magnitude of -0.2dB. This confirms that the RF power is fully transmitted to the input of the Schottky diode (RF output).

As a first experiment, the fabricated rectifier shown in Figure 16(b) is fed via an RF signal generator and the corresponding PCE results are obtained for a wide range of

input power. The measured and simulated power conversion efficiency (PCE) and dc output voltage results are shown in Figure 19. This rectifier's efficiency rises to above 57% around 0dBm. The circuit achieves a peak voltage of 1.2 V for an input power level of 0dBm with a load RL = 2470 Ω.

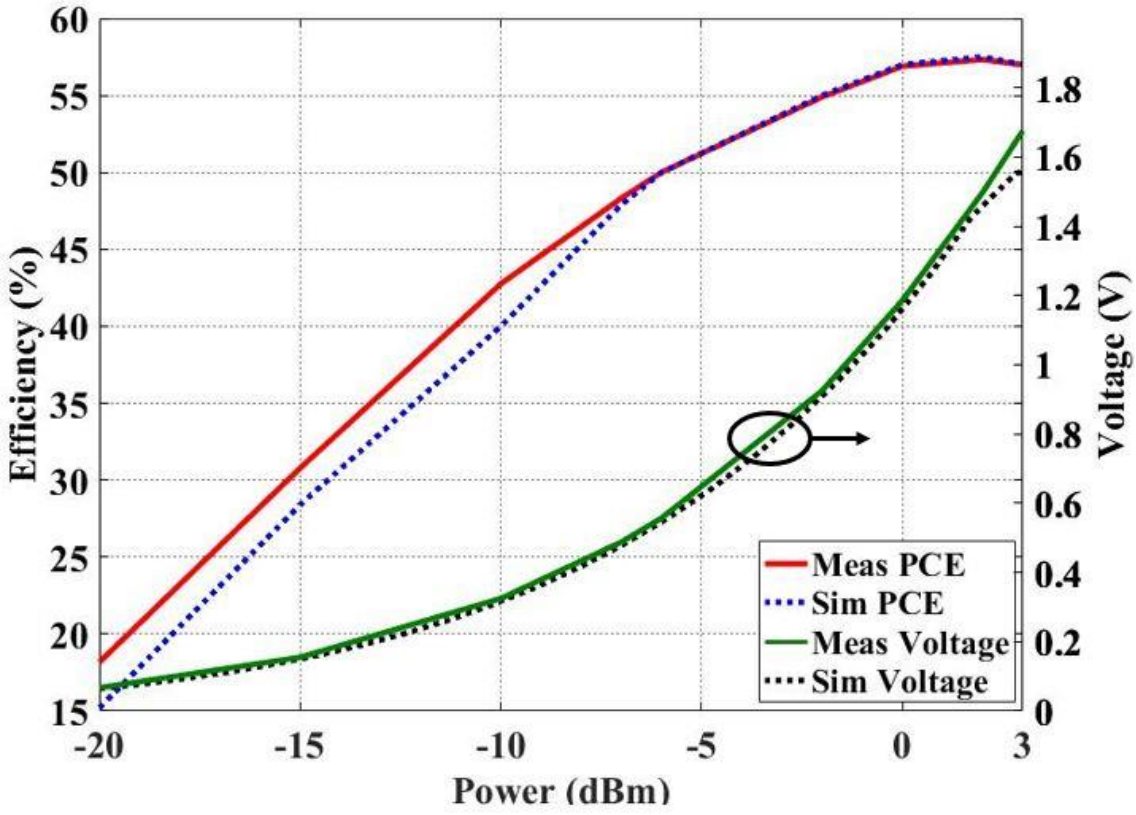

Figure 19: PCE and output voltage results for the proposed rectifier for RL = 2470 Ω.

For validation purposes, this rectifier is connected to a slot antenna and placed facing another slot antenna for a second experiment of output voltage measurement. The slot antenna is composed of three layers. The top layer has a conductive sheet out of which a rectangular slot is etched as shown in Figure 20(a). The second layer is a 109 mm x 82 mm, 1.6 mm-thick, FR4 epoxy substrate, whose dielectric constant is 4.4. The third layer, shown in Figure 20(b), is a microstrip line of length 59.35 mm which is

equivalent to 7*λg/8 and a width of 3.1 mm which corresponds to a characteristic impedance of 50 Ω. The designed antenna is simulated using a high frequency EM simulator. It covers the channels of the Wi-Fi 802.11 b/g bands at 2.45 GHz. Figure 21 shows a comparison between the measured and simulated reflection coefficients of the slot antenna, where a good agreement is clearly noticed. The gain pattern of the fabricated antenna is bidirectional and exhibits both front and back lobes as presented in Figure 22 (a). Accordingly, a 118 mm x 88 mm copper sheet is positioned at a distance of 17 mm, which stands for λg/4, as illustrated in Figure 22 (b). As a result, better gain values are achieved due to the directive radiation pattern that is associated with the ground plane incorporation from behind the bottom layer of the antenna structure. A difference of approximately 3 dB is noticed in the gain plots that are shown in Figure 22(a). Also, a reduction in the back-lobe radiation from 3.5 dB to -4.1 dB is realized. The antenna operation at 2.45 GHz is maintained even in the presence of the ground plane as shown in Figure 21.

(a) (b)

Figure 20: Slot antenna prototype: (a) Top view, (b) Bottom view.

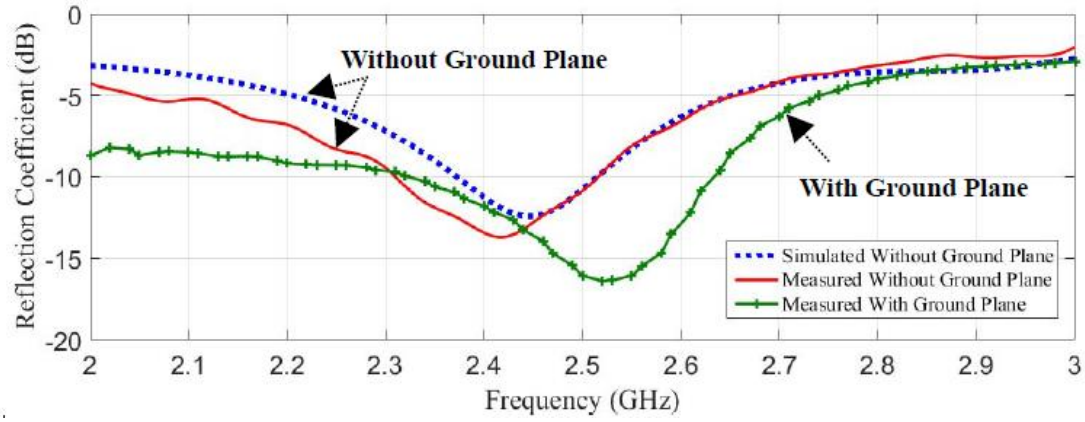

Figure 21: Reflection coefficient of the slot antenna.

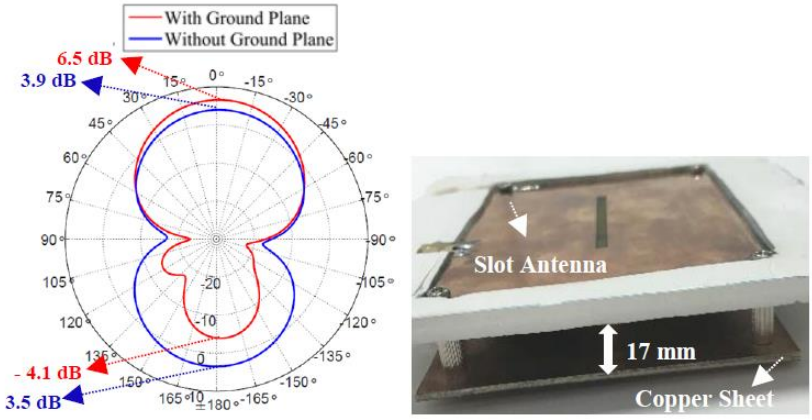

(a) **(b)**

Figure 22: (a) Gain plots for the slot antenna with and without ground plane (at f = 2.45 GHz and φ = 0˚, θ), (b) Slot antenna with a λg/4 distant copper sheet from beneath.

In this experiment, the rectifier connected to the slot antenna, is placed at a distance 50 cm (far field zone) away from a transmitting slot antenna as shown in Figure 23. The distance of separation between the transmitter and receiver antennas ensures that the rectenna system receives a -10dBm power. The expected voltage has matched the reading on the multi-meter and results achieved in this experiment verify the PCE results obtained from the first experiment.

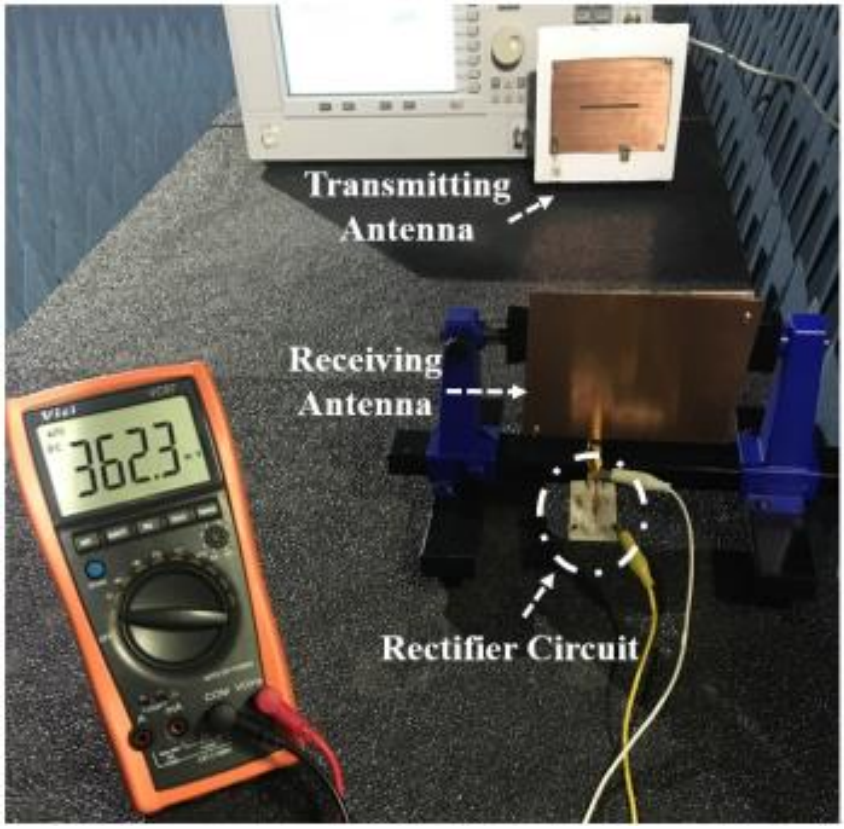

Figure 23: Experiment with the transmitting-receiving system.

A variation in the load is also investigated and efficiency results are measured for three different input power levels of -15dBm, -10dBm and -5dBm. As shown in Figure 24, this circuit preserves an efficiency higher than 50% at -5dBm over most of the considered load variation range. It also presents an efficiency stability that is above 40% and 30% for -10dBm and -15dBm input power levels, respectively. Therefore, this circuit presents a stable response with respect to load variation and makes it suitable for applications requiring abrupt changes in load values.

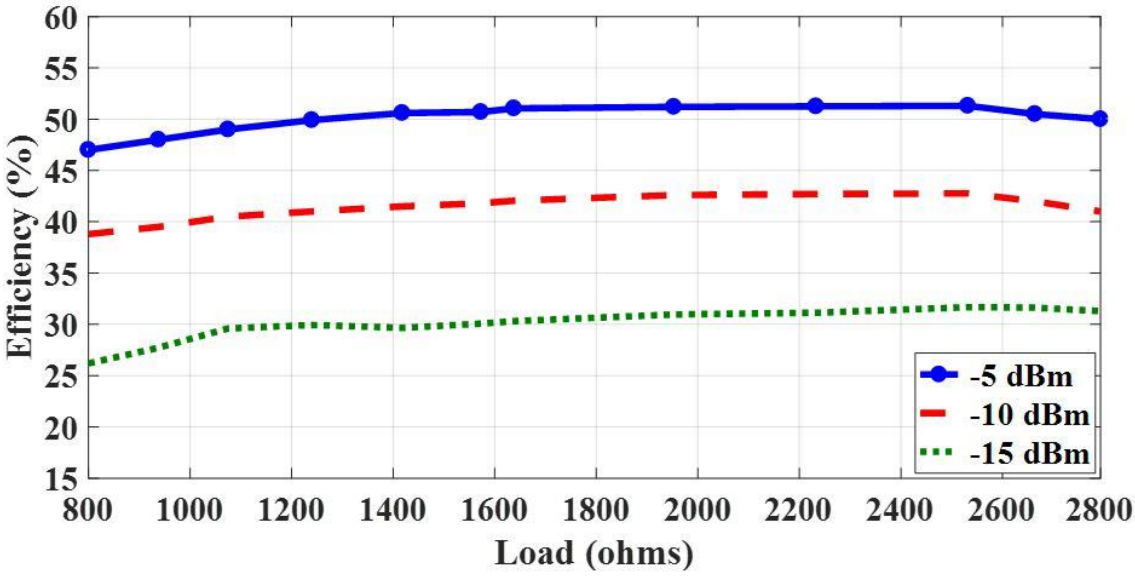

Figure 24: Measured flat efficiency results for the proposed rectifier for Pin = -5 dBm, -10 dBm and -15 dBm with a wide range of load values.

In order to understand the PCE flat response obtained over a wide range of load variation, the variation in the input impedance of the network is illustrated.

For the same input RF power, a stable PCE response is translated through collecting similar output DC power for different load values. This means that the Schottky diode's rectification rate is approximately stable. The rate remains stable when the percentage of RF power this diode is receiving is not strictly dependent on the load variation. This independence is provided through the tapering "T1" and "T2" shown in Figure 17, which are widening the matching ability of the network's operational range.

In order to validate this statement, the input impedance is plotted versus the load ranging between 800 Ω and 2800 Ω for three different power levels as shown below in Figs. 25(a) and (b). It can be noticed from these plots that for each case of input power, the input impedance is slightly affected by the load of the circuit. For example, taking the third case where the system is fed with a power of -15dBm, we can see that sweeping the load between 800 Ω and 2800 Ω forces the real part to decrease from

27.48 Ω to 19.37 Ω (8.11 Ω variation only) and the imaginary part from –j13 Ω to –j25 Ω (-j12Ω variation only). The same applies for the other input powers where the decrease is limited within a certain range. With a very good matching, the RF power fed at the input is able to reach the diode even with the changes in the load, therefore allowing the diode to rectify a similar percentage of the power received each time and thus producing a dc power at the same rate. This mechanism is reflected in the PCE flatness within the corresponding load range.

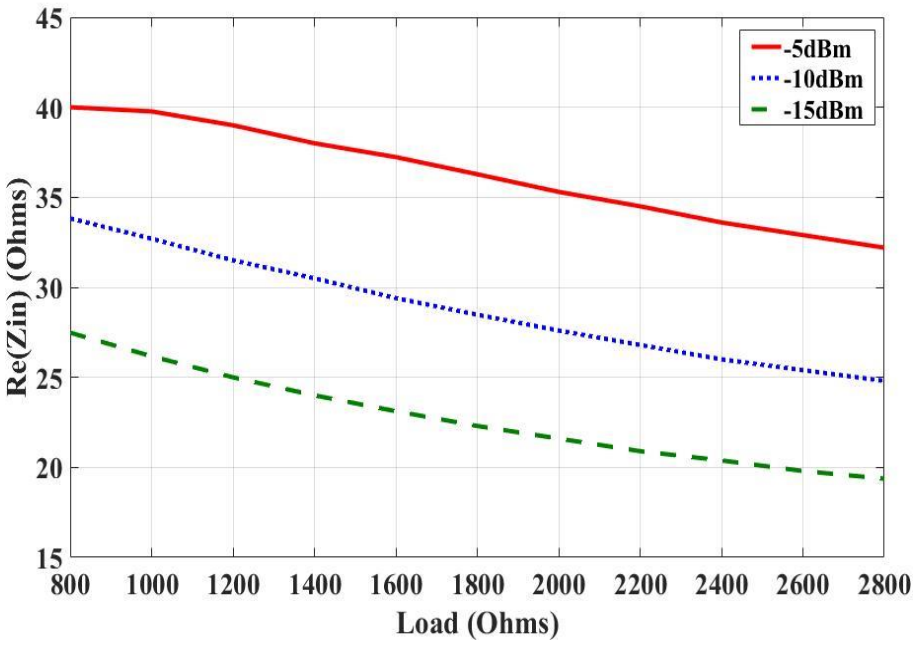

(a)

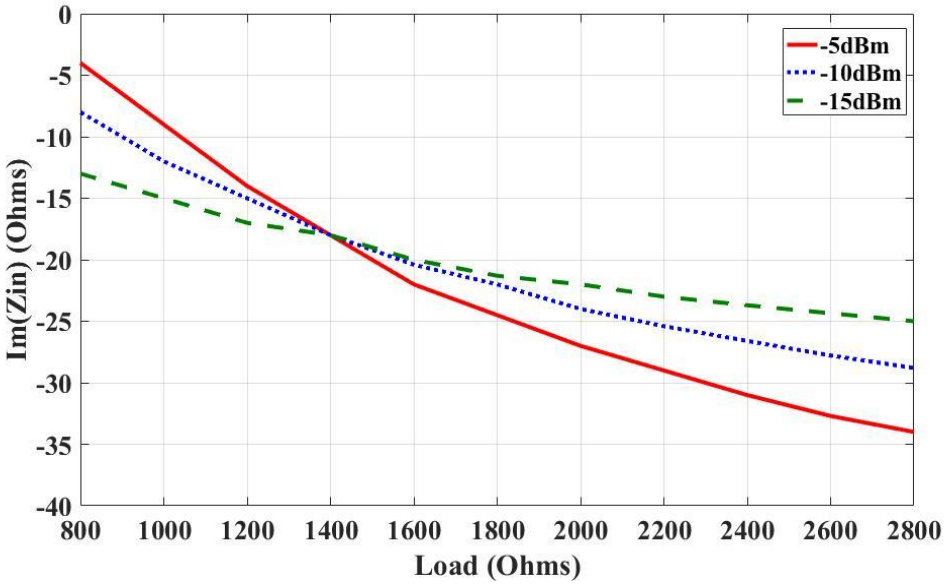

(b)

Figure 25: Variation of the input impedance with respect to the load: (a) Real part, (b) Imaginary part.

D. Summary

In this chapter, an efficient RF energy harvesting rectifier operating over the Wi-Fi 802.11 b/g band is presented and tested. This rectifier is based on a new matching technique that is based on a network of dual line topology with different characteristic impedances. The purpose of this network is to match the Schottky diode's input impedance in a rectifying circuit to the 50 Ω source impedance. The integrated matching network topology helps achieve good and stable efficiency results over a range of load variation. The system is tested as a receiving unit with a slot antenna and as standalone. In both experiments, a great agreement is realized with the simulated results.

CHAPTER IV

A COMPACT RF ENERGY HARVESTER WITH AN IMPROVED MATCHING NETWORK

A. Introduction

The novelty of the work presented in this chapter is based on pushing the limits of Schottky diode's rectification abilities, while investigating optimal matching networks. An initial introduction of this work is found in [38], [39] and [40]. The first novelty aspect is based on proposing a novel matching network that relies on a tapered topology in order to provide a stable, almost flat efficiency response across a variation of load and frequency of operation. The second novelty aspect relies on implementing meandering techniques for size reduction in order to result in a compact circuit design. Various matching network topologies are compared together to end up with the best candidate that exhibits a compact size, which is almost $\lambda g/2 \times \lambda g/4$ (40 mm x 20 mm at f = 2.45 GHz). The resulting circuit displays a 58% efficiency for an input power of 0 dBm. The circuit also maintains an efficiency above 50% for a large range of load variations and a wide frequency bandwidth.

B. RF Energy Harvesting System Overview

The work presented in this paper is focused on harvesting RF energy in the frequency band that extends from 2.412 GHz to 2.484 GHz. This work relies solely on Schottky diodes, and in particular, the SMS7630 zero-bias, from Skyworks [36]. In

particular, the rectifier system proposed herein relies on a shunt connected Schottky diode as shown in Figure 26.

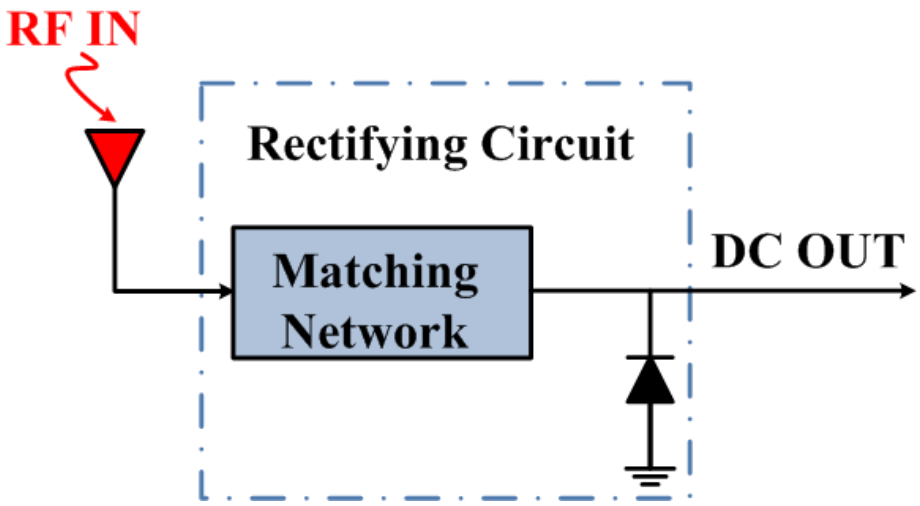

Figure 26: Block diagram of the proposed RF energy harvesting system.

The full rectifying system is composed of a receiving antenna and a matching network followed by a single Schottky diode. The focus is to improve the matching conditions between the antenna and the rectifying element in order to minimize the losses across the full designed network.

More specifically, at low power levels (< 0dBm), the PCE requires the convenient choice of the non-linear diode element as well as the suppression of the generated harmonics and the incorporation of a well-designed matching network for an optimized dc load. The goal of the work presented in this paper is to end up with a compact design having good efficiency results with respect to a varying input power. The harvesting system must maintain an almost flat efficiency curve over the Wi-Fi frequency band along with a robust efficiency response for a wide range of load variations. The end goal

is to integrate the optimal circuit in a multiport system that extends the harvesting capability of a single circuit element.

C. Rectifier Designs with a Stub Based Meandered Matching Network

In this section, the size reduction of the harvesting circuit is achieved using meandering of the stub based matching network. Various meandered stub matching networks are analyzed. The networks are employed to match the load impedance to the 50 Ω source. In this work, the load is the SMS7630 zero-bias diode whose impedance (Z_{out}) varies with both frequency and input power. More specifically (Z_{out}) is taken to be (229-j*252) Ω at 2.45 GHz and for an input power level of -10 dBm.

1. Shorted Shunt Stub Matching Network

Matching the Schottky diode with an impedance (Z_{out}) = 229-j*252 Ω to the 50 Ω source, which represents the antenna, can be achieved by resorting to two lines with 50 Ω characteristic impedance as seen in Figure 27(a). One line defines the length of the short-circuited stub L_{SC_stub} and the other one determines its distance away from the load d_{SC_stub}. The rectifier is designed and simulated with the Agilent Advanced Design System (ADS) software, using large signal S-parameters (LSSP) and harmonic balance (HB) simulations.

The impedance transformation is achieved by having the short-circuited stub to be 0.438λg (35 mm) long and 0.19λg (15 mm) away from the load. For compactness, a meandering technique is applied on both the shunt and series lines. The meandering technique results in a reduction of 70% in the rectifier's size in comparison to a non-meandered stub. The two lines are curved in a way to achieve the required size

reduction while minimizing the coupling between the turns to around -30 dB. The corresponding circuit layout is shown in Figure 27(b) with an overall dimension of 30.5 mm x 17.6 mm. A 1 µF capacitor is placed before the diode as shown in Fig. 27(b) to block any dc leakage to the RF source. The diode is placed in a reverse shunt configuration followed by a 110 nH inductor operating as an RF choke. The substrate used in this work for all designs is Rogers 3203 with a thickness of 0.508 mm and a dielectric constant of 3.02. The fabricated prototype is presented in Figure 27(c).

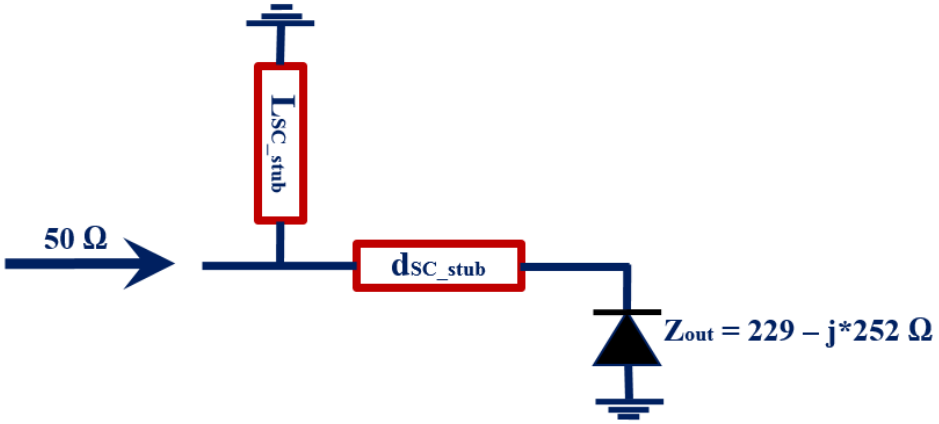

(a)

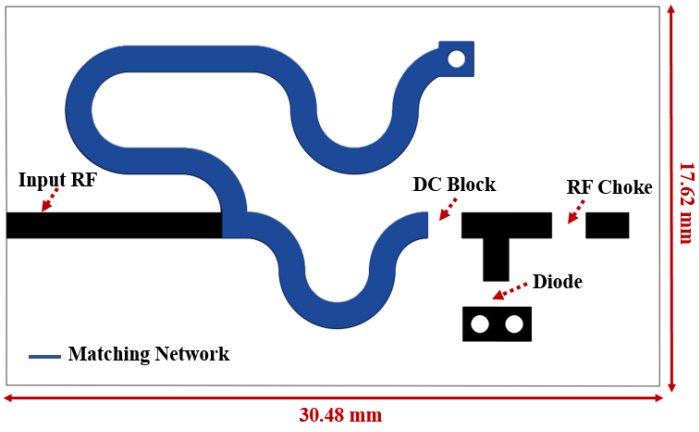

(b)

(c)

Figure 27: Rectifier design with short-circuited stub (a) Schematic, (b) Layout, (c) Fabricated prototype.

The simulated and measured dc output voltage and power conversion efficiency are presented in Figure 28. This rectifier operates within the targeted band, in particular at 2.41 GHz. The voltage results are extracted at the operating frequency along with the choice of an optimal load. For this circuit, the voltage and PCE plots are taken for RL (optimal) = 660Ω. An agreement between the simulated and measured results is attained. A peak voltage of 0.562 V is obtained at 0 dBm input power leading to an efficiency of 47.85 %. The efficiency maintains an increasing state until it reaches a peak efficiency of 50.5% at 3 dBm as displayed in Figure 28.

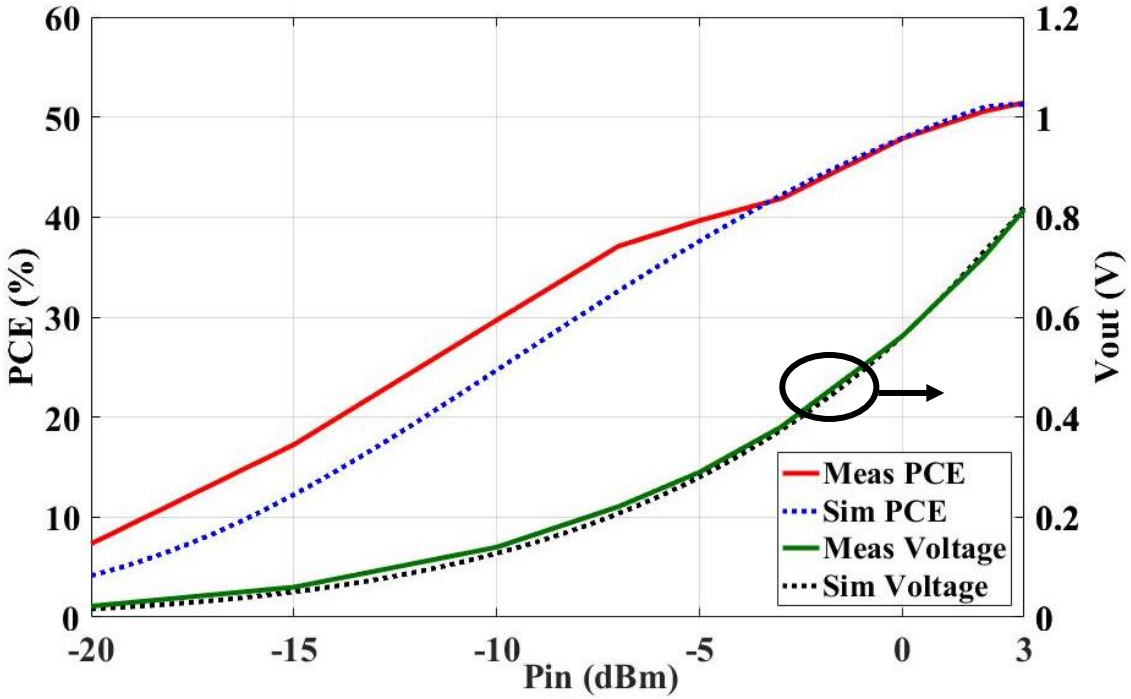

Figure 28: Efficiency and output voltage results for the rectifier design with single short-circuited stub matching network.

2. Shorted Shunt Stub Matching Network

In order to compare the effect of the matching technique on the rectifier performance, a different stub termination is applied to the same matching topology as shown in Figure 29(a). A stub with an open circuit end with length $L_{OC\_stub} = 0.198\lambda g$ (15.8mm) and a distance $d_{OC\_stub} = 0.16\lambda g$ (12.8mm) away from the load is adopted. The same meandering technique is applied to the two lines to keep the resulting rectifier compact in size. The corresponding rectifier layout along with the fabricated prototype are shown in Figure 29(b) and Figure 29(c). The rectifier's dimensions are 30.22 mm x 15.13 mm thus achieving a 51% reduction in size in comparison to a non-meandered stub. Similar to the previous design, a 1 μF dc-blocking capacitor and a 110 nH RF choke are integrated within the matching network.

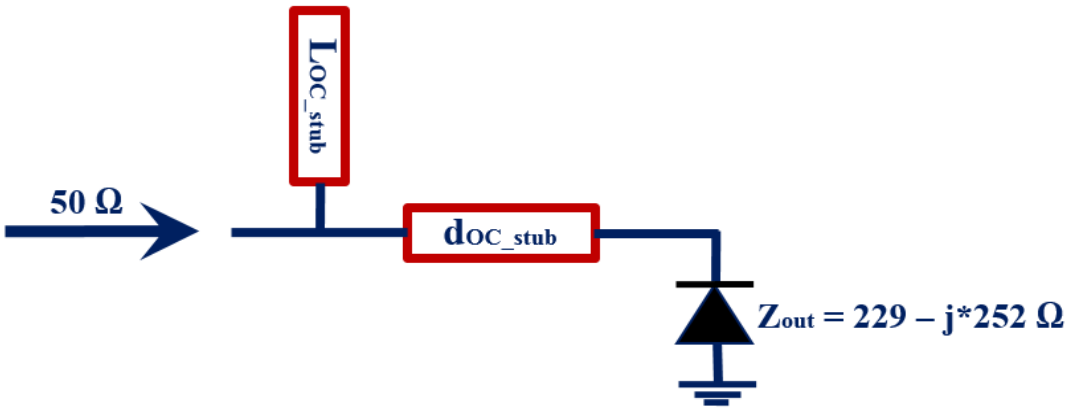

(a)

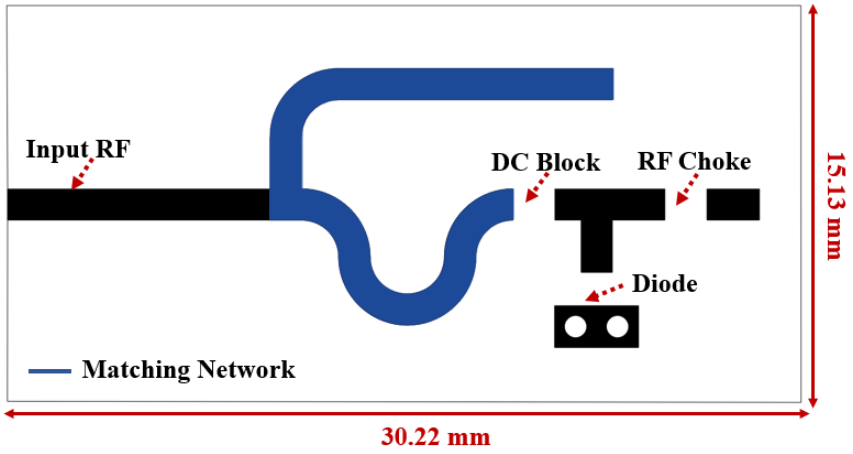

(b)

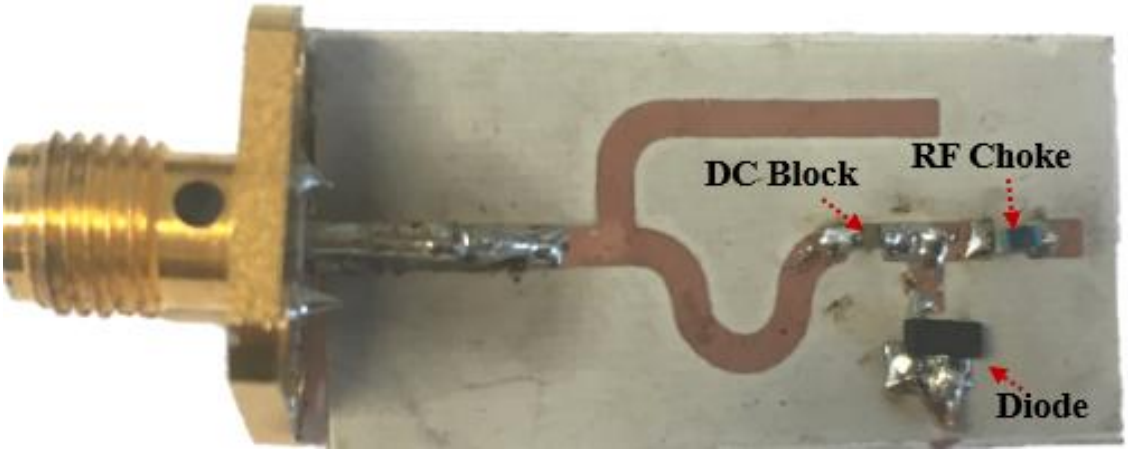

(c)

Figure 29: Rectifier design with open-circuited stub (a) Schematic, (b) Layout, (c) Fabricated prototype.

The simulated and measured voltage and PCE for the open circuit configuration are given in Figure 30. This rectifier is matched over the entire desired band and exhibits a good efficiency of 51.26% at 0 dBm with a peak measured voltage of 0.716 V and an optimal load of 1 kΩ.

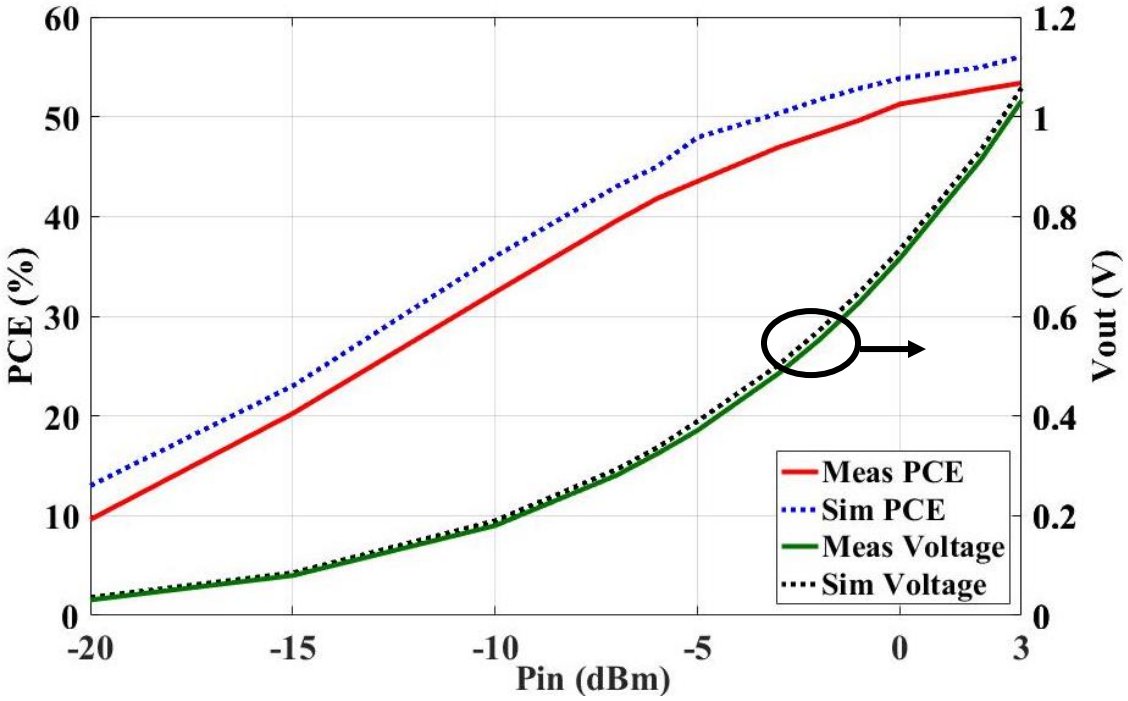

Figure 30: Efficiency and output voltage results for the rectifier design with single open-circuited stub matching network.

3. Performance comparison between the open- and short-circuited stub matching techniques

Upon comparing the performance of both rectifier designs, it's obvious that the open-end shunt stub presents a slightly more superior performance. First of all, the open-ended stub is shorter in length (0.198λg) as opposed to (0.438λg) for the short-ended stub. Also, the open stub results in a more efficient rectifier at the desired frequency band. However, both techniques do not meet the design requirements in

achieving a PCE greater than 55% for an input power of 0 dBm. In addition, these networks do not exhibit a stable, robust and almost flat PCE curves across various loads and different operating frequencies. Table 1 summarizes the comparison of results between both circuits.

Table 1: Comparison between short and open shunt stub MN

Design Parameter	Short Stub MN	Open Stub MN
VIA	**YES**	**NO**
L_{stub}	**$0.438\lambda_g$**	**$0.198\lambda_g$**
d_{stub}	**$0.19\lambda_g$**	**$0.16\lambda_g$**
Size (mm^2)	**30.48 x 17.62**	**30.22 x 15.13**
PCE (%)	**47.85**	**51.26**

D. Rectifier Designs with a Stub Based Meandered Matching Network

In this section, a new matching network topology that aims at matching the SMS7630 zero-bias diode to the 50 Ω source is proposed. In this design, the SMS-7630 diode is used with internal resistance R_s = 20 **Ω** and a junction capacitance C_{j0} = 0.36pF.

1. Proposed dual lines matching technique

The topology of the proposed matching network is shown in Figure 31. The transmission line, characterized by an impedance *(Z_{0L})*, a length *(L_L)* and a width *(W_L)*, constitutes the "load transmission line *(TL)*". The purpose of this line is to transform the diode impedance *(Z_{out})* into *(Z_l)*. The second transmission line in series is the "feed TL"

that is characterized by an impedance *(Z_{0F})*, a length *(L_F)* and a width *(W_F)*. By tuning the lengths and characteristic impedances of both transmission lines' sections, the input impedance *(Z_{in}')* of the entire network is optimized to be 50 Ω. By assuming negligible conductor and dielectric losses, the impedances *(Z_I)* and *(Z_{in}')* can be calculated as displayed in (2) and (3).

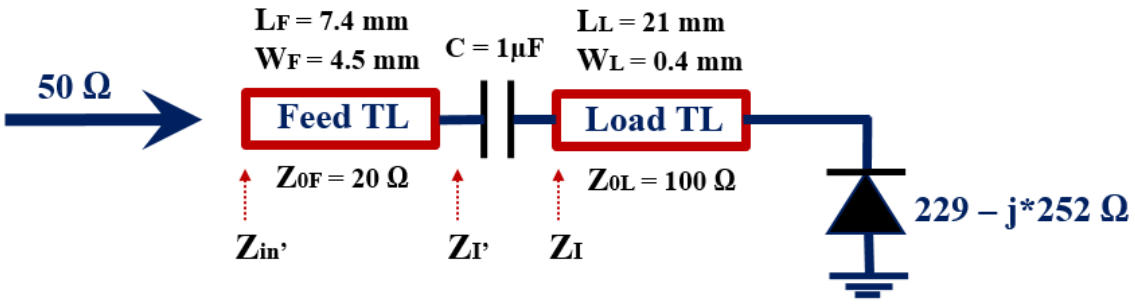

Figure 31: Rectifier design along with the proposed impedance transformer network.

The lengths of both transmission lines are iteratively swept and optimized over a full spatial period (0 to 0.5*λg). The change in the impedance at various points along the proposed matching network is demonstrated in Figure 32.

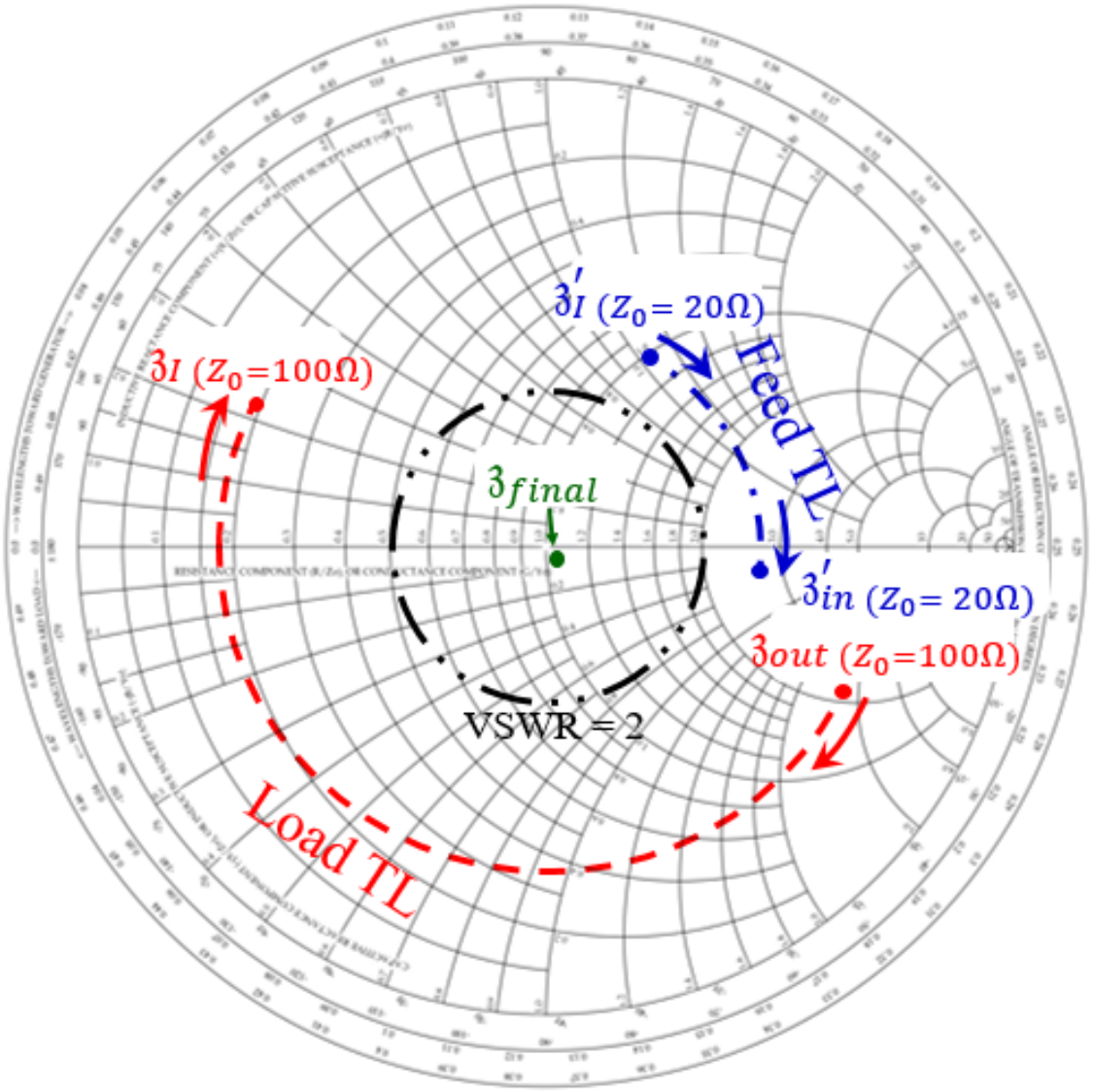

Figure 32: Smith chart representation of the proposed impedance transformer matching network.

The diode is located on the line with 100 Ω characteristic impedance. Therefore, its impedance is first normalized to 100 Ω and placed on the smith chart as ($\mathcal{Z}_{out}$). The $\lambda_g/4$ load transmission line transposes the diode impedance from ($\mathcal{Z}_{out}$) to ($\mathcal{Z}_I$) as shown in Figure 32. At this stage, the impedance faces the "feed TL" that has a characteristic impedance of 20 Ω. The transformation from 100 Ω to 20 Ω is done by first de-normalizing ($\mathcal{Z}_I$) to 100 Ω and then normalizing it back to 20 Ω. This corresponds to the point ($\mathcal{Z}_I'$) on the smith chart of Figure 32. This point is then moved by a distance of

$0.0986\lambda_g$ to reach the point $(\mathcal{Z}_{in}')$. Such distance is equivalent to the length of the "feed TL". De-normalizing this point to 20 Ω leads to the input impedance of the circuit being equal to (52 – j4) Ω. The resulting impedance is now normalized to 50 Ω, which results in the point $(\mathcal{Z}_{final})$ =1.04-j0.08 as indicated on the smith chart inside the VSWR=2 circle.

The layout of the proposed rectifier circuit is presented in Figure 33(a). The matching network consists of two lines "feed TL" and "load TL" with different characteristic impedances. A meandering technique is applied on the load TL of length 21 mm to minimize the resulting rectifier's size. A dc block capacitor prevents the dc voltage generated by the diode from reaching the generator.

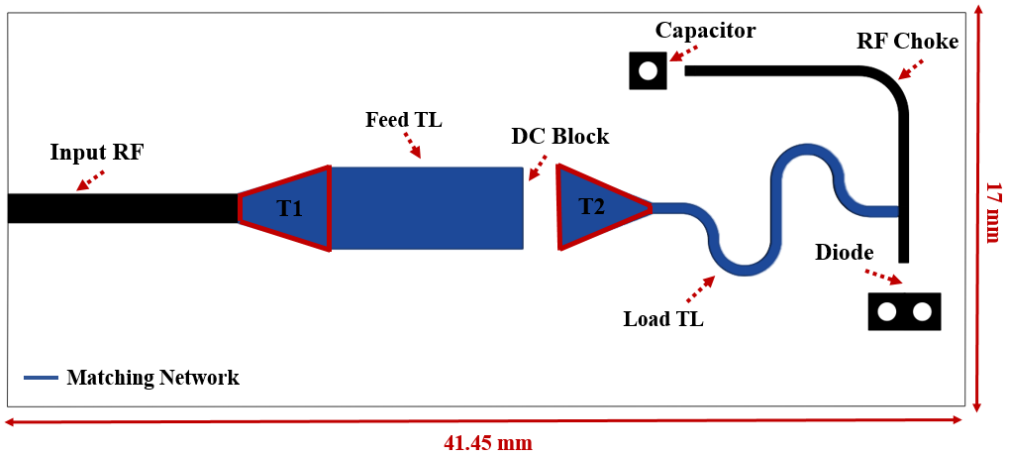

(a)

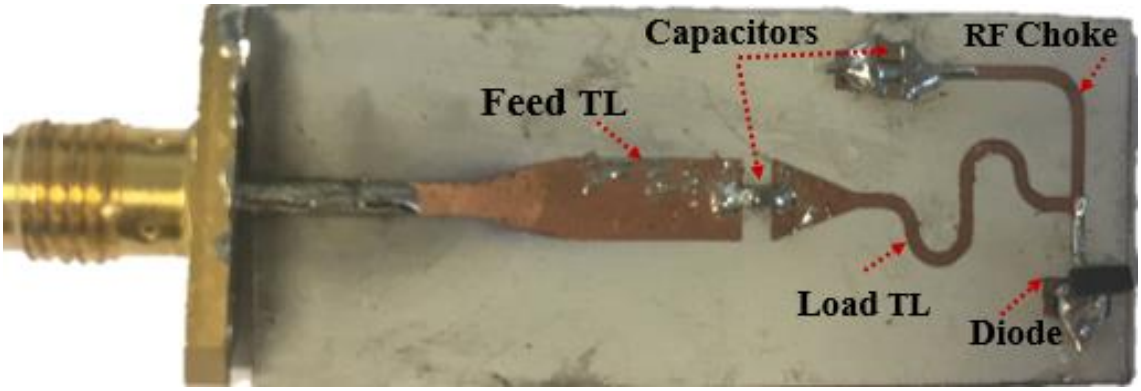

(b)

Figure 33: Rectifier design for the proposed impedance transformer matching network (a) Layout, (b) Fabricated prototype.

A tapering technique is applied first between the 50 Ω input line and the “feed TL” as well as between the “feed TL” and the “load TL”. A triangular tapered connection “T1” is used for transition from the feeding line to the “feed TL” of Z0 = 20 Ω. Another transition “T2” is required to avoid the abrupt transition from 20 Ω to 100 Ω that is the characteristic impedance of the “load TL”. Such tapered section ensures a smooth transition between the two transmission lines.

In reality, the tapered behavior of the impedance can be explained from equations (4) and (5), where the impedance of a tapered line is studied in function of the position.

The design is built using Rogers 3203 with thickness 0.508 mm as shown in Figure 33(b). The total network dimension is equal to 41.45 mm x 17 mm. The “RF Choke” functionality is achieved using a shorted quarter-wavelength (λg/4) stub. The shorting of the λg/4 stub is achieved through 1 μF capacitors. The λg/4 stub behaves as an open circuit impedance at the fundamental and third harmonic frequencies. However, it short-circuits the second harmonics.

Figure 34 presents a comparison between the simulated and measured dc voltage and PCE values at f=2.43 GHz. Placing the two matching TLs in this configuration

yields an efficiency of around 50% at 0 dBm with a measured voltage of 0.65V for an optimal load of 850 Ω. The attained efficiency is close to the one achieved by the single stub matching. Therefore, the proposed technique must be enhanced further to lead to higher efficiency values with better performance and a more compact size.

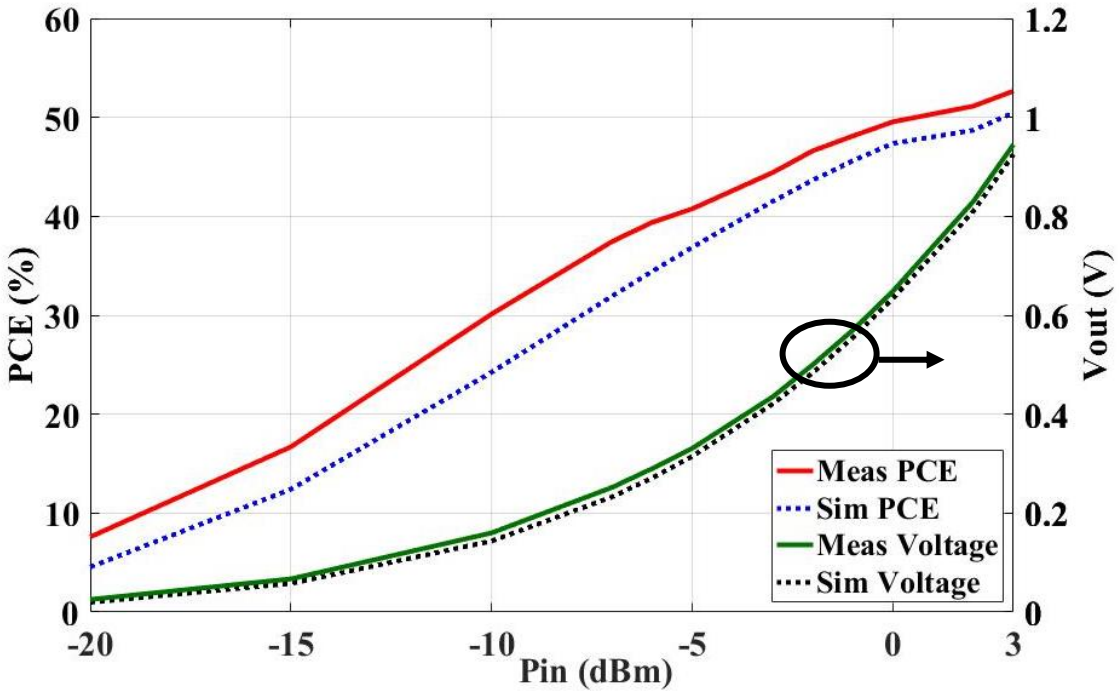

Figure 34: Efficiency and output voltage results for the rectifier with tapered series lines matching technique.

2. Improved matching network technique

The proposed matching network is optimized in this subsection for better results. The dimensions of both TLs are kept the same; however, the position of the "load TL" is tuned with respect to the Schottky diode. The new layout is presented in Figure 35 along with the fabricated prototype, which has a compact size of 32.21 mm x 17.54 mm.

Part of the "load TL" is kept in series with the "feed TL" whereas the other part is suspended in shunt with the Schottky diode at its end. This topology maintains the

matching between the two impedances and creates a symmetrical design. Changing the position of the “load TL” with respect to the “feed TL” and the Schottky diode improves the efficiency response. The results for the voltage and efficiency are shown in Figure 36 for the proposed layout at f = 2.45 GHz. The rectifier is matched for operation within the whole desired frequency range. By inspecting the voltage and efficiency results, an increase to 58% is observed at 0 dBm with a peak voltage of 0.76V measured for a 1 kΩ load. Such topology provides a compact design accompanied with an almost 10% increase in the efficiency over the entire power range from -20 dBm to 3 dBm.

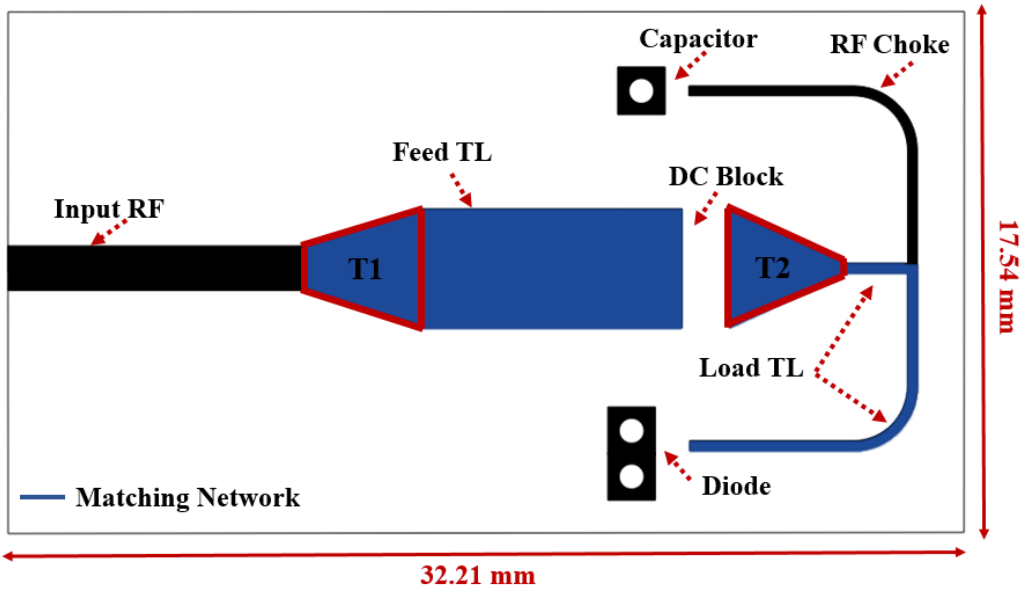

(b)

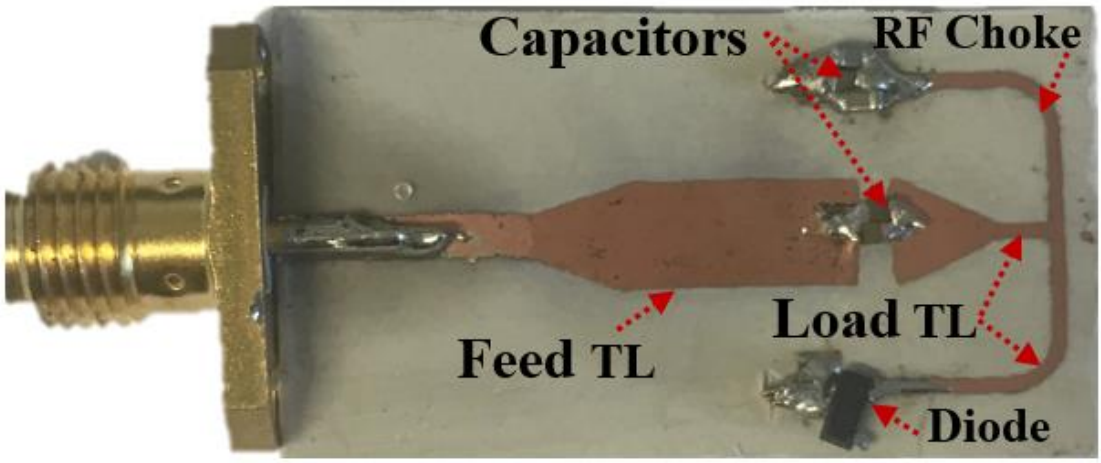

(b)

Figure 35: Rectifier design with improved matching network (a) Layout, (b) Fabricated prototype.

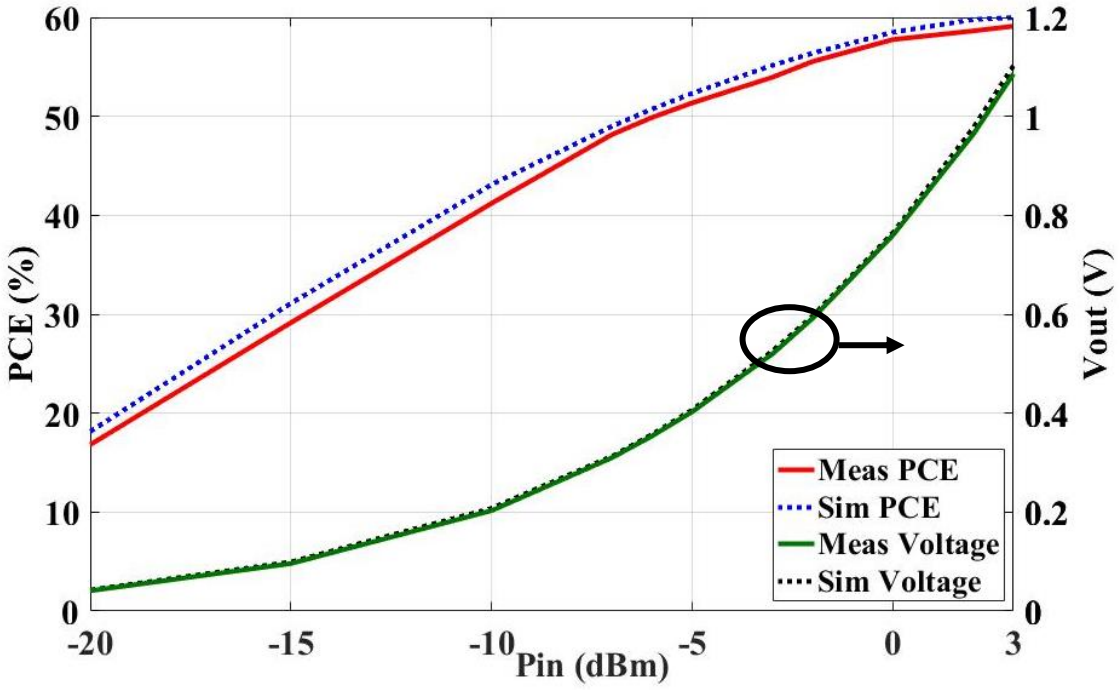

Figure 36: Efficiency and output voltage results for the rectifier with improved matching technique.

E. Rectifiers' Performance Comparison with Respect to Frequency, Load and Input Power

The input impedance of the Schottky diode implemented herein varies not only with frequency but also with the RF power fed to the rectifier. A comparative analysis is executed in this section to analyze the performance of the rectifier in various matching topologies. The four rectifiers that are discussed in Sections C and D are now tested over a wide range of load variations from 0.1 kΩ to 10 kΩ. These four rectifiers are denoted as: "SS" for the first design (presented in subsection C.1) with a shorted shunt stub matching network, "OS" for the second rectifier with an open shunt stub (presented in subsection C.2), "TSL" for the third composed of tapered series lines (presented in subsection D.1), and "IMN" for the last rectifier with an improved matching technique (presented in subsection D.2).

The PCE behavior of each circuit with respect to load variations for an RF fed power of 0 dBm at 2.45 GHz is shown in Figure 37. The efficiency peaks at the optimal load value of each design. The tapered line topology exhibits a larger difference in comparison to the other matching network techniques. The circuit with the improved matching network starts with an efficiency of 27% at RL = 0.1 kΩ, peaks to a value of 58% at 1kΩ, then returns to 27% at RL = 10 kΩ. The tapered series lines "TSL" allows the rectifier to return to its initial PCE value (23%) at RL = 7 kΩ. On the other hand, the rectifiers with open ended stubs "OS" and shorted stubs "SS" regain their initial PCE value (25%) when the load is around 4.5 kΩ. This comparison shows that rectifying circuits that resort to tapered non-uniform TLs are able to reliably maintain their efficiencies over a wider range of load values.

In order to explain such performance, the input impedance of two rectifying circuits is studied as shown in Figure 38. The first one is the "OS" rectifier that

represents the 50Ω TLs. The second one is the “IMN” rectifier that is based on the tapered matching technique. It can be noticed that for the rectifiers with tapered lines, the real part of the input impedance increases from 16 Ω to 58 Ω when the load goes from 0.1 kΩ to 2 kΩ. Then, it is stabilized around 60 Ω along all the remaining load range. A similar performance is achieved by the imaginary part of the input impedance where it decreases from j28 Ω to j19 Ω before getting stabilized at about j22 Ω. However, when it comes to analyzing rectifiers with matching networks that resort to 50 Ω single stub matching, the real part increases from 20 Ω to 88 Ω throughout the range while the imaginary part decreases from j21.5 Ω to a stable state of around –j5 Ω. Therefore, the tapering technique implemented between the lines of different characteristic impedances allows the circuit to maintain better efficiency figures over a wider drift of load values.

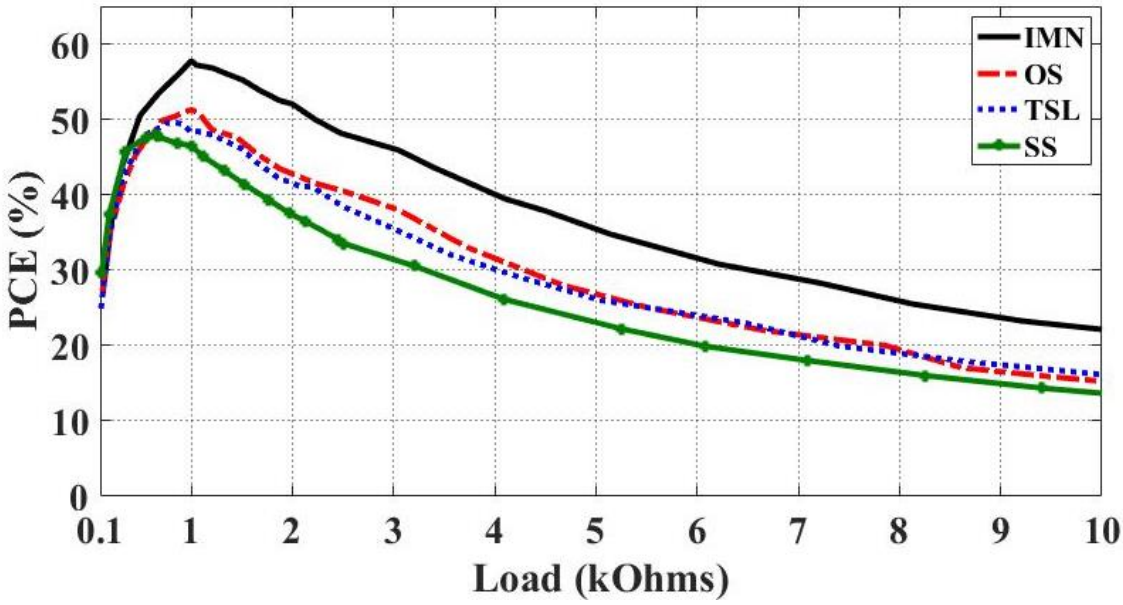

Figure 37: Measured PCE results for different load values of all rectifiers at Pin = 0dBm and f = 2.45GHz.

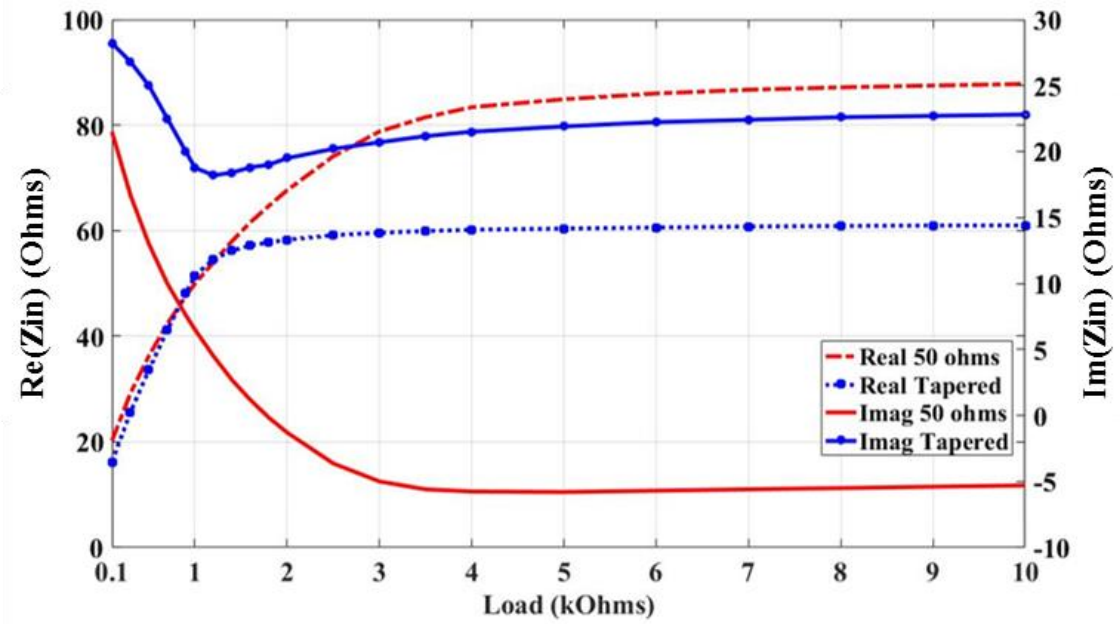

Figure 38: Input impedance plots with respect to load variations for the proposed rectifier "IMN" and the 50 Ω single stub MN rectifier "OS".

The PCE performance of each of the four rectifiers is also studied when the frequency is varied between 2.3 GHz and 2.5GHz as shown in Figure 39. Such study is done for an input power of 0 dBm and for the corresponding optimal load. The load for the "IMN" and "OS" designs is RL (optimal) = 1kΩ, for the "TSL", RL (optimal) = 850 Ω and for the "SS", it is equal to 660 Ω.

From Figure 39, it is concluded that the "IMN" rectifier maintains an almost stable efficiency around 55% over the whole frequency range. This is due to its tapered matching network. The "TSL" rectifier maintains an approximate efficiency of 49%, which is close to its optimum efficiency (50%) over 75% of the frequency range. The PCE curves of the "OS" and "SS" rectifiers show more dependency with respect to the variation of the frequency. It can be noticed that the efficiency flatness for these two rectifiers appears in a very small fraction of the frequency band. This behavior is explained by the use of 50 Ω TLs, which offer a narrower bandwidth with respect to

tapered lines. The input impedances of the “IMN” and “OS” rectifiers are plotted with respect to frequency in Figure 40 for an input power of 0 dBm and an optimal load. The tapered line circuit displays smoothness in the input impedance with respect to frequency. The real part of the “IMN” circuit starts at 42 Ω, increases until it reaches 50 Ω and then returns to 46 Ω while the imaginary part smoothly changes as the frequency increases. On the other hand, the “OS” rectifier reacts differently to the changes in frequency. The input impedance variation shows abrupt increases and decreases within a smaller frequency range. The rigidness of the tapered circuit response is due to the triangular tapered part of the circuit as explained in [1].

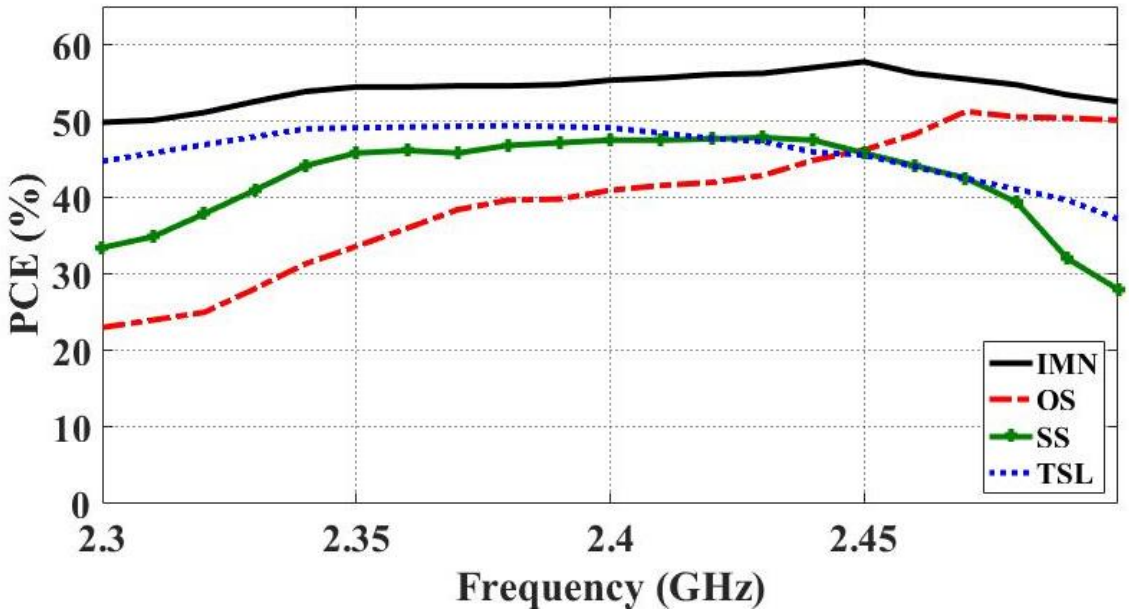

Figure 39: Measured PCE results with respect to frequency for Pin = 0 dBm and RL (optimal).

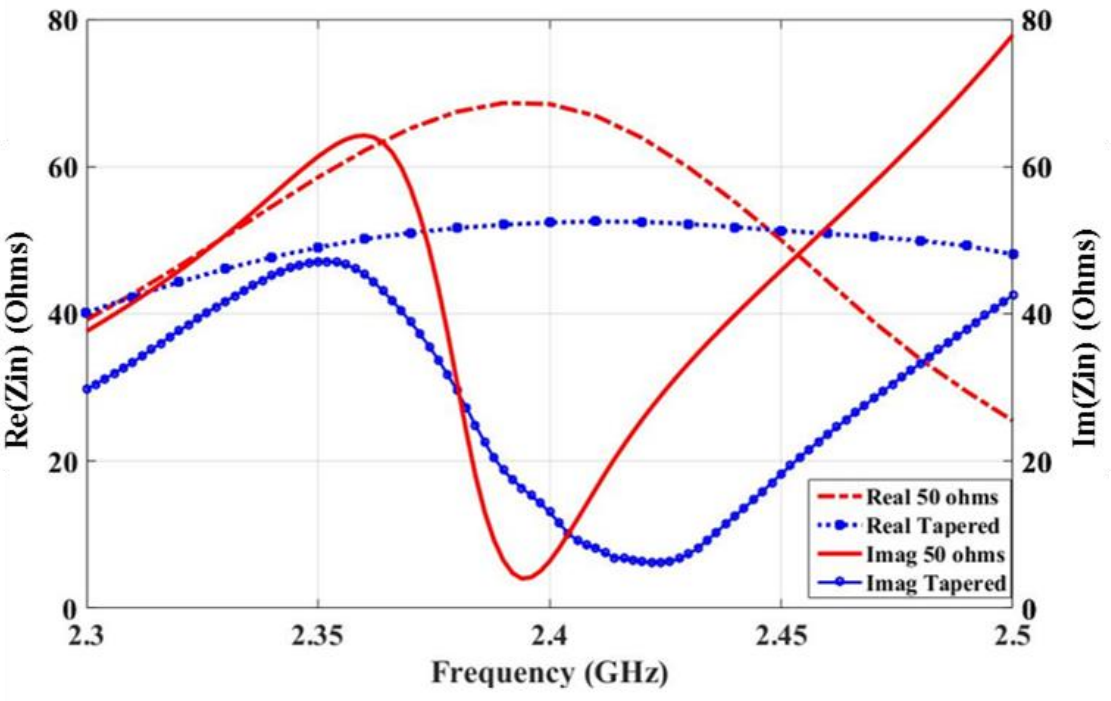

Figure 40: Input impedance plots with respect to frequency for the proposed rectifier "IMN" and the 50 Ω single stub MN rectifier "OS".

The performance of the rectifiers is also affected by the variation in the input RF power levels. Figure 41 illustrates the measured PCE values for an RL = 1kΩ and an optimal frequency of operation with respect to a range of input power spanning from -20 dBm to 3 dBm. Similar to earlier comparisons, the "IMN" circuit presents the highest efficiency followed by the "OS" rectifier. It is then concluded that the "IMN" rectifier with the tapered matching technique constitutes the most suitable candidate circuit for RF energy harvesting and can be proposed for integration into the multiport RF harvesting system that is discussed in the next section.

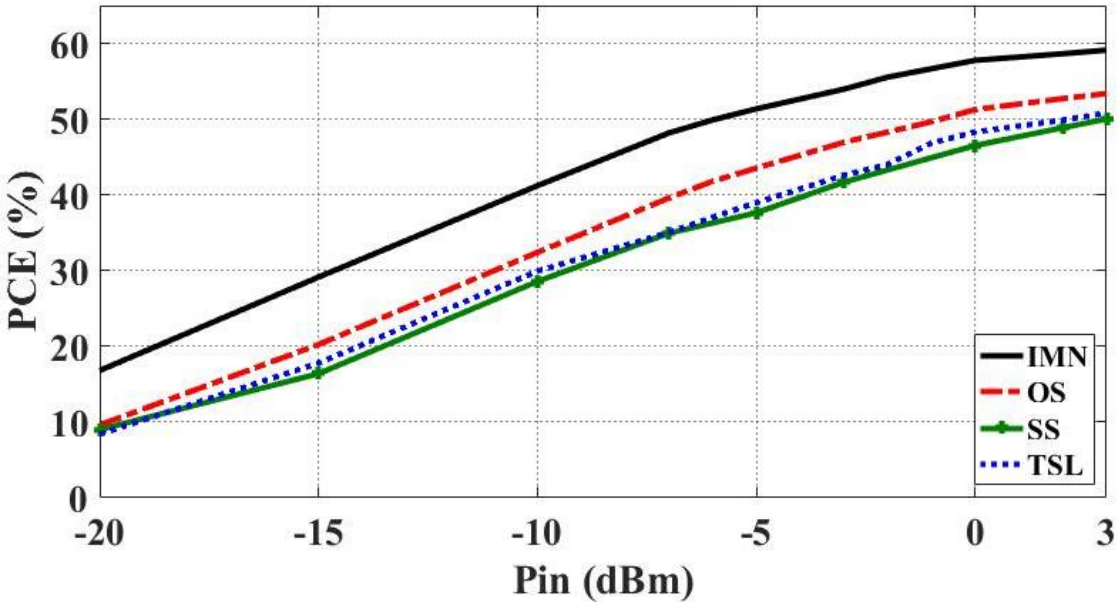

Figure 41: Measured PCE results with respect to input power at 2.45 GHz and RL= 1kΩ.

F. Summary

In this paper, a new matching technique that maintains steady efficiency figures for RF rectifiers is discussed. The matching technique is compared against typical and conventional matching networks. It is mainly based on a tapered topology that results in a better impedance matching. The proposed network reflects the ability of matching a real source impedance to a complex load impedance, while resorting to two series lines of non-uniform widths. A validation of the proposed methodology is provided by simulating, designing and measuring a corresponding rectifier. A great agreement between simulated and measured results is obtained with a peak efficiency of around 60% at 0 dBm.

CHAPTER V

MULTIPORT RF ENERGY HARVESTERS

A. Introduction

In order to increase the harvested energy by extending the scavenging capability, a multiport RF energy harvester is proposed in this section. The objective of implementing such a multiport harvester is to increase the dc output power, while maintaining the same transmitted power. A multiport system can include multiple inputs and/or multiple outputs. In this work, we will adapt two separate strategies: combining multiple inputs using RF combining and combining multiple outputs using DC combining.

B. Design of the Multiport System

Two combining architectures are implemented: RF combining and dc combining. Two different antennas are used for transmission and reception in the multiport energy harvester. On the transmitting side, the slot antenna described in section C of chapter III is used. The receiving antenna is 1x2 array antenna. Each antenna element design is composed of a meandered line patch with a length of 166 mm corresponding to multiples of $\lambda/2$, and a width of 5 mm that corresponds to 50 Ω at 2.42 GHz. The microstrip line feeding each antenna element has a trapezoidal configuration at the end of a 10 mm feeding line matched to 50 ohms. Figure 42 displays the designed single element on HFSS with a size of 65x79 mm2, it exhibits operation at 2.45 GHz along with a 7dB gain. The design is printed over Rogers RO5880 substrate with dielectric constant of 2.2 and a thickness of 1.6 mm.

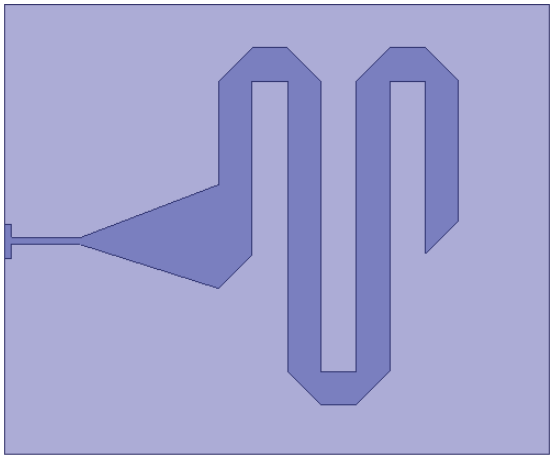

Figure 42: Single element meander antenna design on HFSS.

An array of two meandered line antennas is then built resulting in a size of 183 mm x 120 mm. This antenna operates at 2.45 GHz. It is characterized by a full ground plane and a measured gain of 12.65 dB. Figure 43 shows the array fabricated prototype. The antennas used for transmission and reception are simply examples to prove the concept. Other antenna types can also be implemented to achieve the same purpose.

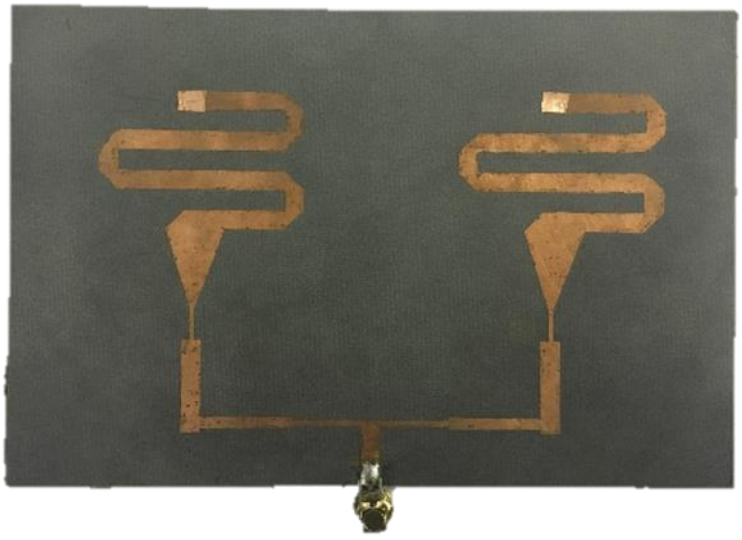

Figure 43: Photo of fabricated meander antenna array.

The comparison between the simulated and measured reflection coefficients as well as gain plots are shown in Figure 44 and Figure 45 respectively.

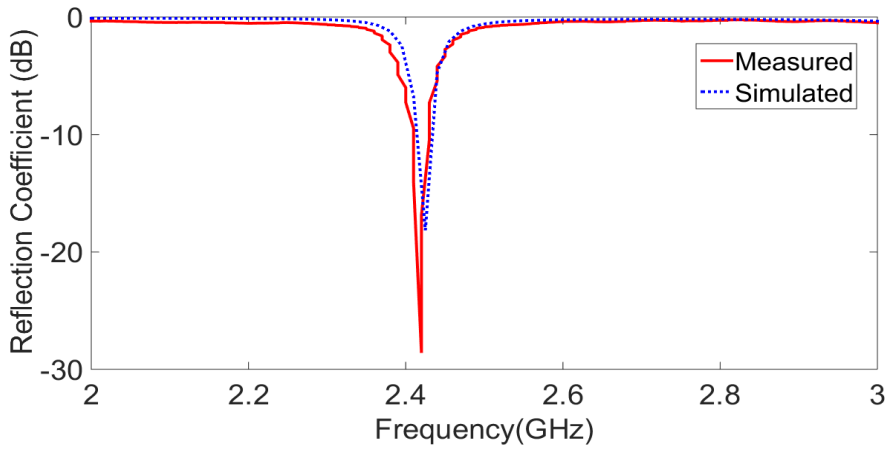

Figure 44: Plot of simulated and measured reflection coefficient of meander antenna array.

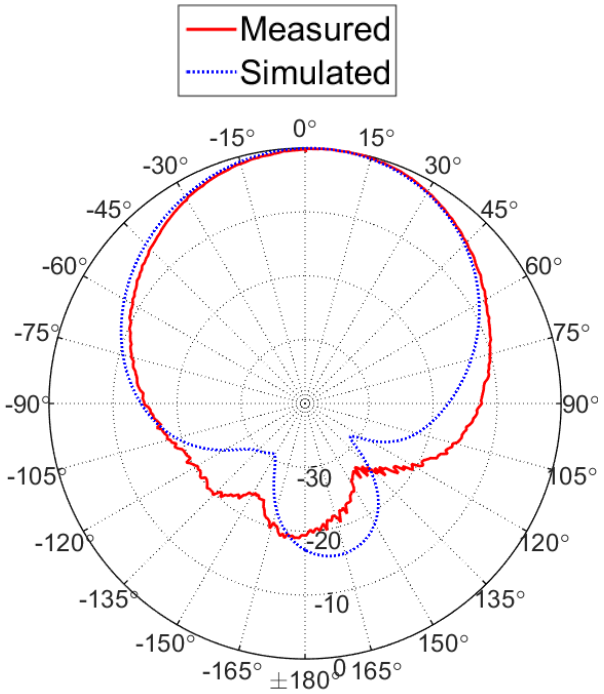

Figure 45: Plot of simulated and measured radiation pattern of meander antenna array.

A multiport system is based on either combining the RF input or combining the dc output as discussed in [41]. Section C discusses the scenario when one slot antenna is used for transmission and four meandered line array antennas are integrated for reception. The purpose of such setup is to demonstrate that the dc output can be boosted without changing the transmitter configuration. The rectifier used in all the multiport setups is the rectifier "IMN" discussed in Chapter IV that presents the highest desired efficiency behavior. Section D displays the RF combining capabilities in combining the RF signal in a point to point communication system between multiple meandered line antenna arrays as transmitters and multiple slot antennas as receivers.

C. Single Transmitter - Multiple Receivers -RF Energy Harvesting System

1. RF Combining

RF combining happens when RF signals obtained from multiple receiving antennas are combined to one output port as represented in Figure 46. The resulting single RF signal constitutes the input to one rectifier. The rectifier converts the RF combined signal into a dc voltage output. In this case, multiple antennas and one rectifier are employed. This configuration offers efficient power transfer schemes because higher power is fed to a single rectifier, hence operating within the diode most efficient rectification region.

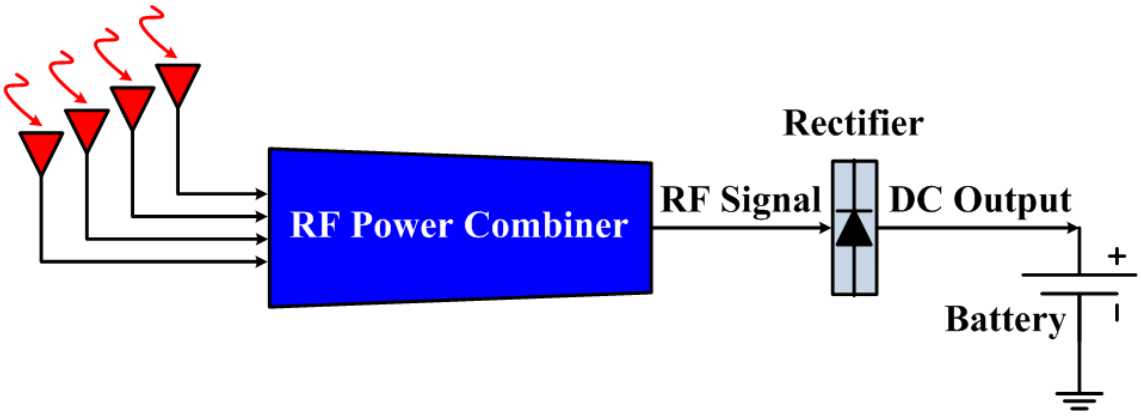

Figure 46: RF combining schematic.

To test the effectiveness of the RF combining technique, the experiment starts with a one-to-one setup. One meandered line array is placed facing a transmitting slot antenna at a distance of 50 cm (far field region). By Friis transmission equation [42], this distance insures that by sending 10 dBm through the slot antenna, -6.5 dBm is captured by the receiving antenna. This amount of received power generates around 0.35 V for an R_L = 1kΩ, and this stands for the same value measured in the voltage plot of Figure 36 for Pin = -6.5 dBm. The second step is setting up a two-to-one combining architecture by using a two-to-one RF combiner [43]. For this scenario, the received power increases to -4.2 dBm for the same transmitted power of 10 dBm by the slot antenna. The dc output voltage from the rectifying circuit also increases to 0.48 V accordingly. The last step is to build a four-to-one combining setup by the integration of additional RF power combiners and four meandered line antenna arrays as shown in Figure 47. For all tested RF combining setups, one rectifier is used to receive the combined RF signal at the output port of the RF combiner. This setup yields an increase in the power received to -2 dBm with a generated voltage of around 0.6 V. This result is validated in Figure 36 for an input power of -2 dBm and a load of 1 kΩ. Therefore, the

RF combining of four RF signals has increased the power by 4.5 dB, which is expected to be less than 6 dB mainly due to the losses in the RF power combiners and the cables that are calculated to be around 1.5 dB. Therefore, the RF combining technique proves the ability of increasing the output voltage with only one source of transmission and one rectifying circuit.

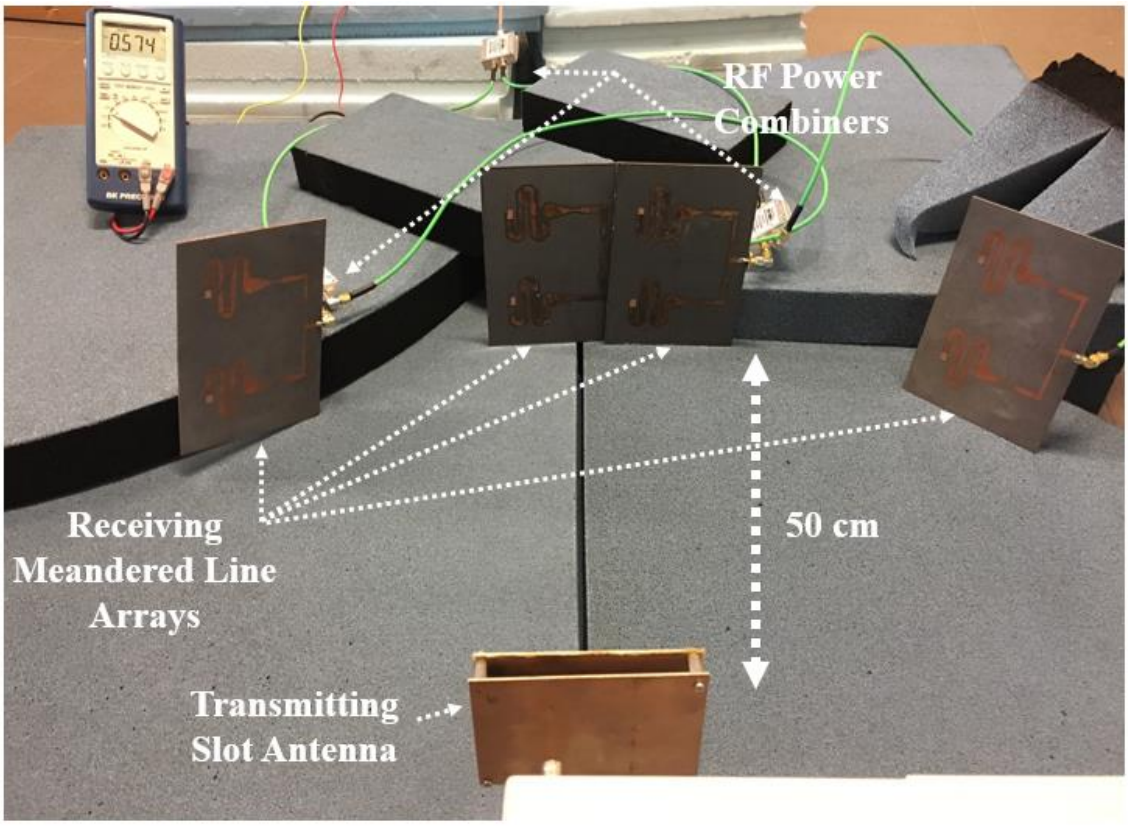

Figure 47: Four-to-one RF combining experimental setup.

2. DC Combining

Implementing an RF harvesting system using dc combining requires the use of multiple antennas with each attached to a rectifier. Each rectifier will output a certain amount of dc power which will then be combined to get one source of dc output. The dc

combining scheme is shown in Figure 48. The harvested dc power from all rectifiers can then be combined in parallel, series, or a hybrid manner. For this setup, the same type of antennas is used as before for transmission and reception of RF signals. The only difference is that now each of the four rectifiers is attached to a receiving meandered line antenna array and the output dc voltages are combined in series.

To start with the comparison, the one-to-one setup realized in the previous part yields a voltage of 0.35 V. The second step is to implement a dc combining topology from two rectifiers. Therefore, two meandered line antenna arrays are placed facing the slot antenna at a distance of 50 cm. Two rectifiers are connected each to an antenna array with their outputs connected in series. An output voltage of 0.68 V is collected at the output of the dc combiner. The dc output of the two combined rectifiers surpasses the output voltage of the four-to-one RF combining architecture. The last setup is done by implementing the dc combining of four rectifiers connected to four receiving antennas as shown in Figure 49. The series connection among the outputs of the four rectifiers gives the summation of the four voltages generated by each one. Therefore, a voltage of around 1.34 V is collected at the output of the dc combiner. Accordingly, combining at the dc level increases the overall output voltage by approximately 1V for the same transmitted power.

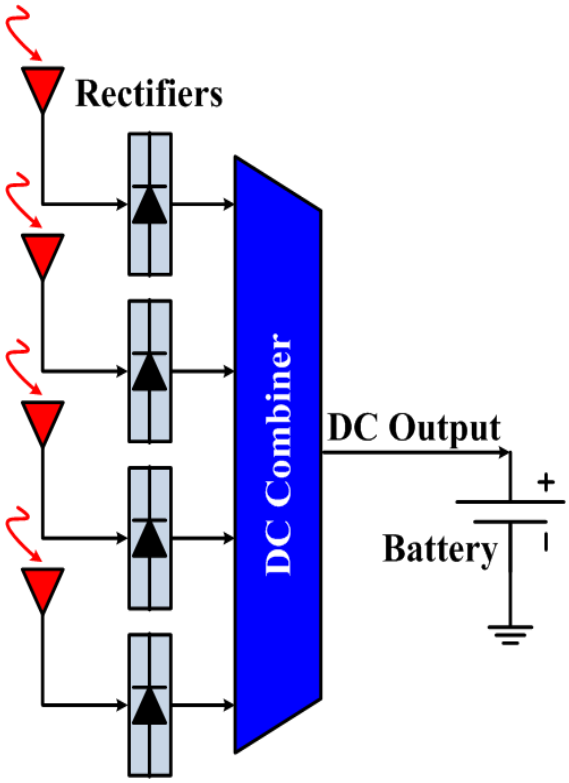

Figure 48: DC combining schematic.

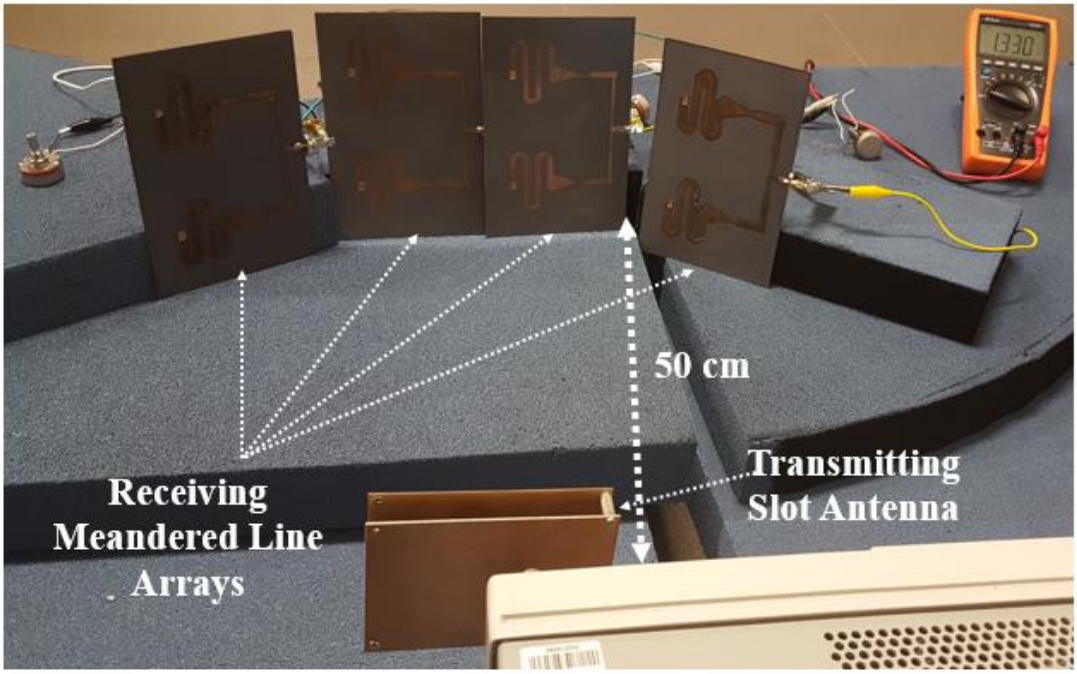

(a)

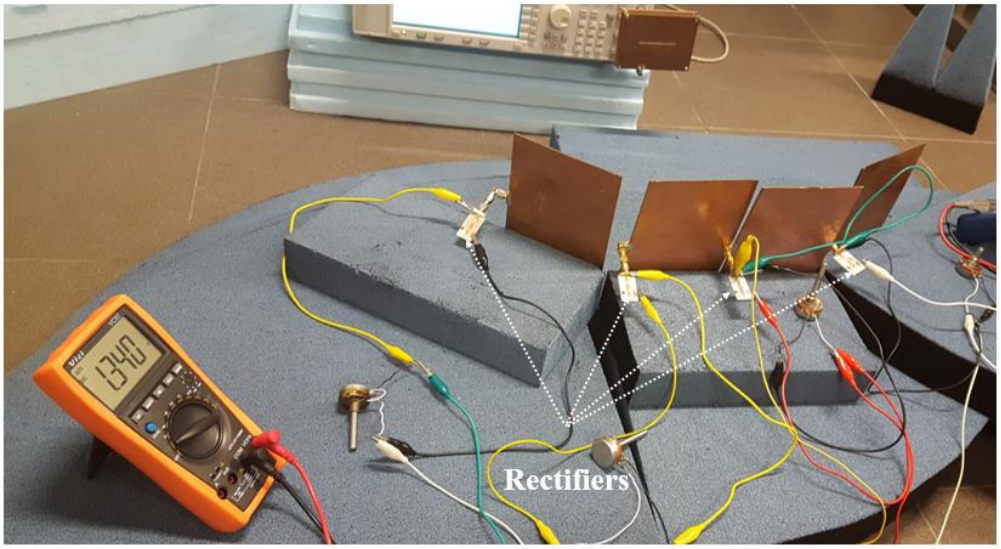

(b)

Figure 49: DC combining experimental setup of four rectifying circuits.

3. RF combining vs dc combining

This subsection compares the results obtained from applying the RF combining technique versus the ones obtained from the dc combining techniques. In the case of transmitting from one source, the same number of antennas is used. Although RF combining requires a single rectifier, where the combined RF signal is the input, the collected dc output from four RF sources is still less than that generated by two series dc combined outputs. In this experiment, RF combining is facing losses due to the presence of a single source, thus loosing direct line of sight with some receiving antennas. Also, the presence of RF power combiners and cables adds to the losses that appear at the last stage of the RF combining. This has been shown in the limited gain of 4.5 dB instead of 6 dB for the four-to-one RF combining architecture, where the overall dc voltage is 0.6 V for a load of 1 kΩ. On the other hand, dc combining requires only a series combination of output voltages that presents minimal losses compared to RF combining.

Even if each receiving antenna is not capturing the maximum power, summing the voltages of the four rectifiers contributes to a better performance for the same transmitted power. Accordingly, a voltage of 1.34 V, which is around 2.5*$V_{RFcombining}$, is collected at the output of the dc combiner. On the other hand, dc combining requires the output combination of multiple rectifiers instead of a single one. Thus, one must resort to the constraints imposed on the system's performance to determine which combining technique to employ for a higher harvesting ability.

D. Multiple Transmitters - Multiple Receivers- RF Energy Harvesting System

A four-to-one power combiner [44] is used to combine four different RF signals captured by four antennas. Such technique also results in an increase in the harvested dc power at the output of the rectifying circuit, however the collected RF signal at the input of the rectifier is expected to increase to a higher level than in the case of a single transmitter-multiple receivers. This is due to the fact that each receiver antenna will be facing another transmitter antenna. Such scenario yields a better line of sight connection, which results in capturing more RF power. Before implementing the RF combining technique, the same slot antenna is placed at a distance of 70 cm away from the meandered line array as shown in Figure 50(a). The rectifier used is the one presented in chapter III.

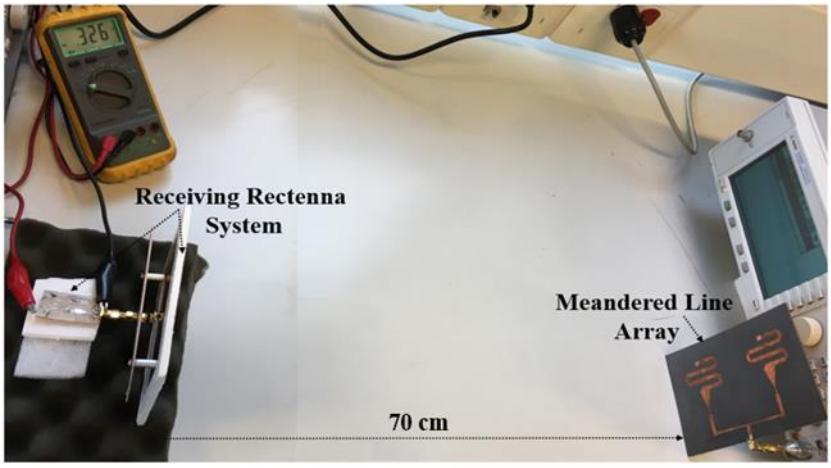

(a)

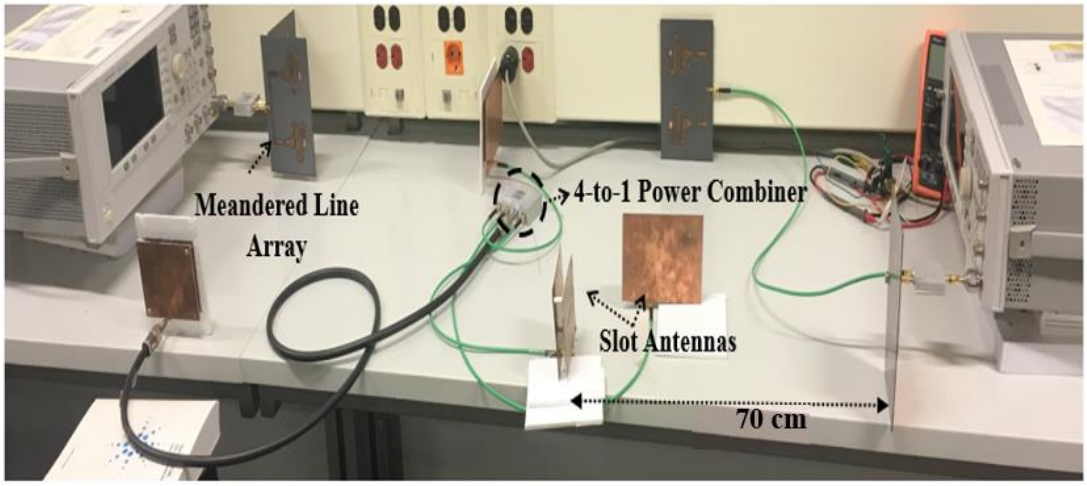

(b)

Figure 50: (a) The one to one transmitting-receiving system, (b) RF combining experimental setup.

For this input power, the slot antenna is collecting around -9.5dB. The dc output voltage from the rectifier is 0.326 V. The next scenario is based on using four slot antennas and combining the RF received power as shown in Figure 50(b). Under this scenario, the received power increases to -4 dBm for the same transmitted power of 10 dBm by the meandered line array. The dc output voltage from the rectifying circuit also increases to 0.75 V accordingly.

E. Summary

In this chapter, the single port system presented in the previous chapter is transformed into a multiport RF energy harvester by the implementing RF and dc combining architectures. Measurement results show that dc combining can result in a higher dc output voltage in comparison with an RF combining architecture under the same conditions. Such benefit is observed at the cost of integrating additional rectifiers into the multiport system. Thus, with an improved matching network and a multiport RF harvesting system, a larger dc power output can be reached over a wider range of load variations and frequency of operation.

CHAPTER VI

AMBIENT RF ENERGY HARVESTING FROM WI-FI

A. Introduction

In this section, a novel technique for harvesting Wi-Fi 802.11 b/g band signals is proposed. The harvesting circuit here-in operates on all different Wi-Fi channels while providing a flat efficiency response. The implemented technique enables the routers to send an almost continuous signal, thus encouraging the harvesting process. A commercial access point having a transmission power up to 17 dBm is used as the source for the RF harvesting. Along its ability to harvest efficiently, this system produces a minimal effect on Wi-Fi users. The system is then analyzed with respect to several important parameters such as frequency and distance variation, and most importantly compared to the harvesting from direct dedicated RF signals.

B. Principles of Harvesting from Ambient Wi-Fi signals

This harvesting scenario differs from the case where the transmitted RF signal is dedicated for a specific receiver. In this case, the RF power must be collected from ambient Wi-Fi signals that are scavenged from actual wireless local area networks (LAN) access points. In order to achieve this objective, a rectenna system is positioned facing a wireless router. It is immediately noticed that when the rectenna system is scavenging the RF signals from commercial routers, the resulting efficiency data and voltage output levels are shockingly much less significant in comparison to the harvesting scenario from dedicated RF sources. Figure 51(a) displays the harvesting scenario from dedicated

signals while Fig. 51(b) shows the same setup but while harvesting from a wireless router. While 0.55 V are collected from the slot antenna fed by an RF signal generator, only 0.022 V (22 mV) are generated by the rectenna system facing a wireless router for the same transmitted power.

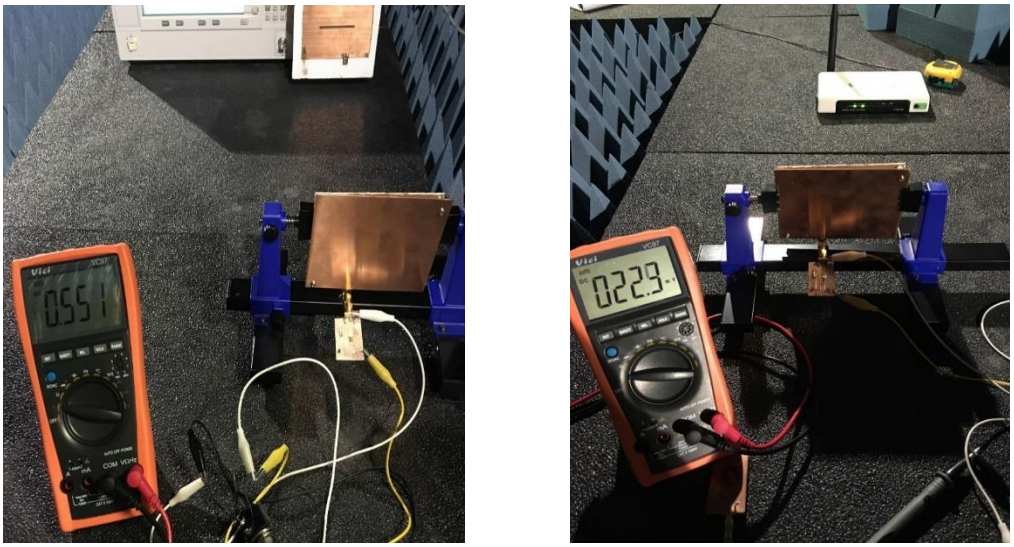

(a) **(b)**

Figure 51: RF Energy Harvesting: (a) Dedicated signals, (b) Ambient Wi-Fi signals.

To that extent, with same transmitted power level, the two setups have resulted with two completely different results. The only difference is that in the second scenario, the transmitter is a commercial router and not a dedicated signal. In reality, routers transmit intermittent signals following IEEE 802.11 a/b/g/n standards and protocols. The router used for the experiments can be any commercial router with any data rate, however in this experiment setup we resorted to the router TL-WR541G 54 Mbps Extended Range with a 3dBi antenna [45]. An antenna monitoring the Wi-Fi signal, when connected to a spectrum analyzer, displays intermittent signals. Figure 52 shows the normal router activity as visualized on Wireshark [46]. This tool is a packet analyzer we used to

understand the performance observed on the spectrum analyzer. We can notice from this figure that this router is sending the packets at a very low rate and non-continuous manner which explains the inability of the rectifier to rectify these signals. The silent periods shown in this figure are inherent to a distributed medium access protocol such as Wi-Fi, where multiple devices share the same wireless medium.

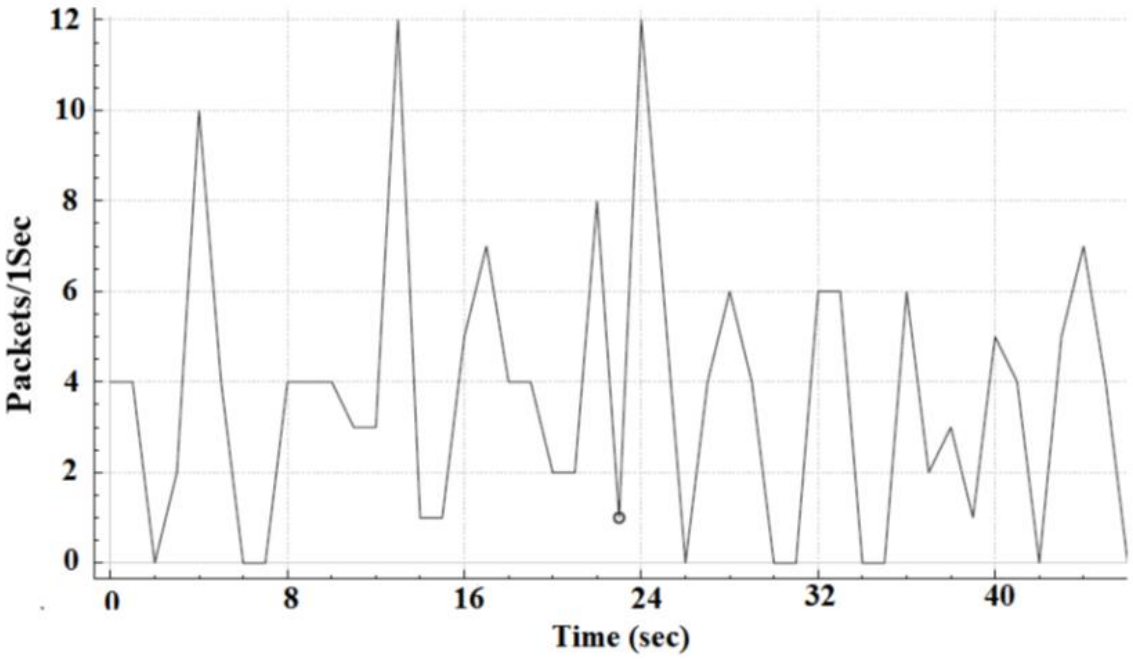

Figure 52: Router normal activity.

Therefore, the main problem faced in ambient harvesting from Wi-Fi is based on the fact that routers send bursts of signals that are very fast and highly unstable. This fluctuation makes harvesting tricky and challenging. In order to solve these issues, packet building and network transmission is achieved. Such approach requires some algorithm manipulation and no hardware change at the router. The algorithm targets the physical layer messages at the router and no upper layer change. Hence, the router continues its natural performance while harvesting energy from it. No chipsets are needed here only

the software bearing this algorithm. Ethernet II packets that have a frame size ranging from 64 to 1518 bytes without a preamble and start/end delimiters are fundamentally used here. The size of the packet used is 1000byte, and it reaches an average packet rate of 600packets/sec. Furthermore, fluctuations are minimized and stability is re-gained. Once this is visualized with Wireshark, the continuous peak becomes clear on the spectrum analyzer. Figure 53 shows the activity in the router when the algorithm with 600packet/sec is applied. The difference between the periods where the packet injection is ON or OFF is clearly observed. The continuity of the Wi-Fi signal is visualized on Wireshark as well as on the spectrum analyzer.

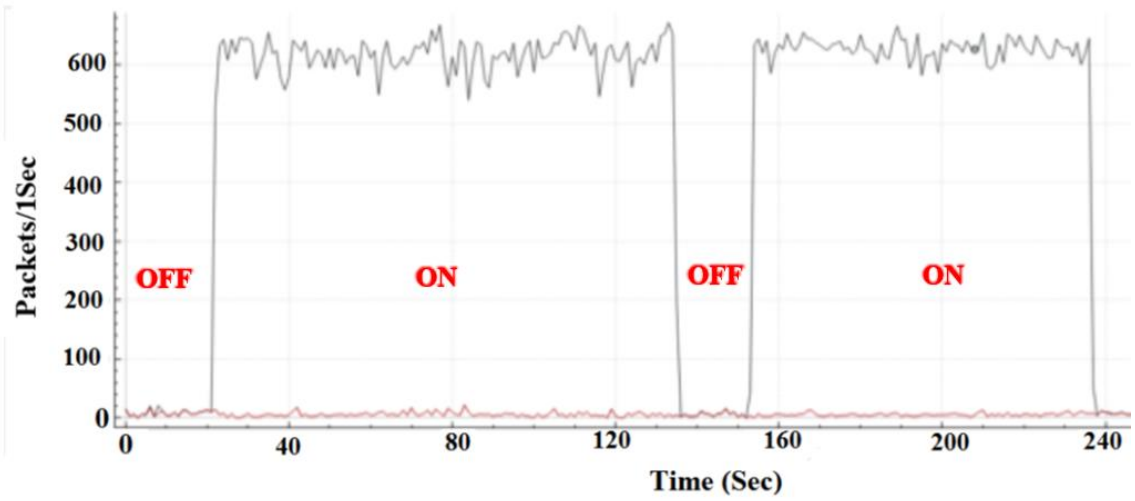

Figure 53: Router activity after applying the packet injection algorithm.

C. Ambient RF Energy Harvesting Experimental Setup

After insuring a continuous activity at the spectrum analyzer, the router is tested for RF energy harvesting. Testing is performed with respect to three important parameters. First the efficiency of the ambient RF energy harvesting is compared to that of a dedicated RF signal. Then, the efficiency is tested with respect to frequency and distance variation.

The rectifier used is the rectifier "IMN" discussed in Chapter IV that presents the highest desired efficiency behavior. The meandered line array antenna described in chapter V is used as the receiver antenna connected to the rectifier while the wireless router is the transmitter. The router's monopole antenna has a gain of 3dB. In order to gain control over the power transmitted, bandwidth, and channels of the router DD-WRT is used. DD-WRT is a Linux based Open Source firmware that aids users in changing the router's specification as needed. The router offers a power range between 0 and 17dBm. It covers the first 11 channels (2.412 − 2.462GHz). The bandwidth can be set to either 5, 10, 20 or 40MHz.

1. Ambient Wi-Fi Signals Vs Dedicated Point to Point RF Signals Energy Harvesting

In this subsection, the goal is to compare the ambient harvesting performance after implementing the algorithm on the router with a dedicated harvesting scenario. Figure 54 holds the description for two different setups. Figure 54(a) illustrates the ambient RF energy harvesting scenario. The router is placed at a distance of 50 cm (far field region) facing the receiving rectenna system. The rectenna is composed of the antenna array connected to the rectifier circuit. At this distance, the power received varies between -23 and -5dBm after transmitting at a power level between 0 and 17dBm. In order to mimic the first setup, the monopole is now detached from the router and connected to a dedicated RF source for the same distance and power transmitted as seen in Figure 54(b). From each of the two different experiments, voltage results are extracted at a load of 1KΩ, at channel 3 (2.422GHz). The efficiency is then calculated and plotted in Figure 55. This figure shows an agreement between the efficiency results of harvesting from a dedicated RF

source and an ambient source. The harvester is now able to rectify signals coming from ambient wireless router while resulting with a very similar efficiency obtained from the dedicated signals scenario. The resulting efficiency values are also very close to the ideal scenario shown in Figure 56 where voltage results are extracted by directly connecting the rectifier to the RF signal generator. This proves the successful implementation of the algorithm on the commercial router.

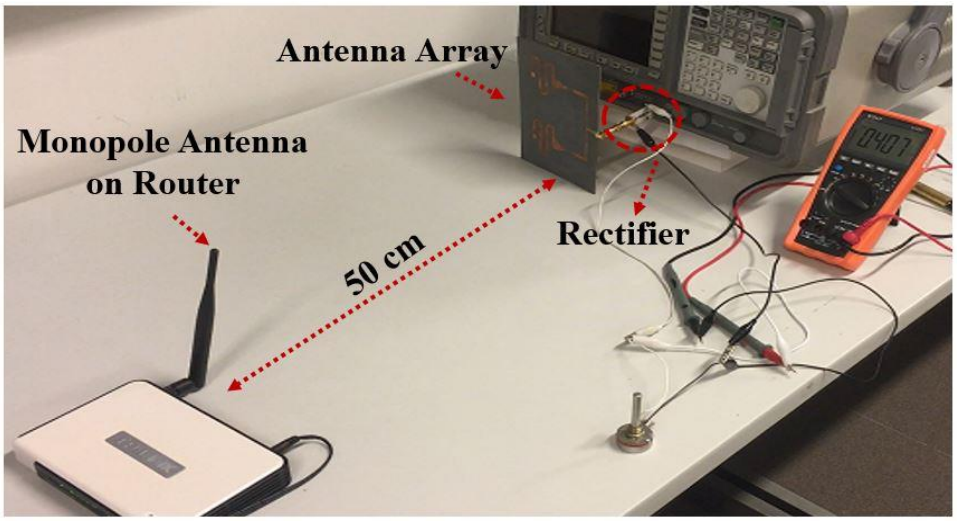

(a)

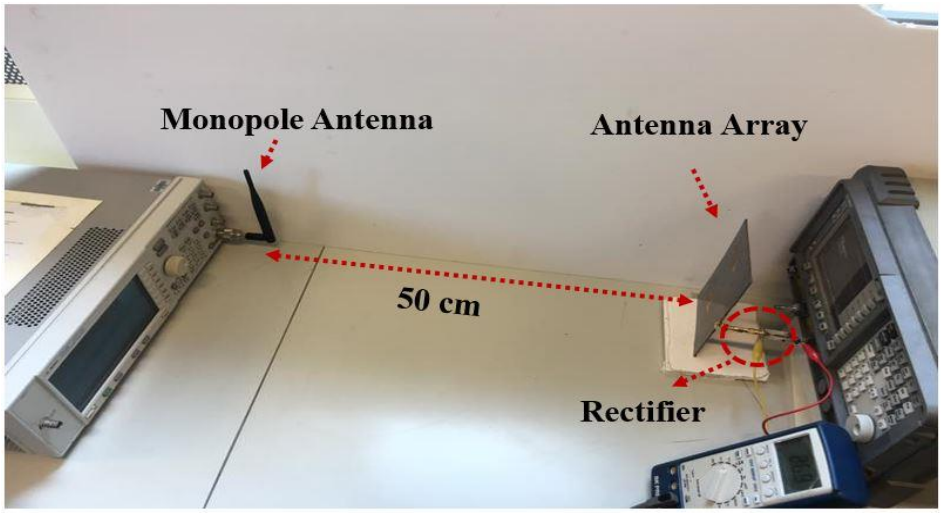

(b)

Figure 54: Experimental setups: (a) Ambient harvesting setup, (b) Dedicated harvesting setup.

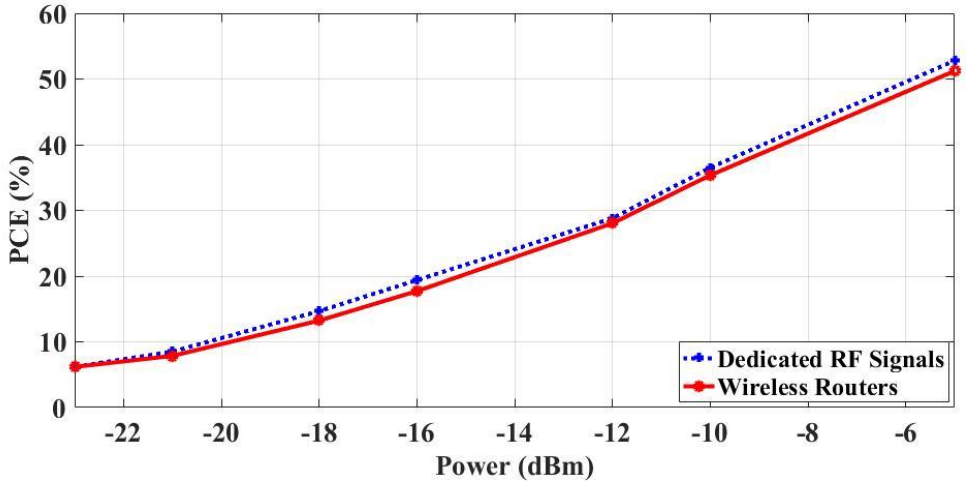

Figure 55: Efficiency comparison between Dedicated and Ambient energy harvesting scenarios.

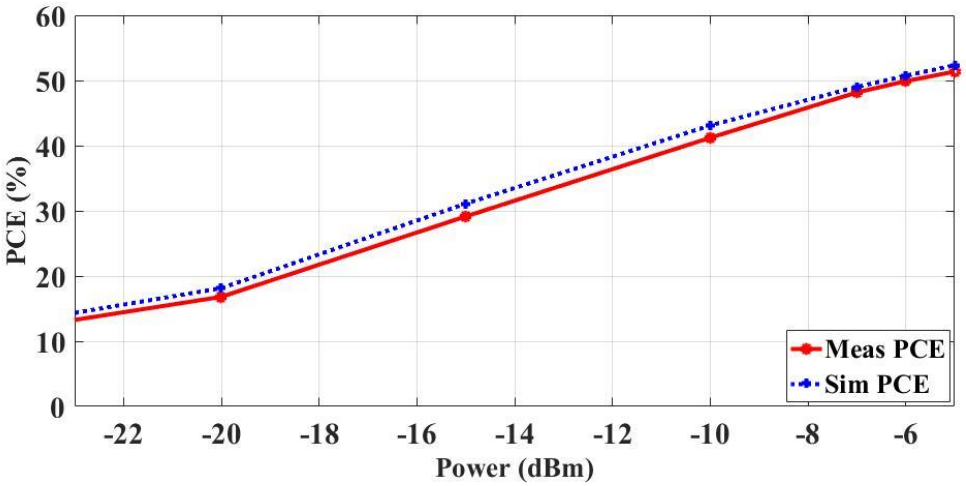

Figure 56: Efficiency results for the used rectifier.

2. Efficiency Response with Respect to Frequency

The tapering technique implemented in the rectifier circuit creates a smooth efficiency response with respect to frequency. In order to verify this aspect, this rectifier is tested on all Wi-Fi channels. The setup presented in Figure 54(a) is repeated while sweeping the frequency from channel 1 to channel 11. For a transmitted power set to 17,

12, and 10 dBm at a distance of 50cm, the expected received powers are -5, -10, -12 dBm respectively. In Figure 55, such a power corresponds to around 50%, 37% and 29% efficiency respectively. Voltage results are extracted and the calculated efficiency is shown in Figure 57. The rectifier presents a stable efficiency response due to the applied tapering technique at all power levels along the whole band.

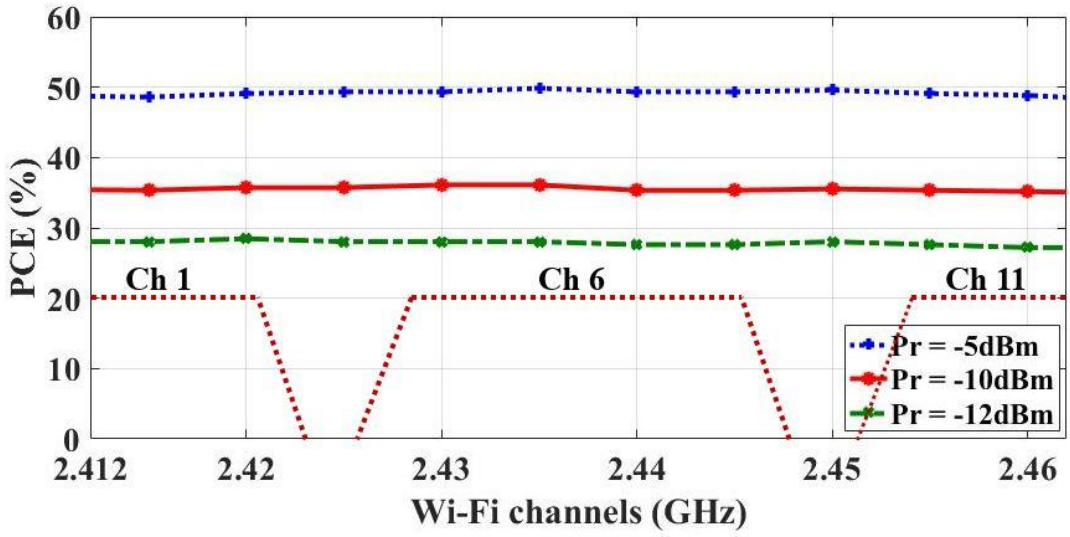

Figure 57: Measured PCE results with respect to frequency for Pr = -5dBm, Pr = - 10dBm, and Pr = -12dBm.

3. Efficiency Response with Respect to Distance

In this part, the rectifier is evaluated for its ability to harvest from wireless routers at its threshold distance. The power transmitted from the router is fixed to 17dBm while its position is swept between 40 cm and 420 cm. The lower bound denotes the beginning of the far field region while the upper bound represents the sensitivity level of the Schottky diode. At these two limits, the power received is -3 and - 30dBm respectively. Figure 58 shows the variation of the received power and the efficiency with respect to distance. For the same transmitted power, the received power decreases

with distance which leads to a fall in the efficiency from 56.1% to a 2.6%. This experiment shows that the rectifier is able to harvest up to a distance of 420cm. This relates to the Schottky diode sensitivity limitation described in details in [5], [6].

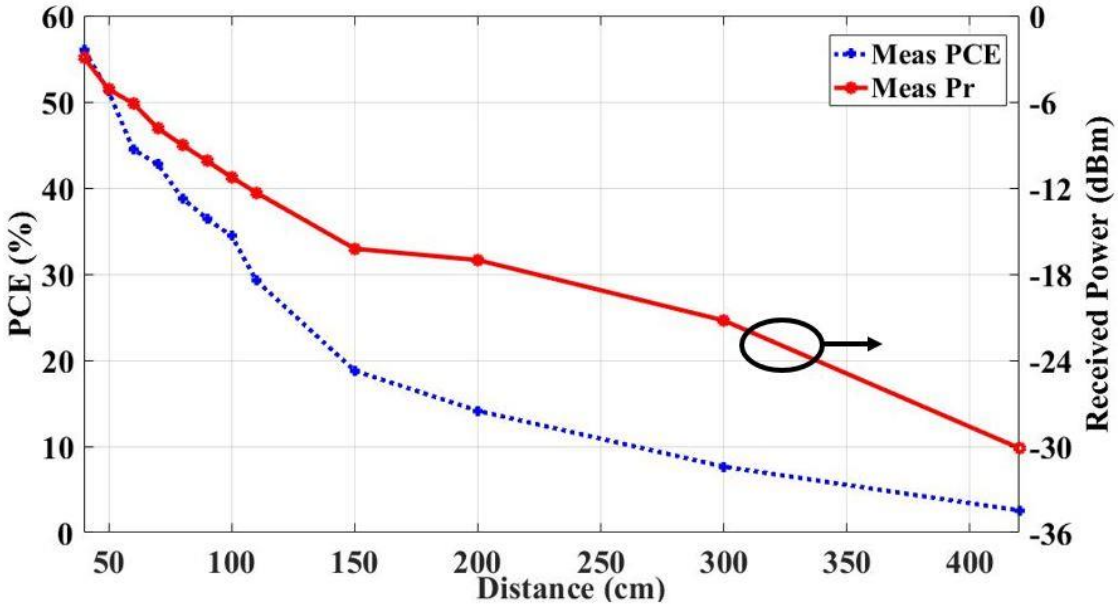

Figure 58: Efficiency plot with respect to distance.

D. Ambient RF Harvesting Effect on Wi-Fi Users

Finally, the technique applied on the router is tested for impact on other Wi-Fi users. Therefore, tests are done on active users connected to the router while running this algorithm. The results show a minimal effect on the user's data rate and the time needed for download. Tests are done on four Samsung S4 devices while downloading a video of size 16.81MB These devices have the CoCodi application [47]. The latter application is used with a MATLAB code to check the user's bitrate and duration to download the video while applying packet injection. The comparison is done on scenarios with and without the algorithm. As expected the quality of the video remained

the same but the duration is longer and the bit rate slightly decreases as seen in Figure 59 and Figure 60.

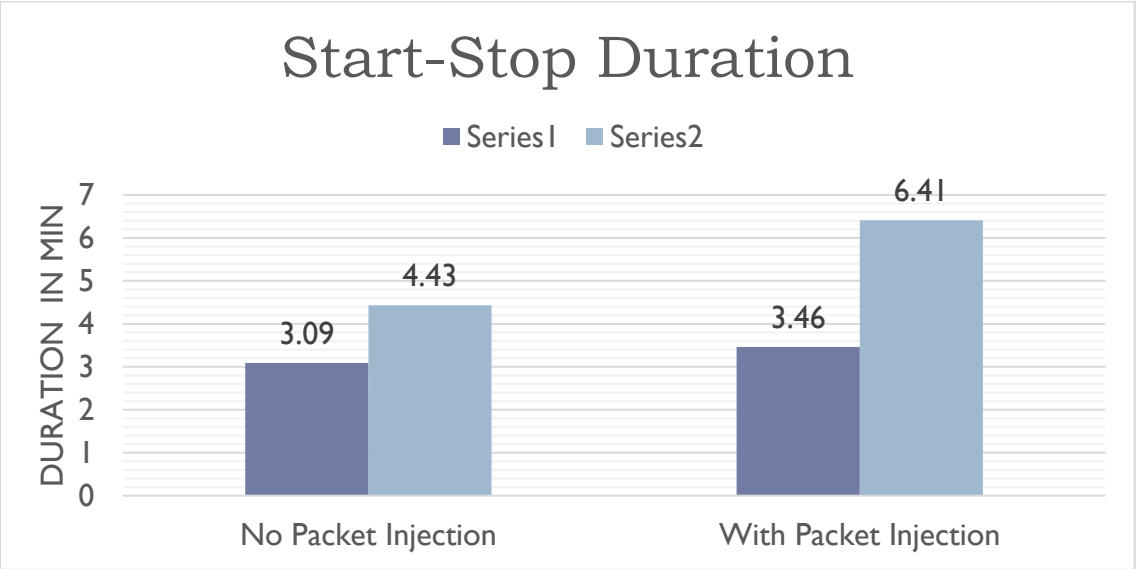

Figure 59: Video streaming duration for router with and without packet injection.

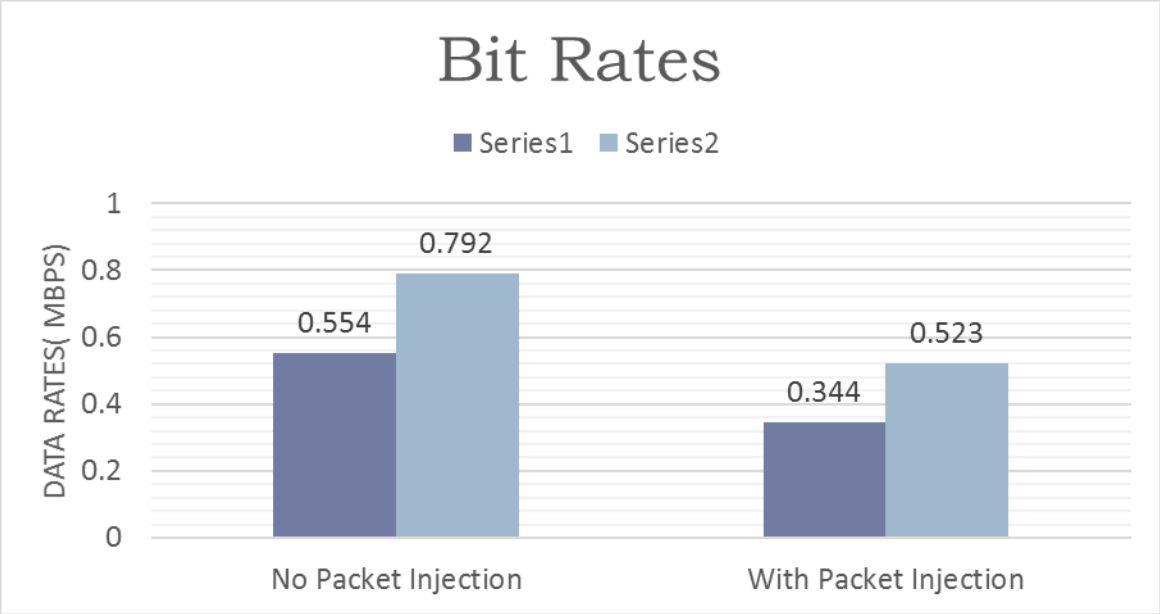

Figure 60: Data Rates for router with and without packet injection.

E. Summary

In this chapter, a novel technique is proposed to enable the RF energy harvesting from daily wireless routers. Moreover, the novelty that encompasses the use of software manipulation rather than hardware adjustment on the router's front-end makes this approach easy to be used on any commercial router. The proposed algorithm is tested on a commercial router and results in an almost continuous transmission. This router is then used as a transmitter in an RF energy harvesting system and tested with respect to several parameters: power, frequency and distance. The effect of this applied algorithm on Wi-Fi users is also studied resulting in minimal effects on the duration and bit rate.

CHAPTER VII

IMPROVING WI-FI HARVESTING EFFICIENCY USING SUPPORT VECTOR MACHINES

A. Introduction

Besides the design structure of the harvester, RF energy harvesting relies on the source generating the RF signal. Throughout this thesis, improving the rectification efficiency is proposed through several techniques either concerned with the receiving system such as: proposed matching techniques and combining architectures or the transmitting system like the technique proposed in chapter VI. This chapter also targets the rectification optimization of the collected signal, however from a different perspective. Several parameters are taken into account to build a system that is able to predict the best operation by finding the locations with the highest available RF power.

It is explained earlier that harvesting ambient RF energy is very challenging since it is dependent on many factors. A particular case is the harvesting from daily wireless routers where the transmitted power is dependent on factors such as the type of the router, its configuration, its location, the number of users connected to it, and many others. Therefore, there is a need for a systematic approach to help direct the rectifying device to the maximum input power. To serve this purpose, machine learning algorithms constitute the best way to learn about a system by looking through data for patterns. Machine learning is robust to noise and fast in classification. In that it learns for different systems their characteristics leading to a predicted model.

B. Wi-Fi Activity Prediction Methodology

1. Data Collection and Preprocessing

To study the Wi-Fi power and understand its behavior with respect to time and location, data is collected for three consecutive months from five locations of one building. One personal laptop device “Acer 5251” is used for the data collection using Wi-Fi analyzer - Acrylic Wi-Fi professional application [48]. In each time, the data is collected in a different location, the device is placed at a constant distance of 3.5 meters away from the router to insure reliability of the collected data. The system is programmed to measure the available power in the location each ten minutes. The collected data consists of the following parameters:

- Location of the five wireless routers of interest defined as location A through E.
- The day in which the data is taken in the form of a number from 1 to 5 corresponding to the five working days of the week. Saturdays and Sundays along with the holidays are not taken into account since the Wi-Fi usage pattern will be different. This helps maintain the consistency in the gathered data.
- The time at which the data is measured: a number going from 8 to 24 corresponding to the data taken from 8 A.M. till 12 A.M.
- The signal strength measured in dBm.

For illustration purposes, data collected from location A for three consecutive Tuesdays is plotted in Figure 61.

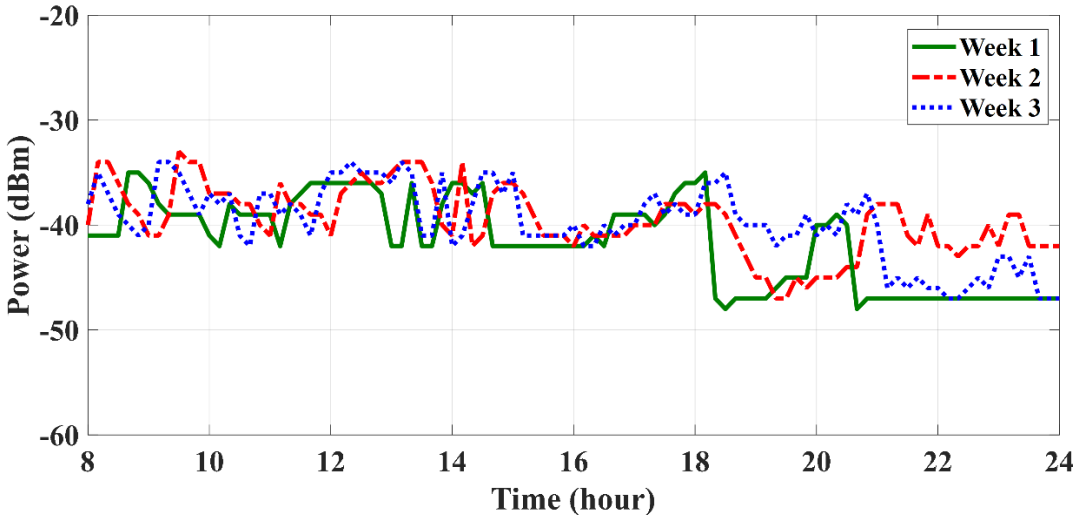

Figure 61: Data collected for three consecutive Tuesdays in location A.

By looking into these plots, it can be noticed how the router's transmission fluctuates between an upper and lower limit with a huge dependency on the day and time. The pattern characterizing the signal strength varies with several parameters and is not easily visualized and interpreted. Therefore, to model the Wi-Fi activity pattern, this data will be trained using a widely used learning technique that is based on SVM.

SVM is a powerful tool in classification, regression and novelty analysis due to its foundation in statistical theory. The fundamental feature of an SVM is to locate a maximum-margin hyperplane whose position is determined by maximizing its distance from the support vectors to optimally identify the predictive model [27].

In this system, the collected datasets contain thousands of points representing the five locations. Since the data is not collected simultaneously for all places, Wi-Fi power from each location at the same time is not available. Therefore, it is possible to implement one SVM that describes each one of the five locations. By implementing this design, each SVM output yields the predicted RF power in each location. The output is composed of a regression layer denoting the Wi-Fi power in each location. The input is

a vector containing the date as a number from 1 to 5 corresponding to the five working days, the time in minutes from 480 to 1440, and the previous power or P(t-1) describing the power 10 minutes earlier.

For the same location, data is collected for the same weekday two to three times. 80% of the input data is used to train and validate SVM while 20% are used for testing. Among each five consecutive points, four are chosen for training and one for testing.

SVM relies on a kernel function to solve nonlinear problems. The gaussian radial basis function is used for this purpose. Two parameters C (soft margin parameter) and γ (kernel parameter) are selected before training the SVM through a cross validation technique to select the best values leading to the highest accuracy.

2. Wi-Fi activity prediction approach

As shown in Figure 61, the RF power transmitted from wireless routers exhibits two different patterns; a high RF power level is maintained for a certain period of time whereas a low level appears for the remaining time. Based on this observation, two classifiers are assigned per location to cover the “high power” and the “low power". Figure 62 describes the adopted approach. The total average power for the location is calculated for all working days and marked by the black horizontal cut in Figure 62. The day is partitioned to smaller sections of two hours each. The data for each classifier is selected upon comparing the average power of the section to the total average power. If the data appears to be higher than the total average, it then belongs to the “high power” classifier as marked in the horizontally hatched blue region of Figure 62. Otherwise the data will be part of the “low power” classifier as highlighted in the diagonally hatched green region.

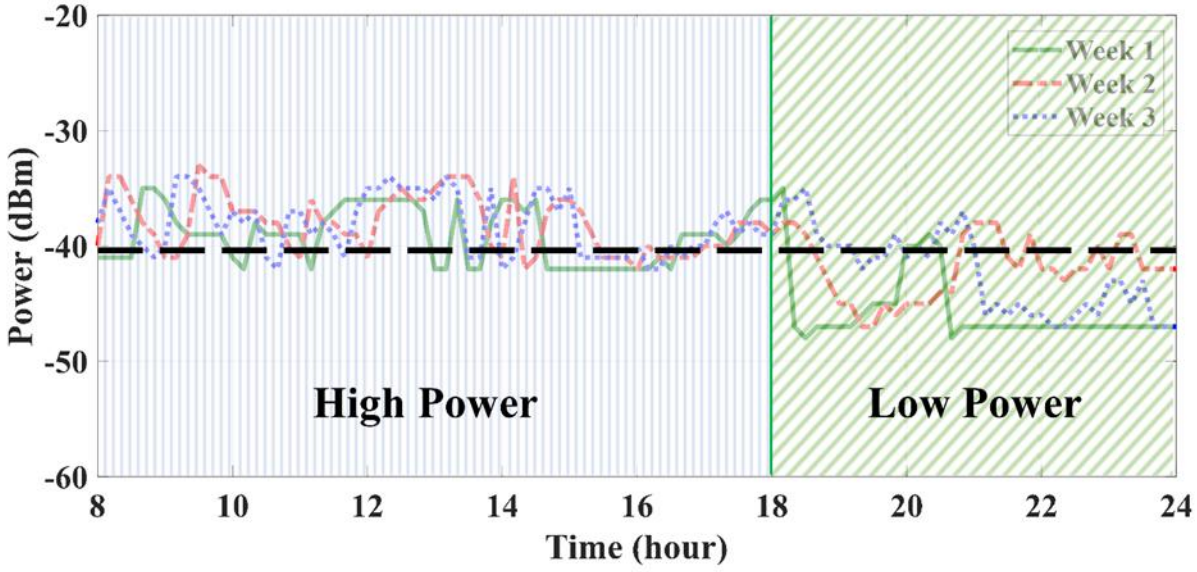

Figure 62: Power Patterns for three consecutive Tuesdays in location A.

C. Results Interpretation

The proposed approach is now tested by building two SVMs for each location. The algorithm is responsible for predicting the maximum available power along with its location. The accuracy is calculated using Eq. 6.

$$Accuracy = \frac{100}{n} \sum_{t=1}^{n} A_t = P_t \tag{6}$$

where A is the actual power in the location, P is the predicted power and n is the maximum number of observations.

Figure 63 shows the prediction performance of SVM and Artificial Neural Networks (ANN) compared to the actual values for location A. ANN is implemented for validation purposes. Its architecture illustrated in Figure 64 is based on five hidden layers of 200, 150, 100, 50 and 10 neurons consecutively. The sigmoid is used as an activation function between the layers. The applied training function is the scaled

conjugate gradient and the performance is measured using mean squared error (MSE). The tested accuracy on the 20% of the data yields a 30% accuracy for ANN and 35% for SVM with an average prediction error of 1.5 dBm.

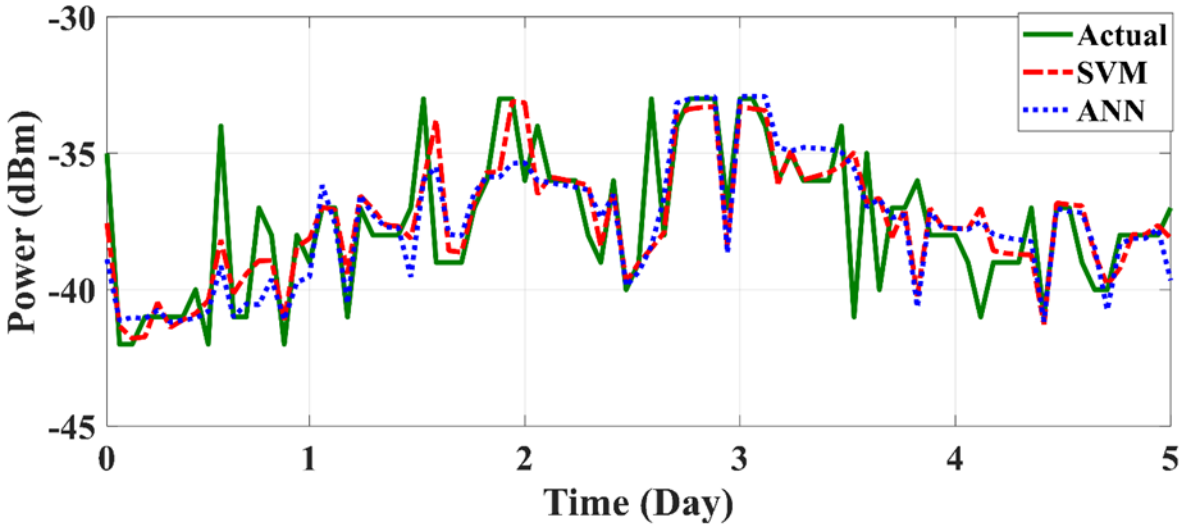

Figure 63: Comparison of actual power with predicted power using ANN and SVM in location A for a week period.

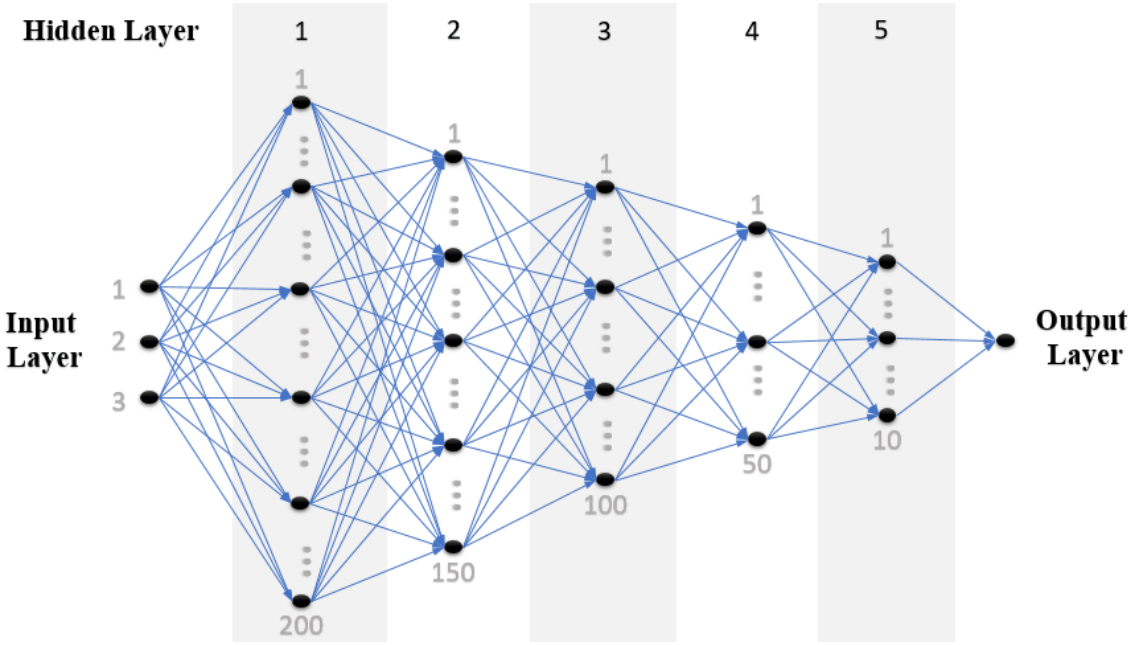

Figure 64: ANN Architecture.

One location is chosen as a reference, where its data sets are selected for comparison with data sets collected from other locations. Accordingly, the data having a matching input (day/time) in the other locations is chosen. This way, we can guarantee that the data used for testing possess the same input. For all of these locations, a table similar to Table 2 is created. This table holds the input along with the "Actual" output or available power and the "Predicted" Wi-Fi powers using SVM at the same input.

From each section of the table, "Actual" and "Predicted", the location with the maximum power is extracted at each time stamp. From the "Actual" section in table 2, the green colored values in each column denote the actual maximum power value among the locations, whereas those that are green colored in the "Predicted" section, denote the correctly predicted values by SVM. The value shown in orange represents the predicted value that doesn't match the actual one. Therefore, the average prediction accuracy is calculated by comparing the selected locations from the table. The accuracy is found to be ranging between 79 and 83%.

Table 2: Sample of actual vs predicted power

	Day	1	3	2	5	5	1	4
	Time	618	720	1010	850	1340	600	910
Actual	Location A	-35	-43	-32	-32	-48	-37	-39
	Location B	-41	-45	-40	-37	-47	-39	-37
	Location C	-43	-46	-40	-33	-35	-44	-38
	Location D	-34	-45	-44	-39	-39	-46	-41
	Location E	-46	-46	-48	-41	-43	-42	-36
Predicted	Location A	-35.61	-41.43	-32.50	-34.75	-49.73	-35.88	-38.15
	Location B	-38.96	-43.78	-42.51	-37.45	-47.74	-38.29	-37.52
	Location C	-43.40	-46.90	-39.43	-32.44	-34.81	-43.62	-39.65
	Location D	-33.49	-44.38	-42.07	-39.25	-39.67	-46.20	-41.64
	Location E	-45.69	-46.96	-48.70	-39.93	-42.27	-43.05	-35.96

To evaluate the effect of applying the SVM algorithm on the daily collected RF power, Figure 65 is provided. This figure describes the measured power in the five locations for a one day period. The straight line curve represents the predicted path leading to the maximum power at these locations using SVM. This curve maintains a higher level compared to the other ones over most of the tested periods. Small inaccuracies are due to few misclassified points.

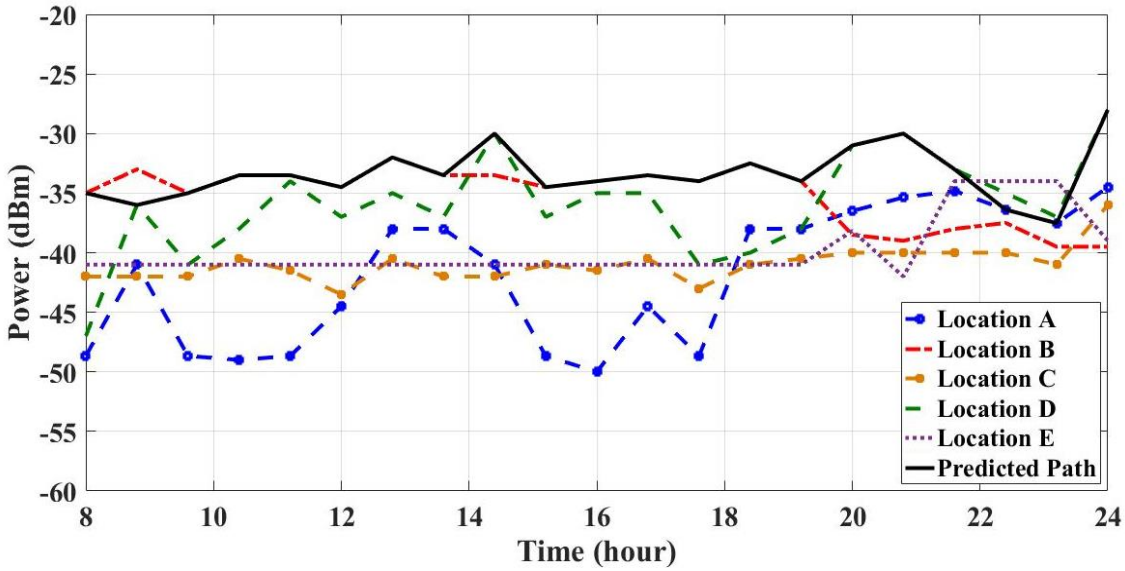

Figure 65: Power on predicted path using SVM for a one day period.

To ensure a reliable performance, energy prediction modelling is a key component for optimizing energy harvesting because it equips the harvesting node with adaptation to energy availability. Using the SVM output for predicting the highest power based on time and location in the rectification process, we plot in Figure 66 the gathered PCE values. The proposed optimization technique proves the ability of collecting a dc output voltage over most of the period of interest. Even though the rectifier is able to provide low efficiency results (around 5%), the harvesting is very challenging because of the low input power levels along with the considered distance of 3.5 meters. The obtained efficiency results agree with Figure 67 where the maximum attained PCE at -30 dBm is 5% and then goes to zero below -38 dBm. Harvesting ambient RF signals from one location without following the predicted path may lead to an almost zero efficiency for the whole period.

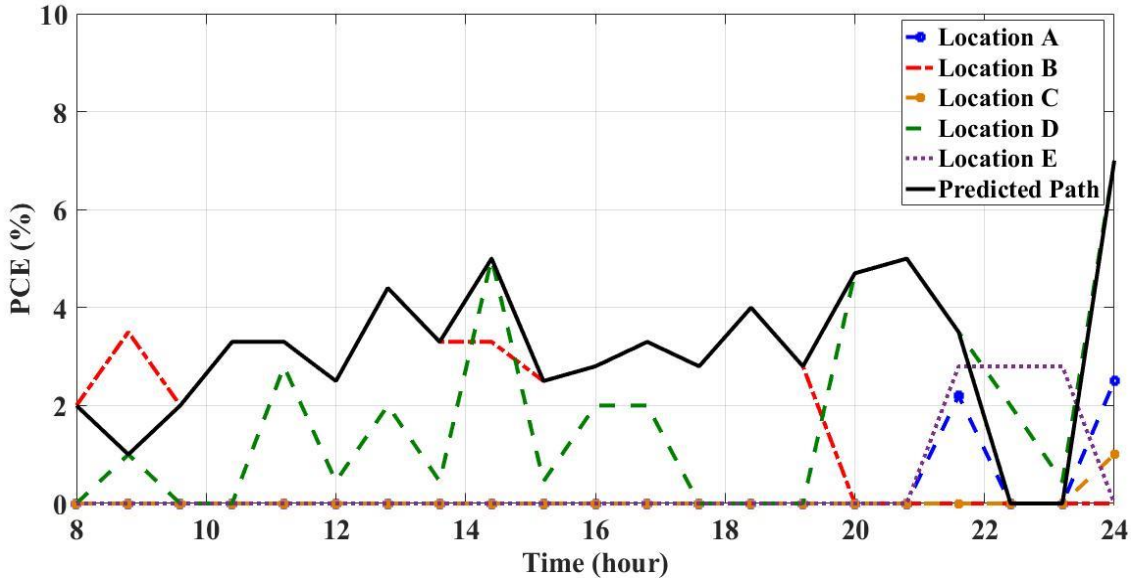

Figure 66: Rectifier's efficiency on predicted path using SVM for a one day period.

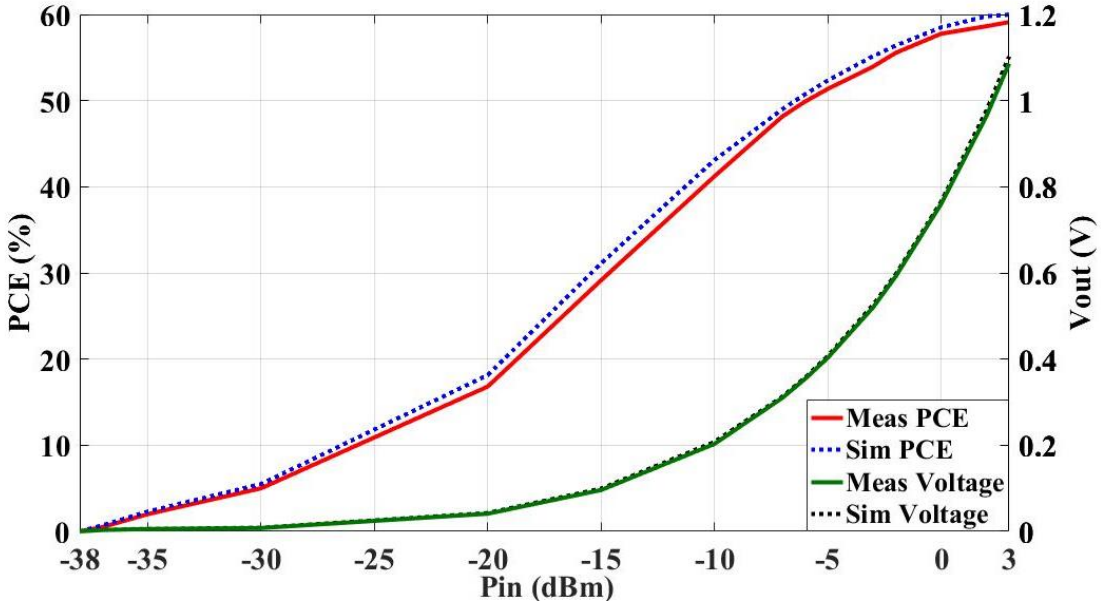

Figure 67: Efficiency and output voltage results for the user rectifier circuit.

With the new predicted approach, other methodologies can be followed to increase the efficiency results. Much higher PCE values are obtained when placing the rectenna system closer to the routers (at 1 meter distance for example). Therefore collecting -30

dBm at a distance of 3.5 meters from the routers is equivalent to getting around -17 dBm at 1 meter. This improvement in the power yields an increase in the average efficiency results from 5 to 25% following the graph of Figure 67.

D. Summary

In this work, pushing the rectification efficiency from ambient RF signals is done through the integration of machine learning techniques. SVM predicts the maximum available powers at different locations over time with an accuracy of 83%. The predicted path helps preserving an almost flat efficiency over time which is very interesting for managing and planning harvested energy. Other experimental techniques can be followed to boost the efficiency of the system, such as resorting to a decreased testing distance.

CHAPTER VIII

CONCLUSION AND FUTURE WORK

In this thesis, RF energy harvesting is studied from different perspectives in the aim of increasing the efficiency of the harvester using a single Schottky diode. The goal is to design a novel system that is able to harvest and rectify RF signals at low power levels. For this reason, in chapter II, a summary of several contemporary rectenna designs available in the literature is presented with the aim of getting familiar with the challenges that exist in this field of study. Chapter III introduces an efficient RF energy harvesting system operating over the Wi-Fi 802.11 b/g band. This system consists of a slot antenna and a new rectifier design. The integrated matching network topology helps achieving good efficiency results over the desired frequency range. It also presents a flat efficiency response over a wide range of load variations. The fabricated rectifier presents an efficiency of 43% at an input power of -10 dBm and a peak efficiency of 57% at 0dBm.The rectenna system is tested for rectification from low dedicated powers and its achieved measured operation matches simulated results.

In chapter IV, the designs of two conventional single stub matching rectifiers are shown. Later, a new matching technique is proposed based on two tapered lines with different characteristic impedances. This network proves the ability of matching a real source impedance to a complex load impedance while resorting to two series lines of non-uniform widths. A demonstration is presented using the smith chart tool then by simulating, designing and measuring the corresponding rectifier. Results show a great agreement between simulated and measured results with a peak efficiency of around 60% at 0dBm. The single port system is then transformed into a multiport RF energy

harvester through the implementation of two combining architectures: RF and dc as discussed in chapter V. This chapter is divided into two sections depending on whether we are considering single or multiple transmitters. Testing shows an advantage of the dc combining over the RF combining, where an increase of 1 V is observed for the same transmitted power after the combination of four rectifiers outputs for the single source transmission.

Chapter VI discusses harvesting very small RF energy at 2.45 GHz from ambient Wi-Fi signals that are collected from commercial Wi-Fi routers. The difference in harvesting scenarios differs from dedicated RF transmission harvesting capability since the RF power must be collected from ambient Wi-Fi signals that are scavenged from actual wireless local area networks (LAN) access points. Therefore, a new technique is proposed to overcome the challenge of harvesting Wi-Fi signals from ambient Wi-Fi. The rectifier is tested in ambient conditions and measured results are found agree closely with the ones obtained through harvesting from dedicated RF signals.

In chapter VII, we resort to Support Vector Machines (SVM) to yield a system that is able to predict with a good accuracy the location and level of maximum power available at a certain day and time. Experimental design shows that SVM reaches an accuracy of 83%. The predicted path leading to the maximum available power in several locations helps preserving an almost flat efficiency over time and motivates follow on research.

Thus, in this thesis, the limits of Schottky diode's rectification abilities are pushed, while investigating optimal matching networks. The systems designed are deployed in a multiport scenario when combined input and output are used. Such system, not only

harvests from dedicated RF signals but also collects ambient Wi-Fi signals with a prediction ability of the maximum available power.

The research carried out in this thesis can be further commenced in the future on different levels such as the investigation of the new matching techniques such as wideband matching networks, or even eliminating the matching network by resorting to conjugately matched antennas. Moreover, all tested rectifiers used shunt reverse-connected Schottky diodes. It might be useful to consider other configurations such as series or voltage multipliers. Also, CMOS based rectifying circuits can be integrated to enable RF energy harvesting at very low power levels.

REFERENCES

[1] D. M. Pozar, “Electromagnetic Theory”, in Microwave Engineering, 4th ed, United States: John Wiley & Sons 1998.

[2] S. Lee, R. Zang and K. Huang, “Opportunistic Wireless Energy Harvesting in Cognitive Radio Networks", IEEE Transactions on Wireless Communications, Vol. 12, No. 9, September 2013 4788.

[3] W. C. Brown, “The History of Power Transmission by Radio Waves,” IEEE Transactions on Microwave Theory and Techniques, vol. 32, no. 9, pp. 1230-1242, Sep. 1984.

[4] S. Hemour et al., "Towards Low-Power High-Efficiency RF And Microwave Energy Harvesting, "IEEE Transactions on Microwave Theory and Techniques, vol. 62, no. 4, pp. 965–976, Apr. 2014.

[5] C. H. P. Lorenz, S. Hemour, and K. Wu, “Physical Mechanism and Theoretical Foundation of Ambient RF Power Harvesting Using Zero-Bias Diodes,” IEEE Transactions on Microwave Theory and Techniques, vol. 64, no. 7, pp. 2146–2158, Jul. 2016.

[6] C. R. Valenta, “Fundamental Limitations for Schottky Diode RF Energy Harvesting”, IEEE International Conference on RFID Technology and Applications (RFID-TA), 2015.

[7] M. Stoopman, S. Keyrouz, H. J. Visser, K. Philips and W. A. Serdijn, “Co-Design of a CMOS Rectifier and Small Loop Antenna for Highly Sensitive RF Energy Harvesters”, IEEE Journal of Solid-State Circuits, Vol. 49, No. 3, March 2014.

[8] H. Liu, X. Li, R. Vaddi, Ka. Ma, S. Datta and V. Narayanan, “Tunnel FET RF Rectifier Design for Energy Harvesting Applications”, IEEE Journal on Emerging and Selected Topics in Circuits and Systems, Vol. 4, No. 4, December 2014.

[9] S. D. Assimonis, S.-N. Daskalakis, and A. Bletsas, "Sensitive and efficient RF harvesting supply for Batteryless Backscatter sensor networks," IEEE Transactions on Microwave Theory and Techniques (MTT), vol. 64, no. 4, pp. 1327–1338, Apr. 2016.

[10] Y. Huang, N. Shinohara, and H. Toromura, "A wideband rectenna for 2.4 GHz-band RF energy harvesting," in IEEE Wireless Power Transfer Conference (WPTC), 2016.

[11] J. Kimionis, M. Isakov, B. S. Koh, A. Georgiadis, and M. Tentzeris, "3D-Printed Origami Packaging with Inkjet-Printed Antennas for RF Harvesting Sensors," IEEE Transactions on Microwave Theory and Techniques, vol. 63, no. 12, pp. 4521–4532, Dec. 2015.

[12] C. Song, Y. Huang, J. Zhou, J. Zhang, S. Yuan, and P. Carter, "A High Efficiency Broadband Rectenna for Ambient Wireless Energy Harvesting," IEEE Transactions on Antennas and Propagation, vol. 63, no. 8, pp. 3486–3495, Aug. 2015.

[13] C. Song, Y. Huang, P. Carter, J. Zhou, S. Yuan, Q. Xu and M. Kod, “A Novel Six-Band Dual CP Rectenna Using Improved Impedance Matching Technique for

Ambient RF Energy Harvesting", IEEE Transactions on Antennas and Propagation, Vol. 64, No. 7, July 2016.

[14] Z. Popović, S. Korhummel, S. Dunbar, R. Scheeler, A. Dolgov, R. Zane, E. Falkenstein and Joseph Hagerty, "Scalable RF Energy Harvesting", IEEE Transactions on Microwave Theory and Techniques, Vol. 62, No. 4, April 2014.

[15] C. Song, Y. Huang, J. Zhou, S. Yuan, Q. Xu, and P. Carter, "A Broadband Efficient Rectenna Array for Wireless Energy Harvesting", 9th Europeoan Conference on Antennas and Propagation (EuCAP), 2015.

[16] H. Sun, Y. Guo, M. He, and Z. Zhong, "A dual-band Rectenna using Broadband Yagi antenna array for Ambient RF power harvesting," IEEE Antennas and Wireless Propagation Letters, vol. 12, pp. 918–921, 2013.

[17] J. Bito, R. Bahr, J. G. Hester, S. A. Nauroze, A. Georgiadis, and M. Tentzeris, "A Novel Solar and Electromagnetic Energy Harvesting System With a 3-D Printed Package for Energy Efficient Internet-of-Things Wireless Sensors", IEEE Transactions on Microwave Theory and Techniques.

[18] J. H. Kim, J. Bito and M. Tentzeris, "Design Optimization of an Energy Harvesting RF-DC Conversion Circuit Operating at 2.45GHz", IEEE International Symposium on Antennas and Propagation 2015.

[19] I. Ramos and Z. Popovic, "A Compact 2.45 GHz, Low Power Wireless Energy Harvester with a Reflector-Backed Folded Dipole Rectenna", IEEE 2015.

[20] C. Song, Y. Huang, J. Zhou, P. Carter, S. Yuan, Q. Xu and Z. Fei, "Matching Network Elimination in Broadband Rectennas for High-Efficiency Wireless Power Transfer and Energy Harvesting", IEEE Transactions on Industrial Electronics, 2016.

[21] D.-K. Ho, I. Kharrat, V.-D. Ngo, T.-P. Vuong, Q.-C. Nguyen, and M.-T. Le, "Dual-band rectenna for ambient RF energy harvesting at GSM 900 MHz and 1800 MHz," 2016 IEEE International Conference on Sustainable Energy Technologies (ICSET), 2016.

[22] T. B. Lim, N. M. Lee, B. Kiat, "Feasibility Study on Ambient RF Energy Harvesting for Wireless Sensor Network," 2013 IEEE MTT-S Microwave Workshop Series on RF and Wireless Technologies for Biomedical and Healthcare Applications (IMWS-BIO), International, 2013.

[23] N. Tung, "Multi-Band Ambient RF Energy Harvesting Rectifier for Autonomous Wireless Sensor Networks," 2016 IEEE Region 10 Conference (TENCON), 2016.

[24] Y. Zhao, V. C. M. Leung, X. Sun, Z. Chen, and H. Ji, "Energy-Efficient Resource Allocation in Cellular Network with Ambient RF Energy Harvesting," 2017 IEEE Wireless Communications and Networking Conference (WCNC), 2017.

[25] J. F. Ensworth, S. J. Thomas, S. Y. Shin, and M. S. Reynolds, "Waveform-Aware Ambient RF Energy Harvesting," 2014 IEEE International Conference on RFID (IEEE RFID), 2014.

[26] V. Talla, B. Kellogg, B. Ransford, S. Naderiparizi, S. Gollakota, and J. Smith, "Powering the Next Billion Devices with Wi-Fi," IEEE, May 2015.

[27] M. Awad and R. Khanna, Efficient Learning Machines: Theories, Concepts, and Applications for Engineers And System Designers. Berkley: Apress Open, 2015.

[28] F. Azmat, Y. Chen, and N. Stocks, “Predictive Modelling of RF Energy for Wireless Powered Communications,” IEEE Communications Letters, vol. 20, no. 1, pp. 173–176, 2016.

[29] M. M. Ababneh, S. Perez, and S. Thomas, “Optimized Power Management Circuit for RF Energy Harvesting System,” 2017 IEEE 18th Wireless and Microwave Technology Conference (WAMICON), 2017.

[30] J. Bito, M. M. Tentzeris, and A. Georgiadis, “A Hybrid Heuristic Design Technique for Real-Time Matching Optimization for Wearable Near-Field Ambient RF Energy Harvesters,” 2016 IEEE MTT-S International Microwave Symposium (IMS), 2016.

[31] S. Shen and R. D. Murch, “Impedance Matching for Compact Multiple Antenna Systems in Random RF Fields,” IEEE Transactions on Antennas and Propagation, vol. 64, no. 2, pp. 820–825, 2016.

[32] J. Costantine, Y. Tawk, E. A. Zuraiqi, S. E. Barbin, and C. G. Christodoulou, “Applying Graph Models and Neural Networks on Reconfigurable Antennas for Cognitive Radio Applications,” 2011 IEEE-APS Topical Conference on Antennas and Propagation in Wireless Communications, 2011.

[33] N. Xu, C. G. Christodoulou, S. E. Barbin, and M. Martinez-Ramon, “Detecting Failure of Antenna Array Elements Using Machine Learning Optimization,” 2007 IEEE Antennas and Propagation International Symposium, 2007.

[34] M.M. Ramon, N. Xu, C.G. Christodoulou, “Beamforming Using Support Vector Machines,” IEEE Antennas and Wireless Propagation Letters, vol. 4, no. 1, pp. 439-442, 2005.

[35] C. Christodoulou, J. Rohwer, and C. Abdallah, “The Use of Machine Learning in Smart Antennas,” IEEE Antennas and Propagation Society Symposium, 2004., 2004.

[36] Skyworks Solutions, Inc. (2016, July. 5). “Surface Mount Mixer and Detector Schottky Diodes,” [Online]. Available: http://www.skyworksinc.com/ /uploads/documents/Surface_Mount_Schottky_Diodes_200041AB.pdf [Sept. 15, 2016].

[37] Advanced Design System, ADS 2009, Keysight Technologies, Santa Rosa, CA.

[38] A. Eid, J. Costantine, Y. Tawk, A. H. Ramadan, M. Abdallah, R. ElHajj, R. Awad, I. B. Kasbah, “An Efficient RF Energy Harvesting System”, IEEE European Conference on Antennas and Propagation (EuCAP), pp. 896-899, 2017.

[39] A. Eid, J. Costantine, Y. Tawk, M. Abdallah, A. H. Ramadan, C. Christodoulou, “Multiport RF Energy Harvester”, IEEE International Symposium on Antennas and Propagation (APS), 2017.

[40] J. Costantine, A. Eid, M. Abdallah, Y. Tawk, A. H. Ramadan, “A Load Independent Tapered RF Harvester”, IEEE Microwave and Wireless Components Letters (MWCL), 2017.

[41] U. Olgun, C.-C. Chen, and J. L. Volakis, "Investigation of Rectenna array configurations for enhanced RF power harvesting," IEEE Antennas and Wireless Propagation Letters, vol. 10, pp. 262–265, 2011.

[42] C. A. Balanis, Modern Antenna Handbook, John Wiley and Sons, 2007.

[43] Mini-Circuits, “ZN2PD-63-S+”, Power Splitter/Combiner,” [Online] Available: https://www.minicircuits.com/pdfs/ZN2PD-63-S+.pdf [Jan. 12, 2017].

[44] Mini-Circuits, “ZB4PD-42+, Power Splitter/Combiner,” [Online] Available: https://www.minicircuits.com/pdfs/ZB4PD-42+.pdf [Jan. 12, 2017].

[45] TP-Link, TP-Link TL-WR541G 54 Mbps Extended Range Wireless Router. [Online]. Available: http://static.tplink. com/resources/software/200977201065 .pdf.

[46] Wireshark, 2017. [Online]. Available: https://www.wireshark.org/download/docs/ user-guide-a4 .pdf.

[47] QMIC, D-COCODI: Framework for Cooperative Multimedia Multi-casting in Dense Environments, July 2017. [Online].
Available: http://www.qmic.com/solutions/de-cocodi/.

[48] WiFi analyzer – Acrylic WiFi Professional, [online] Available: https://www.acrylicwifi.com/en/wlan-software/wifi-analyzer-acrylic-professional